

Higher order trade-offs in hypergraph community detection

Jiaze Li¹, Michael T. Schaub², Leto Peel¹

¹Department of Data Analytics and Digitalisation , Maastricht University, 6200 MD
Maastricht, The Netherlands

²RWTH Aachen University, Aachen, Germany

Extending community detection from pairwise networks to hypergraphs introduces fundamental theoretical challenges. Hypergraphs exhibit structural heterogeneity with no direct graph analogue: hyperedges of varying orders can connect nodes across communities in diverse configurations, introducing new trade-offs in defining and detecting community structure. We address these challenges by developing a unified framework for community detection in non-uniform hypergraphs under the Hypergraph Stochastic Block Model. We introduce a general signal-to-noise ratio that enables a quantitative analysis of trade-offs unique to higher-order networks, such as which hyperedges we choose to split across communities and how we choose to split them. Building on this framework, we derive a Bethe Hessian operator for non-uniform hypergraphs that provides efficient spectral clustering with principled model selection. We characterize the resulting spectral detectability threshold and compare it to belief propagation limits, showing the methods coincide for uniform hypergraphs but diverge in non-uniform settings. Synthetic experiments confirm our analytical predictions and reveal systematic biases toward preserving higher-order and balanced-shape hyperedges. Application to empirical data demonstrates the practical relevance of these higher-order detectability trade-offs in real-world systems.

Introduction

Community detection is central to interpreting mesoscale network structure, revealing groups of nodes with similar connectivity patterns that provide a coarse-grained summary often aligned with functional organization [1, 2]. In the classical setting of dyadic, or *pairwise*, networks, this intuition translates most commonly into identifying densely connected subgraphs, and a broad range of algorithmic and theoretical tools have been developed, including modularity maximization [3], spectral clustering [4], and probabilistic generative models such as the stochastic block model (SBM) [5]. The SBM has enabled a comparatively mature theoretical understanding of community detection, particularly in the case of sparse graphs. These theoretical contributions include sharp detectability thresholds, near-optimal inference algorithms and closely related efficient spectral methods based on the non-backtracking and the Bethe Hessian operators [6–8].

Yet, many complex systems cannot be faithfully represented by pairwise interactions alone. In domains ranging from scientific collaboration and human contact patterns to microbial consortia and chemical reaction networks, interactions regularly involve more than two entities at a time, reflecting intrinsic multiway dependencies [9–11]. Recognizing the importance of such higher-order interactions has led to growing interest in higher-order network representations and corresponding models and algorithms, with hypergraphs emerging as a natural and widely used framework; see, e.g., recent reviews [9, 12, 13]. Here we consider aspects of applying the established utility of community detection to the broadly applicable setting of hypergraphs.

Transferring the notion of community structure from graphs to hypergraphs is far from straightforward. In dyadic networks community structure can be largely described by edge density: the strength of community structure corresponds to the relative difference in the density of edges within communities compared to across communities. Hyperedges connect varying numbers of nodes, and these multiway interactions can couple nodes from different communities in a variety of configurations. Figure 1 illustrates some examples of these different configurations in community partitions in graphs and hypergraphs. The resulting structural heterogeneity has no direct analogue in graphs and raises fundamental questions: how should community structure be defined and detected when interactions span multiple orders, and how do different hyperedge orders and “shapes” (i.e., how hyperedges split across communities) jointly influence the recoverability of planted structure? Unlike the graph setting, where detectability and algorithmic optimality are now relatively well understood, the theoretical understanding of community detection in hypergraphs remains much less developed.

In particular, higher-order interactions introduce new trade-offs in describing strength of community structure that have not been characterized systematically so far. Existing work has focused on extending graph-based community detection methods to hypergraphs without explicitly addressing these higher-order trade-offs. The study of hypergraph analogues of modularity maximization [14], spectral methods based on hypergraph Lapla-

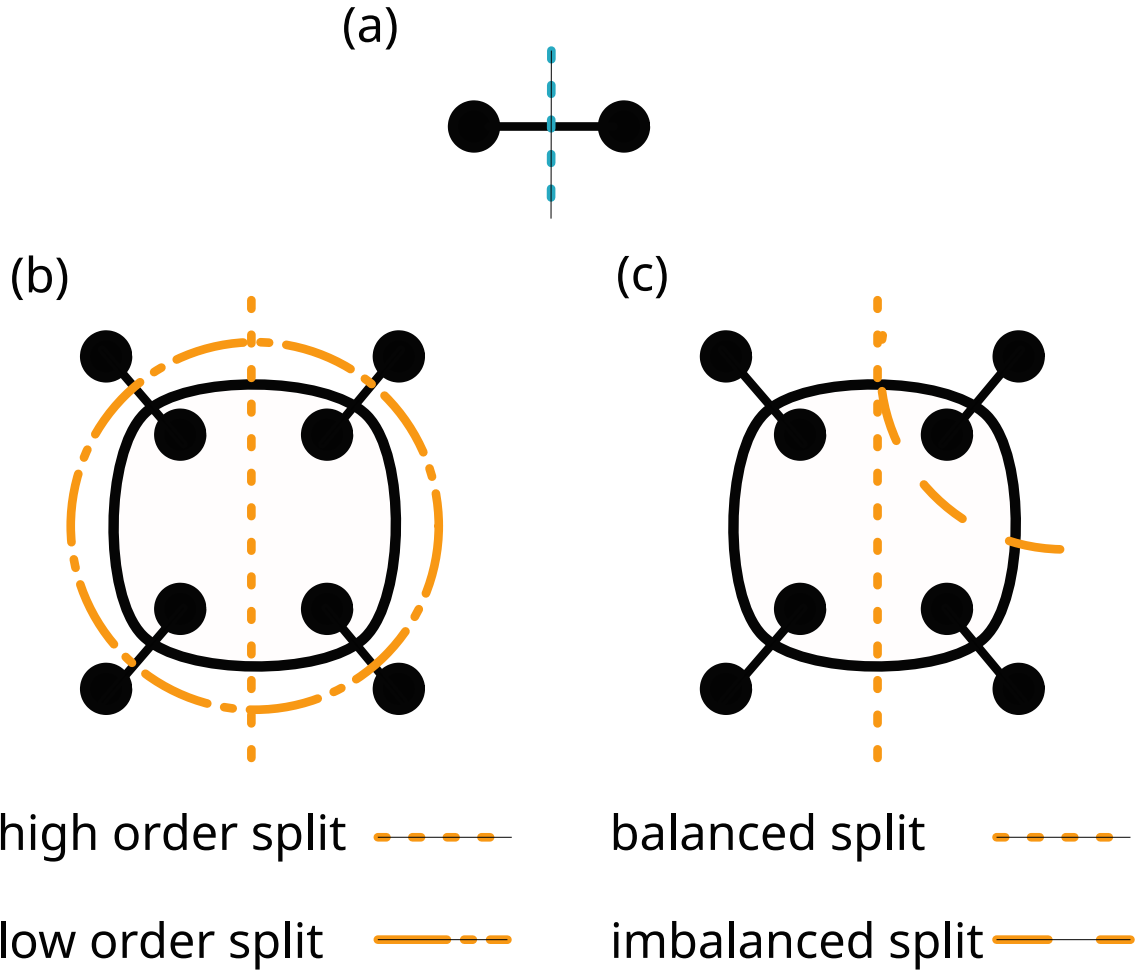


Figure 1: *Different configurations of community structure in graphs and hypergraphs.* (a) In dyadic networks, there is a single type of edge connecting pairs of nodes and edges can only be split across communities in one way. (b) In hypergraphs, hyperedges of different orders connect varying numbers of nodes and we must choose which order of hyperedge to split across communities, e.g., do we prefer to preserve the higher order 4-hyperedges or the lower order 2-hyperedges? (c) Hyperedges can connect more than two nodes and can be split across communities in multiple ways. Here, we consider two different shapes of a 4-hyperedge, a balanced shape and an imbalanced shape.

cians [15], non-backtracking operators [16], and approximate-inference schemes derived from belief propagation [17, 18] provide useful building blocks, but a more unified picture of detectability in general non-uniform hypergraphs is still lacking.

In this work, we take an important step toward such a picture by studying the detectability of community structure in hypergraphs under the Hyper Stochastic Block Model (HSBM) [16, 17]. In the HSBM nodes are assigned to latent communities and hyperedges of various orders are generated according to community-dependent probabilities. This framework generalizes the SBM to higher-order interactions and provides a clear link between observed hypergraph structure and latent communities, enabling principled evaluation of community detection methods via their ability to recover planted structure.

Importantly, the HSBM also allows us to formulate and analyze detectability of communities in hypergraphs. Previous work has derived BP-based detectability thresholds for uniform HSBMs, where all hyperedges have the same order [17], and for specific cases of non-uniform settings [16, 18]. Here we generalize these results by introducing a unified signal-to-noise ratio (SNR) for hypergraphs that applies to arbitrary mixtures of hyperedge orders and any number of communities. This SNR quantifies the relative strength of different hyperedge orders and shapes, and thereby provides an important tool to analyze the novel trade-offs that arise in hypergraph communities.

Our algorithmic approach builds on spectral clustering via the Bethe Hessian (BH) [8]. We derive a BH operator for non-uniform hypergraphs that serves as a symmetric, $n \times n$ linearization of belief propagation for the HSBM and retains a spectral correspondence to the hypergraph non-backtracking operator [16, 19]. This correspondence inherits principled model-order selection via negative BH eigenvalues and provides node-level embeddings via BH eigenvectors, while offering substantial computational advantages over non-backtracking operators. Using our BH formulation, we characterize a spectral detectability threshold in terms of our SNR and compare it to a more general theoretical detectability limit derived for the same HSBM family using belief propagation. We show that the two thresholds coincide in the uniform case, implying that BH-based spectral clustering reaches the theoretical limit, whereas for non-uniform HSBMs the BH spectral threshold is strictly weaker.

Synthetic experiments confirm these analytical predictions and further highlight systematic biases in BH-based clustering according to the order and shape of hyperedges, which we can explain in terms of our analytical SNR framework. In particular, we identify situations where partitions favored by higher-order or more balanced shape hyperedges dominate the detected community structure, even when alternative partitions are equally or more strongly supported by lower-order interactions. These phenomena exemplify detectability trade-offs that are unique to higher-order networks. Finally, we apply our method to empirical hypergraphs, demonstrating its scalability, interpretability, and the practical relevance of these higher-order trade-offs in real-world data.

Community detection and detectability limits for hypergraphs

Consider a hypergraph G_H with a set of nodes $\mathcal{V} = \{1, \dots, n\}$, and a set of hyperedges $\mathcal{E} \subseteq \{e_j | e_j \subseteq \mathcal{V}, j = 1, \dots, m\}$ containing $|\mathcal{E}| = m$ hyperedges. We can represent such a hypergraph using an incidence matrix $\mathbf{H} \in \{0, 1\}^{n \times m}$, whose rows are indexed by the nodes and columns are indexed by the hyperedges [15]. Specifically, for a node $i \in \mathcal{V}$ and a hyperedge $e_j \in \mathcal{E}$, the value \mathbf{H}_{ij} is

$$\mathbf{H}_{ij} = \begin{cases} 1 & i \in e_j \\ 0 & \text{otherwise} \end{cases}. \quad (1)$$

The degree $d_i = \sum_j \mathbf{H}_{ij}$ of a node i is the total number of hyperedges that include node i and the order of a hyperedge $|e_j| = \sum_i \mathbf{H}_{ij}$ is the number of nodes involved in a hyperedge e_j . We refer to a hyperedge with order $|e| = \kappa$ as κ -hyperedge or a hyperedge of order κ . If every hyperedge in a hypergraph is a κ -hyperedge, the hypergraph is called a κ -uniform hypergraph. Any dyadic network (graph) can be viewed as 2-uniform hypergraph. Hypergraphs with mixed order hyperedges are referred to as non-uniform hypergraphs. In non-uniform hypergraphs, we can distinguish the hyperedges by their order. We denote the set of all κ -hyperedges as $\mathcal{E}^{(\kappa)}$, and the number of κ -hyperedges as $m^{(\kappa)} = |\mathcal{E}^{(\kappa)}|$.

The general Bethe Hessian for heterogeneous hypergraphs

In this work, we consider a spectral approach for the detection of communities in hypergraphs based on the so-called Bethe-Hessian matrix for hypergraphs.

Specifically, the Bethe Hessian matrix for non-uniform hypergraphs, which can be derived from belief propagation and its linearization in terms of non-backing matrices, is defined as follows:

$$\mathbf{B}_\eta^{(\kappa)} = \mathbf{I} - \sum_{\kappa \in \mathcal{K}} \frac{(\kappa - 1)}{(1 - \eta)(\eta + \kappa - 1)} \mathbf{D}^{(\kappa)} + \sum_{\kappa \in \mathcal{K}} \frac{\eta}{(1 - \eta)(\eta + \kappa - 1)} \mathbf{A}^{(\kappa)}, \quad (2)$$

where η is a regularization parameter, $\mathbf{D}^{(\kappa)}$ is the diagonal degree matrix for κ -hyperedges, and $\mathbf{A}^{(\kappa)}$ is the one-mode projection matrix for κ -hyperedges, i.e.,

$$\mathbf{A}_{ij}^{(\kappa)} = \begin{cases} |\{e | i, j \in e \text{ and } |e| = \kappa\}| & i \neq j \\ 0 & i = j \end{cases}. \quad (3)$$

Note that the matrix $\mathbf{A}^{(\kappa)}$ can also be expressed in terms of the κ -hyperedge incidence matrix $\mathbf{H}^{(\kappa)}$ as follows:

$$\mathbf{A}^{(\kappa)} = \mathbf{H}^{(\kappa)} (\mathbf{H}^{(\kappa)})^T - \text{diag}(\mathbf{H}^{(\kappa)} (\mathbf{H}^{(\kappa)})^T). \quad (4)$$

We remark that the Bethe Hessian has many desirable properties and deep connections to a variety of quantities and methods previously considered in the literature (see, e.g., [8, 16–18]). We here consider the Bethe Hessian in its most general form in terms of heterogeneous hypergraphs, which generalizes prior works. The derivation of the Bethe Hessian as well as its relations to the prior literature are discussed in the Appendix B.

The hyper stochastic block model

The hyper stochastic block model (HSBM) is a generative model for uniform [17, 20] and non-uniform hypergraphs [15] with community structure, and is a generalization of the stochastic block model (SBM) [5] for dyadic networks (see Appendix A.1 for further details and definitions related to the SBM).

We can use the HSBM to generate a hypergraph G_H with q communities as follows. We begin by assigning each node $i \in \mathcal{V}$ a community label $\psi_i \in \{1, 2, \dots, q\}$. We define the set \mathcal{K} that collects all the possible hyperedge orders in our hypergraph. If \mathcal{K} only has one element, then the HSBM generates a uniform hypergraph, otherwise it generates a non-uniform hypergraph. For each $\kappa \in \mathcal{K}$, the probability of generating a κ -hyperedge is described by a κ -order tensor $\Omega^{(\kappa)} \in [0, 1]^{q^\kappa}$, i.e., for any set of κ nodes $\{i, j, \dots, \kappa\}$, the probability of generating a κ -hyperedge is given by $\Omega_{\psi_i, \psi_j, \dots, \psi_k}^{(\kappa)}$.

For a fixed number of nodes n and $\kappa \in \mathcal{K}$, the number of possible κ -hyperedges is $\binom{n}{\kappa}$. If we assume that hypergraphs are sparse, in the same way that many empirical dyadic networks are, then the number of κ -hyperedges should be $m^{(\kappa)} \sim O(n)$ as $n \rightarrow \infty$. We can then reparameterize the hyperedge connectivity within and between communities, for hyperedges of order κ :

$$\Omega^{(\kappa)} = \frac{\mathbf{C}^{(\kappa)}}{n^{\kappa-1}}, \quad (5)$$

where $\mathbf{C}^{(\kappa)}$ is a κ -order tensor that is constant with respect to n .

For convenience, we define a symmetric HSBM for both uniform and nonuniform case in which all nodes have equal probability $1/q$ of being assigned to any of the q communities and for any $\kappa \in \mathcal{K}$, the elements of tensor $\mathbf{C}^{(\kappa)}$ satisfy:

$$\mathbf{C}_{\mathbf{z}}^{(\kappa)} = \begin{cases} c_{\text{in}} & \text{if } \mathbf{z}_i = \mathbf{z}_j = \dots = \mathbf{z}_\kappa \\ c_{\text{out}} & \text{otherwise} \end{cases}, \quad (6)$$

where \mathbf{z} represent the κ -dimensional vector of community indices.

Spectral clustering with the Bethe Hessian for hypergraphs

Given a (possibly non-uniform) hypergraph G_H and its Bethe Hessian $\mathbf{B}_\eta^{(\mathcal{K})}$ from Eq. (2), we detect communities by spectral clustering on $\mathbf{B}_\eta^{(\mathcal{K})}$. As in the graph case [8], informative eigenvalues of the non-backtracking operator correspond to negative eigenvalues

of $\mathbf{B}_\eta^{(\mathcal{K})}$ when η is chosen appropriately. Thus, the number of negative eigenvalues estimates the number of communities, and the associated eigenvectors provide an informative embedding of the nodes.

We now partition the hypergraph nodes according to the following procedure:

1. Choose a regularization parameter $\eta > 0$ (e.g., using a simple degree-based rule; see Appendix B.3).
2. Let $\lambda_1(\eta) \leq \dots \leq \lambda_n(\eta)$ be the eigenvalues of $\mathbf{B}_\eta^{(\mathcal{K})}$. Set $\hat{q} = |\{i : \lambda_i(\eta) < 0\}|$ as the estimated number of communities.
3. Form the matrix $\mathbf{U} \in \mathbb{R}^{n \times \hat{q}}$ whose columns are the eigenvectors corresponding to the \hat{q} most negative eigenvalues, and apply k -means to the rows of \mathbf{U} to obtain labels $\hat{\psi}_i$.

This procedure generalizes the Bethe Hessian spectral clustering for graphs [8] and uniform hypergraphs [17] to non-uniform hypergraphs.

Generalized detectability limits for hypergraph community structure

The detectability limit for community structure describes the boundary below which no algorithm can succeed in recovering the true community structure with accuracy better than random guessing. Detectability limits of community structure in dyadic networks have been extensively studied in the literature [6, 21–23]. In contrast, the theoretical understanding of detectability in hypergraphs has received comparatively less attention. Early work by Angelini et al. [17] first analyzed the detectability limit of the uniform symmetric HSBM, employing a theoretical approach based on belief propagation (BP), similar to the analysis in dyadic networks [6]. Subsequently, Chodrow et al. [16] analyzed the spectral features of both the non-backtracking matrix (NB) and the Jacobian matrix of belief propagation (BP Jacobian). They established two limits related to the spectral clustering based on these two matrices for the non-uniform symmetric HSBM. However, their analysis was restricted to the case of only $q = 2$ communities. Chodrow et al. concluded that the limit derived from the NB is weaker than the limit from the BP Jacobian. More recently, the work by Ruggeri et al. [18] derived the theoretical detectability limit using BP for a specialized variant called HySBM, a model structurally constrained by deriving all κ -order affinity tensors from a single underlying probability matrix, thereby limiting the independent modeling of different hyperedge order probabilities.

Here, we significantly extend these contributions. First, we reparameterize and generalize the spectral detectability limit, build upon the work of Angelini et al. [17] and Chodrow et al. [16] for the non-uniform symmetric HSBM with an arbitrary number of

communities. Second, we employ a methodology similar to that of Ruggeri et al. [18] to derive the theoretical detectability limit with BP for the non-uniform symmetric HSBM. Finally, by comparing these two derived theoretical boundaries, we conclude that the spectral clustering limit is precisely equal to the theoretical limit in the uniform HSBM case, but is demonstrably weaker in the more complex non-uniform HSBM case.

Detectability limit for spectral methods on general hypergraphs We can describe the detectability limit for spectral clustering with the Bethe Hessian in terms of the average κ -in-degree $d_{\text{in}}^{(\kappa)}$ and κ -out-degree $d_{\text{out}}^{(\kappa)}$. To this end, we define the average κ -in-degree $d_{\text{in}}^{(\kappa)}$ as the expected number of κ -hyperedges incident on a node in which all κ nodes belong exclusively to the same community. Analogously, the average κ -out-degree $d_{\text{out}}^{(\kappa)}$ is the expected number of hyperedges that connect to at least one node belonging to a different community. Now, consider a network generated from a symmetric HSBM with q equal-sized communities and symmetric tensor \mathbf{C} satisfying (6). Then, $d_{\text{in}}^{(\kappa)}$ and $d_{\text{out}}^{(\kappa)}$ can be computed as (See formulas (62) and (63) in Appendix D for details)

$$d_{\text{in}}^{(\kappa)} = \frac{c_{\text{in}}}{q^{\kappa-1}(\kappa-1)!} \quad d_{\text{out}}^{(\kappa)} = \frac{c_{\text{out}}}{q^{\kappa-1}(\kappa-1)!} , \quad (7)$$

and the average κ -degree for the node is

$$d^{(\kappa)} = d_{\text{in}}^{(\kappa)} + (q^{\kappa-1} - 1)d_{\text{out}}^{(\kappa)} . \quad (8)$$

The detectability limits for spectral methods previously derived in the literature [16, 17] can now be generalized to the non-uniform symmetric HSBM with any q as follows (for details see Appendix D):

$$\text{SNR}_{\text{BH}} := \frac{\left(\sum_{\kappa \in \mathcal{K}} (\kappa-1)(d_{\text{in}}^{(\kappa)} - d_{\text{out}}^{(\kappa)}) \right)^2}{\sum_{\kappa \in \mathcal{K}} (\kappa-1)d^{(\kappa)}} = 1 . \quad (9)$$

Detectability limit in general hypergraphs We also derive the theoretical detectability limit with BP for non-uniform symmetric HSBM, employing a similar methodology as in the work by Ruggeri et al. [18]. To establish the general detectability limit, we first determine two essential characteristics of the network structure: the average degree d of a node and the average order $\hat{\kappa}$ of a hyperedge. Both the average degree d and the average order $\hat{\kappa}$ can be expressed based on the order- κ average degree $d^{(\kappa)}$ given in (8). The average degree d is directly calculated by summing the average degrees across all hyperedge orders:

$$d = \sum_{\kappa \in \mathcal{K}} d^{(\kappa)} , \quad (10)$$

where the average order $\hat{\kappa}$ can be expressed as (See Appendix E.4.2 for details):

$$\hat{\kappa} = \frac{d}{\sum_{\kappa \in \mathcal{K}} \frac{d^{(\kappa)}}{\kappa}} . \quad (11)$$

Now the detectability for belief propagation on the non-uniform symmetric HSBM can be explicitly expressed as:

$$\text{SNR}_{\text{BP}} := d(\hat{\kappa} - 1) \prod_{\kappa \in \mathcal{K}} \left(\frac{d_{\text{in}}^{(\kappa)} - d_{\text{out}}^{(\kappa)}}{d^{(\kappa)}} \right)^{2 \frac{\hat{\kappa} d^{(\kappa)}}{d \kappa}} = 1 . \quad (12)$$

Analogously, to prior works [6], we posit that this represents the theoretical detectability limit for non-uniform hypergraphs with q communities. For simplicity, the detailed derivation of (12) is deferred to the Appendix E.

In the uniform HSBM, The SNR_{BP} (12) will degenerate to SNR_{BH} (9). That means that in the uniform case spectral clustering, e.g., with the Bethe Hessian matrix (or the non-backtracking matrix) can detect community structure down to the same detectability threshold as belief propagation. However in the nonuniform case, the detectability threshold $\text{SNR}_{\text{BH}} = 1$ is weaker than $\text{SNR}_{\text{BP}} = 1$.

We validate the thresholds $\text{SNR}_{\text{BH}} = 1$ and $\text{SNR}_{\text{BP}} = 1$ empirically in the following experiment on synthetic hypergraphs. We fix the average degree d of a hypergraph and vary the ratio $\epsilon = \frac{c_{\text{out}}}{c_{\text{in}}}$ to control the community strength. When ϵ is small, the community structure is strong, and when ϵ is large, the community structure is weak. We denote the critical ϵ for which $\text{SNR}_{\text{BH}} = 1$ as ϵ_{BH}^* , and the critical ϵ that make $\text{SNR}_{\text{BP}} = 1$ as ϵ_{BP}^* . We use the adjusted mutual information AMI [24] to evaluate the community detection result. The AMI score lies in range $[0, 1]$, where 1 indicates perfect agreement between the detected communities and the true communities, while 0 indicates that the detected communities are no better than random guessing.

In Figure 2 we see the results of experiments conducted on non-uniform hypergraphs with $q = 3$ communities. We see that ϵ_{BH}^* is indicates well the point that AMI_{BH} transitions from zero to nonzero. Similarly, ϵ_{BP}^* identifies the transition of AMI_{BP} from zero to nonzero.

Additional trade-offs for detecting hypergraph community structure

In dyadic networks, community structure is often characterized by a higher density of edges within communities compared to the edge-density between communities. This concept of community structure naturally implies that detecting communities involves identifying a partition of the network that maximizes the number of edges within communities while minimizing the number of edges that cross community boundaries.

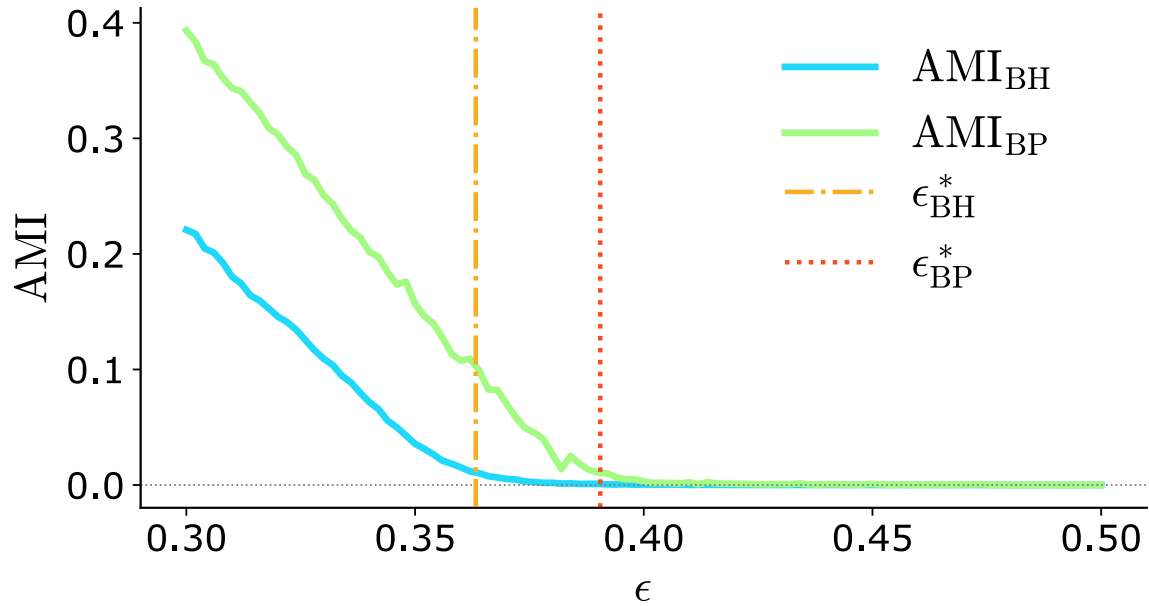


Figure 2: *Spectral methods exhibit a weaker detectability limit in non-uniform hypergraphs.* An experiment with nonuniform hypergraphs with $n = 30,000$ nodes, $q = 3$ communities, $\mathcal{K} = \{2, 3\}$ hyperedge orders and $d = 10$ mean node degree. For each value of ϵ , we run our Bethe Hessian spectral clustering 100 times and belief propagation for 5 times and calculate the mean AMI with the planted community partition. The yellow vertical dash line shows the critical ϵ_{BH}^* , the red vertical dash line shows the critical ϵ_{BP}^* .

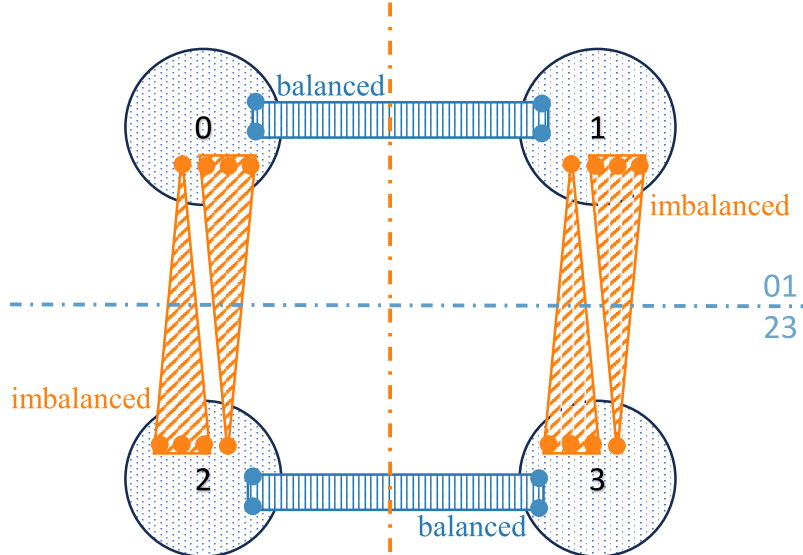
However, for higher-order networks, even this relatively simple density-based notion of community structure is less straightforward to conceptualize, due to the fact that hyperedges can connect more than two nodes and that hyperedges within the same hypergraph can vary in size. For instance, consider the case of detecting a partition of a network into two communities. An edge connecting two nodes that crosses a community boundary will always have one node in each community. For a hyperedge connecting three nodes that crosses a community boundary, there will be one node in one community and two nodes in another community. However, for a hyperedge connecting four nodes that crosses a community boundary, there are two possible configurations: it can connect one node in one community with three nodes in another community, or it can connect two nodes in each community. This observation raises the question of the relationship between these different configurations and the strength of community structure in hypergraphs. To probe this relationship further, we conduct experiments on hypergraphs in which we plant two “competing” community structures and see which one is easier to detect.

Shape preference in hypergraph community structure

We first explore how different configurations of hyperedges crossing community boundaries affect the strength of community structure in hypergraphs. We refer to these different configurations as the *shape* of a hyperedge crossing community boundaries. We consider uniform 4-order hypergraphs with two planted community structures that differ only in the shape of the hyperedges crossing community boundaries: *balanced* hyperedges that connect two nodes in each community, and *imbalanced* hyperedges that connect one node in one community with three nodes in another community. Figure 3(a) illustrates the experimental setup. Each hypergraph has 4 communities, where hyperedges connecting communities $\{0, 1\}$ and $\{2, 3\}$ are balanced, while hyperedges connecting communities $\{0, 2\}$ and $\{1, 3\}$ are imbalanced. We then try to detect a two-community partition of the hypergraph and see which configuration is detected as we vary the ratio $\rho = \frac{m^{\text{imbalanced}}}{m^{\text{balanced}}}$ of imbalanced to balanced hyperedges of the two configurations.

Following the rationale of [25], we predict the relative detectability of the two configurations by calculating which configuration yields a higher value for SNR_{BH} (9). Figure 3(b) shows the results of the experiment, where we plot the AMI of the detected two-community partition with respect to the planted balanced and imbalanced configurations as a function of ρ . We find that the balanced configuration is easier to detect than the imbalanced one, i.e., there is a preference to split the hyperedges such that we have 3 nodes in one community and 1 node in another community, relative to splitting the hyperedges such that we have 2 nodes in each community. This result indicates that preserving more nodes of a hyperedge within the same community creates a stronger community structure. The transition point where the two configurations are equally detectable aligns well with the prediction based on SNR_{BH} and in this case occurs at $\rho^* = 1.33$, indicating that we require 33%.

(a)



(b)

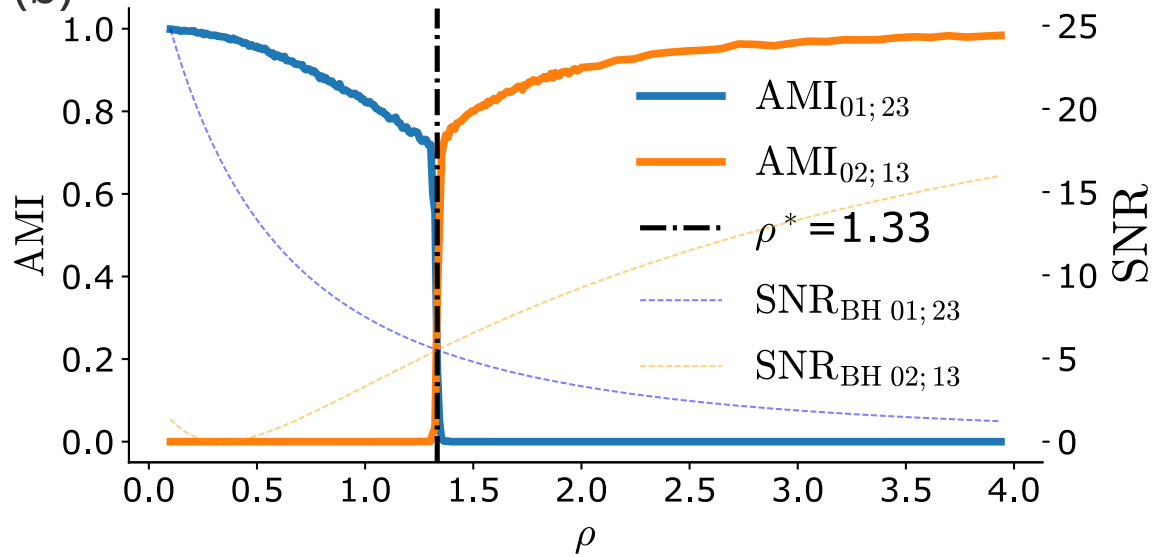


Figure 3: **Hyperedge shape preferences in community detection.** (a) An illustration of the planted community structure in hypergraphs used in experiments to explore the effect of hyperedge shape. All the hyperedges are 4-order and connect 2 of the 4 communities. The balanced hyperedges are represented by rectangle shapes between communities {0, 1} or {2, 3}. The imbalanced hyperedges are represented by triangle shapes between communities {0, 2} or {1, 3}. (b) Experimental results with $n = 8000$ nodes, $d = 10$ mean node degree, $\kappa = 4$ and $\kappa^* = 4$ order hyperedges. We see the $AMI_{01;23}$ and $AMI_{02;13}$ as we vary ρ the ratio of imbalanced to balanced hyperedges. The plot shows that when we have equal number of hyperedges the partition 01; 23 is detected indicating that splitting balanced hyperedges and preserving imbalanced hyperedges is preferred.

Order preference in hypergraph community structure

Now we investigate how hyperedges of different orders crossing community boundaries affect the strength of community structure in hypergraphs. Similar to the previous experiment, we consider non-uniform hypergraphs with planted community structures that differ only in the order of hyperedges crossing community boundaries: low-order hyperedges of order κ and high-order hyperedges of order κ^* . Each hypergraph has 4 communities, where hyperedges connecting communities $\{0, 1\}$ and $\{2, 3\}$ are of order κ^* , while hyperedges connecting communities $\{0, 2\}$ and $\{1, 3\}$ are of order κ . We then try to detect a two-community partition of the hypergraph and see which configuration is detected as we vary the ratio $\rho = \frac{m^{(\kappa^*)}}{m^{(\kappa)}}$ of high-order to low-order hyperedges of the two configurations. Following the same rationale as before, we predict the relative signal-to-noise of the two configurations by calculating which configuration yields a higher value for SNR_{BH} (9). This time, however, the difference in hyperedge orders means that we need to adjust SNR_{BH} accordingly. In the case of non-uniform hypergraphs we find the signal-to-noise ratio for each configuration is equal when

$$\frac{\text{SNR}_{\text{BH} 02;13}}{\kappa + 1} = \frac{\text{SNR}_{\text{BH} 01;23}}{\kappa^* + 1} . \quad (13)$$

Figure 4 shows the results of the experiment, where we plot the AMI of the detected two-community partition with respect to the planted low-order and high-order configurations as a function of ρ . We find that the high-order configuration is easier to detect than the low-order one, i.e., there is a preference to split the lower order hyperedges across community boundaries over splitting higher order ones. This result indicates that hyperedges of lower order create a stronger community structure.

Experiments on empirical data

We test the Bethe Hessian on some hypergraphs constructed from empirical data: two human contact interaction datasets and one user review dataset. The two human contact interaction datasets are from face-to-face interactions using wearable RFID tags in a primary school [26] and a high school [27]. Students and teachers are represented as nodes, and a hyperedge is constructed for each group of individuals who all have a recorded interaction with each other at a given time. The nodes have labels that indicate the school class in which they belong. The user review dataset is from the Yelp website for business reviews in the United States and Canada [28]. The Yelp dataset contains reviews for numerous businesses across 13 states in the United States and one province in Canada. We use nodes to represent the businesses and hyperedges to represent groups of businesses that are reviewed by the same user. We summarize the hypergraphs constructed from these empirical datasets in Table 1.

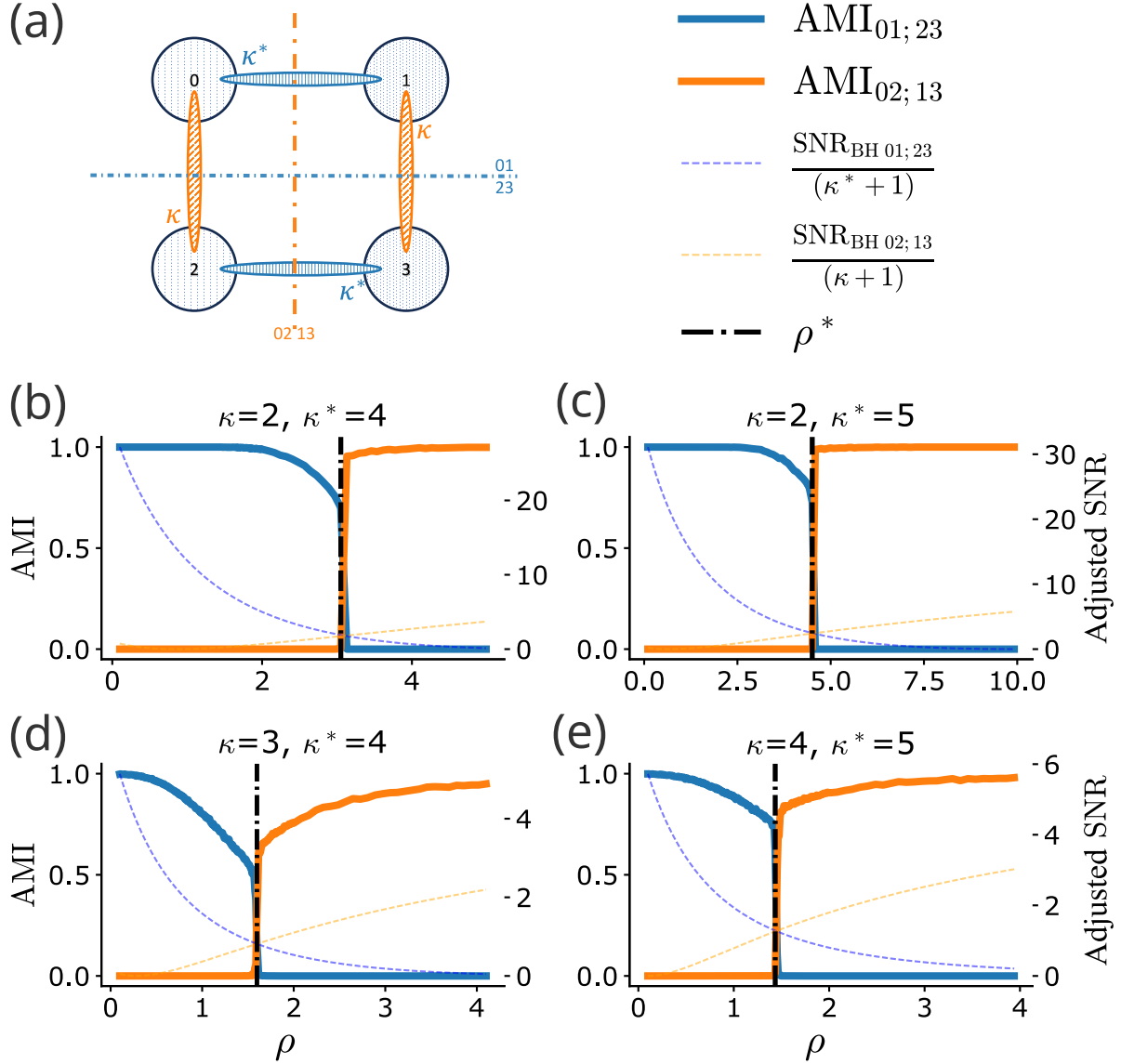


Figure 4: **Hyperedge order preferences in community detection.** (a) Synthetic hypergraphs with 4 planted communities and all the hyperedges between communities $\{0, 1\}$ or $\{2, 3\}$ are of order κ^* , the hyperedges between communities $\{0, 2\}$ or $\{1, 3\}$ are of order κ . All hypergraphs have $n = 8000$ nodes. The average degree is either $d = 50$ (b-c) or $d = 10$ (d-e). We see the $\text{AMI}_{01;23}$ and $\text{AMI}_{02;13}$ as we vary ρ the ratio of high-order to low-order hyperedges. We observe a preference for preserving higher-order κ^* -hyperedges and splitting lower-order κ -hyperedges.

	Hyper Graph	Nodes	Hyperedges	Max Order
primary school	242	12704	5	
high school	327	7818	5	
yelp	150346	851921	3048	

Table 1: Empirical Data

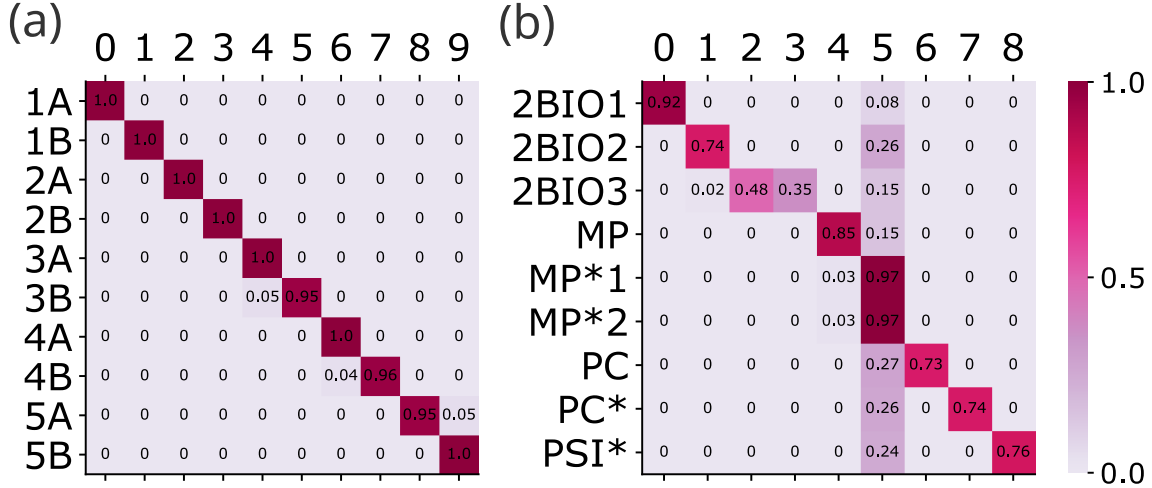


Figure 5: **Comparison between detected communities and class structure in human contact hypergraphs.** Confusion matrices of communities detected and school classes in hypergraphs of human contact interactions in (a) the primary school and (b) the high school. The rows are normalized such that each entry represents the proportion of individuals in the class assigned to each community.

Human contact interaction

First, we detect communities of the primary school detected using spectral clustering with the Bethe Hessian and compare with the school classes. To facilitate comparison, we manually set the number of communities to match the number of classes in the school. Figure 5(a) shows the confusion matrix between the detected communities and the classes. We see an almost one-to-one correspondence between detected communities and classes. This result is similar to community detection results on dyadic networks constructed from the same primary school data [26, 29].

Next we perform a similar comparison on the high school data. Figure 5 (b) shows a less clear correspondence between detected communities and classes compared to the primary school data. This result deviates from the results of community detection on dyadic networks constructed from the same high school data (e.g., using the Bethe Hessian [30]), where the dense within-class connections dominate the mesoscale structure. Instead, we observe that 2BIO3 is split into two main communities (communities 2 & 3), while MP*1 and MP*2 are grouped into a single community (community 5) that also

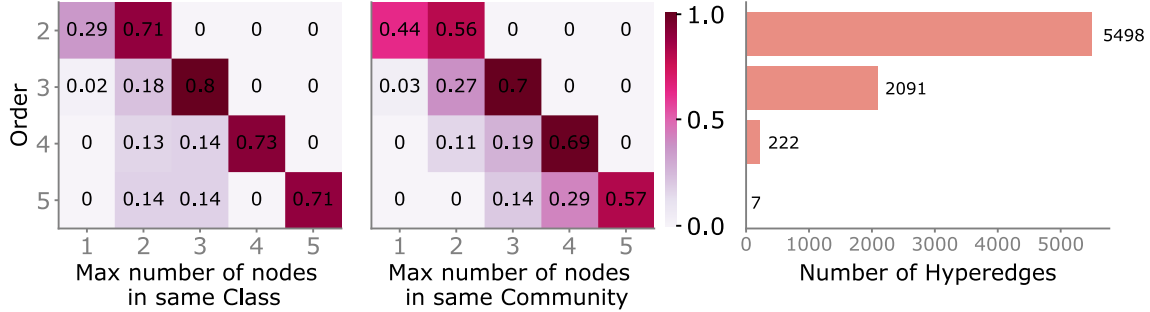


Figure 6: **Hyperedge distributions in the high school data.** The distribution of hyperedges by the maximum number of nodes in the same school class (left panel) and maximum number of nodes in the same detected community (middle panel). The frequency of hyperedges of each order (right panel).

contains a significant proportion of students from all the other classes.

One might be tempted to attribute this deviation from class structure and previous results on dyadic networks as a failure of our method. However, it is important to consider that there may be multiple valid ways to partition the nodes in empirical data [31], and that we should expect a different community structure to emerge when we consider higher-order interactions. To better understand the composition of these hypergraph communities, we analyze the distribution of hyperedges across communities in terms of their order and shape. Figure 6 compares these distributions between the classes and the detected communities. The analysis revealed that the detected communities are not formed by simply increasing the proportion of higher-order homogeneous intra-community hyperedges, in which all nodes belong to the same community. Instead, we observe a general tendency to prefer homogeneous *as well as* the more imbalanced hyperedges that connect a larger number of nodes within the same community. The fact that higher-order hyperedges are not always favored within communities is explained by much larger proportion of lower-order hyperedges in the data (see right panel of Figure 6). These results align with our earlier findings on the preference for imbalanced and higher-order hyperedges in planted community structures.

User reviews of businesses

Finally, we apply our method for spectral hypergraph clustering with the Bethe Hessian to the Yelp dataset. Here, we determine the number of communities according to the number of negative eigenvalues of $\mathbf{B}\mathbf{H}_\eta$, resulting in the identification of 615 communities. Figure 7(inset) presents a confusion matrix between the detected communities and the states in which the businesses are located; for clarity, we merge communities primarily composed of businesses from the same state. We see that most of these communities predominantly consist of businesses located within a single state, except community 0 that

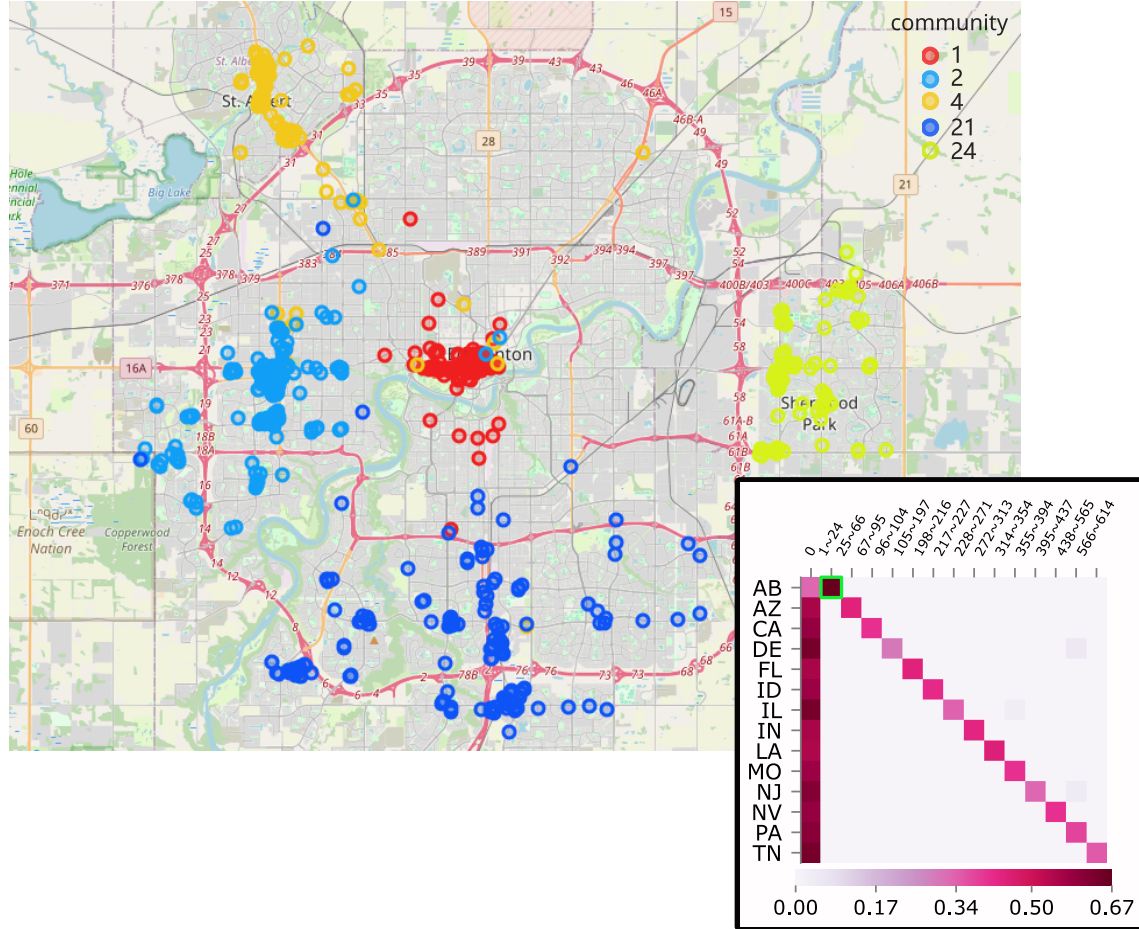


Figure 7: *Geographical distribution of detected communities in the Yelp data.* The bottom right corner is the confusion matrix of communities detected by Bethe Hessian-based spectral clustering with state metadata for yelp data. We highlight some communities composed of business in the Alberta province (AB) and show their geographical distribution.

includes businesses across all states because these businesses are reviewed by users who review businesses across multiple states. We also find geographical organization within states, indicating a hierarchical community structure [30] that corresponds to different resolutions of geographical regions. Figure 7 shows the geographical distribution of businesses in some of the detected communities in the Alberta province in Canada. We see that community 1 is mainly located in the central region of Edmonton, community 2 is in the western region, community 21 is in the southern region, community 24 is in Sherwood Park, and community 4 is in St. Albert.

Discussion

Community detection in hypergraphs presents fundamental challenges that have no direct analogue in dyadic networks. While pairwise networks exhibit a relatively simple trade-off between within- and across-community edge densities, hypergraphs introduce structural heterogeneity through hyperedges of varying orders that can split across communities in multiple configurations. Existing approaches to hypergraph community detection have largely overlooked a critical question: when hyperedges of different orders coexist and can be partitioned across communities in different ways, which structures are preferentially preserved by inference algorithms, and what are the implications for interpreting detected communities? This work provides the first systematic characterization of these higher-order trade-offs, introducing a unified framework for understanding how hyperedge order and splitting shape fundamentally determine what community structure can be detected.

Our main theoretical contributions are a generalized signal-to-noise ratio that quantifies the detectability of communities in hypergraphs for arbitrary mixtures of hyperedge orders and shapes, and a corresponding Bethe Hessian operator for non-uniform hypergraphs that enables efficient spectral clustering. Critically, this SNR framework reveals that the relative detectability of different community partitions depends not only on which hyperedge orders we choose to split across communities, but also on how we split them—a trade-off unique to higher-order networks that has not been considered before. We show that spectral methods exhibit systematic biases toward preserving higher-order hyperedges and those with more balanced shapes within the same community, even when alternative partitions are equally or more strongly supported by lower-order interactions. This finding has direct implications for interpreting communities in real-world hypergraphs: detected partitions reflect not just edge density, but also the order and shape preferences inherent in the detection method. Through comparison with general theoretical limits, we establish that spectral methods based on the Bethe Hessian achieve optimal detectability for uniform hypergraphs but exhibit a weaker threshold in non-uniform settings. Our synthetic experiments confirm these analytical predictions, while empirical applications demonstrate the practical relevance of these order and shape preferences: we recover known structure in human contact networks while revealing alternative organizational patterns that align with preferences for specific hyperedge configurations, and successfully identify hierarchical geographical communities in large-scale data with over 150,000 nodes and hyperedge orders exceeding 3,000.

While we frame these results in terms of hypergraphs, they apply equally to community detection in bipartite graphs, where hypergraphs can be represented via their incidence structure and hyperedge orders correspond to the degrees of one mode. However, the hypergraph perspective provides a more natural lens for understanding these trade-offs, as the notions of order and splitting shape emerge directly from the multiway interaction structure rather than indirectly through degree heterogeneity in one mode of a bipartite network. The connection between hyperedge orders and node degrees in bipartite graphs

suggests that our framework may open new directions for defining detectability limits in degree-heterogeneous networks, a problem that has only been considered in graphs for the restricted cases of two communities [32] or when community structure correlates with degree [33].

Several directions warrant further investigation. First, our current framework assumes homogeneous degree and order distributions within communities. Extending the Bethe Hessian to incorporate degree and order heterogeneity, analogous to degree-corrected models for dyadic networks [34], would broaden applicability to real-world systems. However, beyond developing such extensions, it remains an open empirical question whether degree and order correction are as relevant for hypergraph community detection as degree correction has proven to be for dyadic networks. Second, while our analysis focuses on assortative community structure, disassortative structures in hypergraphs are less straightforward to characterize than in graphs. How should we define disassortativity when hyperedges can split across communities in different shapes? The notion of hyperedge shape introduced here may provide a natural lens for addressing this question, as different splitting patterns could encode various forms of disassortative organization. Finally, rigorous proofs of our conjectured detectability thresholds and signal-to-noise ratio characterizations remain an important theoretical challenge, as does developing spectral methods that close the gap between the spectral and overall theoretical limits in non-uniform settings.

Acknowledgments

JL acknowledges the financial support from the China Scholarship Council under grant number 202106380033. MTS acknowledges support from the European Union (ERC, HIGH-HOPeS, 101039827). Views and opinions expressed are however those of the author(s) only and do not necessarily reflect those of the European Union or the European Research Council Executive Agency. Neither the European Union nor the granting authority can be held responsible for them. LP was supported in part by the Dutch Research Council (NWO) Talent Programme ENW-Vidi 2021 under grant number VI.Vidi.213.163.

References

- [1] S. Fortunato. “Community detection in graphs”. In: *Physics reports* 486.3-5 (2010), pp. 75–174.
- [2] M. A. Porter, J.-P. Onnela, P. J. Mucha, et al. “Communities in networks”. In: (2009).
- [3] V. D. Blondel et al. “Fast unfolding of communities in large networks”. In: *Journal of statistical mechanics: theory and experiment* 2008.10 (2008), P10008.

- [4] U. Von Luxburg. “A tutorial on spectral clustering”. In: *Statistics and computing* 17.4 (2007), pp. 395–416.
- [5] P. W. Holland, K. B. Laskey, and S. Leinhardt. “Stochastic blockmodels: First steps”. In: *Social networks* 5.2 (1983), pp. 109–137.
- [6] A. Decelle et al. “Asymptotic analysis of the stochastic block model for modular networks and its algorithmic applications”. In: *Physical Review E—Statistical, Nonlinear, and Soft Matter Physics* 84.6 (2011), p. 066106.
- [7] F. Krzakala et al. “Spectral redemption in clustering sparse networks”. In: *Proceedings of the National Academy of Sciences* 110.52 (2013), pp. 20935–20940.
- [8] A. Saade, F. Krzakala, and L. Zdeborová. “Spectral clustering of graphs with the bethe hessian”. In: *Advances in neural information processing systems* 27 (2014).
- [9] C. Bick et al. “What are higher-order networks?” In: *SIAM review* 65.3 (2023), pp. 686–731.
- [10] M. Newman. *Networks*. Oxford university press, 2018.
- [11] A. Sanchez-Gorostiaga et al. “High-order interactions distort the functional landscape of microbial consortia”. In: *PLoS biology* 17.12 (2019), e3000550.
- [12] F. Battiston et al. “Networks beyond pairwise interactions: Structure and dynamics”. In: *Physics reports* 874 (2020), pp. 1–92.
- [13] F. Battiston et al. “The physics of higher-order interactions in complex systems”. In: *Nature physics* 17.10 (2021), pp. 1093–1098.
- [14] P. S. Chodrow, N. Veldt, and A. R. Benson. “Generative hypergraph clustering: From blockmodels to modularity”. In: *Science Advances* 7.28 (2021), eabh1303.
- [15] D. Ghoshdastidar and A. Dukkipati. “Consistency of spectral hypergraph partitioning under planted partition model”. In: (2017).
- [16] P. Chodrow, N. Eikmeier, and J. Haddock. “Nonbacktracking spectral clustering of nonuniform hypergraphs”. In: *SIAM Journal on Mathematics of Data Science* 5.2 (2023), pp. 251–279.
- [17] M. C. Angelini et al. “Spectral detection on sparse hypergraphs”. In: *2015 53rd Annual Allerton Conference on Communication, Control, and Computing (Allerton)*. IEEE. 2015, pp. 66–73.
- [18] N. Ruggeri, A. Lonardi, and C. De Bacco. “Message-passing on hypergraphs: detectability, phase transitions and higher-order information”. In: *Journal of Statistical Mechanics: Theory and Experiment* 2024.4 (2024), p. 043403.
- [19] L. Stephan and Y. Zhu. “Sparse random hypergraphs: Non-backtracking spectra and community detection”. In: *Information and Inference: A Journal of the IMA* 13.1 (2024), iaae004.

[20] D. Ghoshdastidar and A. Dukkipati. “Consistency of spectral partitioning of uniform hypergraphs under planted partition model”. In: *Advances in Neural Information Processing Systems* 27 (2014).

[21] E. Mossel, J. Neeman, and A. Sly. “Reconstruction and estimation in the planted partition model”. In: *Probability Theory and Related Fields* 162.3 (2015), pp. 431–461.

[22] L. Massoulié. “Community detection thresholds and the weak Ramanujan property”. In: *Proceedings of the forty-sixth annual ACM symposium on Theory of computing*. 2014, pp. 694–703.

[23] E. Abbe. “Community detection and stochastic block models: recent developments”. In: *Journal of Machine Learning Research* 18.177 (2018), pp. 1–86.

[24] N. X. Vinh, J. Epps, and J. Bailey. “Information theoretic measures for clusterings comparison: is a correction for chance necessary?” In: *Proceedings of the 26th annual international conference on machine learning*. 2009, pp. 1073–1080.

[25] L. Peel and M. T. Schaub. “Detectability of hierarchical communities in networks”. In: *Physical Review E* 110.3 (2024), p. 034306.

[26] J. Stehlé et al. “High-resolution measurements of face-to-face contact patterns in a primary school”. In: *PLoS one* 6.8 (2011), e23176.

[27] R. Mastrandrea, J. Fournet, and A. Barrat. “Contact Patterns in a High School: A Comparison between Data Collected Using Wearable Sensors, Contact Diaries and Friendship Surveys”. In: *PLOS ONE* 10.9 (2015). Ed. by C. Viboud, e0136497. DOI: 10.1371/journal.pone.0136497. URL: <https://doi.org/10.1371/journal.pone.0136497>.

[28] URL: <https://www.yelp.com/dataset>.

[29] N. Tremblay and P. Borgnat. “Graph wavelets for multiscale community mining”. In: *IEEE Transactions on Signal Processing* 62.20 (2014), pp. 5227–5239.

[30] M. T. Schaub, J. Li, and L. Peel. “Hierarchical community structure in networks”. In: *Physical Review E* 107.5 (2023), p. 054305.

[31] L. Peel, D. B. Larremore, and A. Clauset. “The ground truth about metadata and community detection in networks”. In: *Science advances* 3.5 (2017), e1602548.

[32] F. Radicchi. “Detectability of communities in heterogeneous networks”. In: *Phys. Rev. E* 88 (1 2013), p. 010801. DOI: 10.1103/PhysRevE.88.010801.

[33] P. Zhang, C. Moore, and M. Newman. “Community detection in networks with unequal groups”. In: *Physical review E* 93.1 (2016), p. 012303.

[34] L. Dall’Amico, R. Couillet, and N. Tremblay. “Revisiting the bethe-hessian: improved community detection in sparse heterogeneous graphs”. In: *Advances in neural information processing systems* 32 (2019).

- [35] P. Erdős and A. Rényi. “On random graphs I”. In: *Publ. math. debrecen* 6.290-297 (1959), p. 18.
- [36] C. Moore et al. “The Computer Science and Physics of Community Detection: Landscapes, Phase Transitions, and Hardness”. In: *Bulletin of EATCS* 1.121 (2017).
- [37] A. Saade. “Spectral inference methods on sparse graphs: theory and applications”. In: *arXiv preprint arXiv:1610.04337* (2016).
- [38] G. H. Golub and C. F. Van Loan. *Matrix computations*. JHU press, 2013.
- [39] M. Mezard and A. Montanari. *Information, physics, and computation*. Oxford University Press, 2009.

A Detectability limit and the Bethe Hessian for dyadic networks

In this section, we first introduce the Stochastic Block Model, a generative model for networks with community structure. Then we review the non-backtracking matrix and Bethe Hessian matrix used for spectral clustering. Lastly, we briefly review the detectability limit of SBM.

A.1 The stochastic block model

We consider an unweighted, undirected dyadic network G_A with node set \mathcal{V} and edge set \mathcal{E} , where the number of nodes $|\mathcal{V}| = n$, number of edges $|\mathcal{E}| = m$, such that G_A can be represented as an adjacency matrix $\mathbf{A} \in \{0, 1\}^{n \times n}$. For any two nodes $i, j \in \mathcal{V}$, \mathbf{A} is defined as

$$\mathbf{A} = \begin{cases} 1 & \text{if } (i, j) \in \mathcal{E} \\ 0 & \text{otherwise} \end{cases}. \quad (14)$$

The degree of any node is defined by the number of edges connected to that node. For a node i , its degree d_i is

$$d_i = \sum_{j \in \mathcal{V}} \mathbf{A}_{ij} , \quad (15)$$

and the average degree of whole network as d , then

$$d = \frac{\sum_{i \in \mathcal{V}} d_i}{n} = \frac{2m}{n} . \quad (16)$$

We can use the SBM to generate network G_A with q communities. We assign each node $i \in \mathcal{V}$ a community label $\psi_i \in \{1, 2, \dots, q\}$. Let matrix Ω be the edge probability matrix, $\Omega \in [0, 1]^{q \times q}$. For each pair of nodes $i, j \in \mathcal{V}$, we generate an edge (i, j) with probability $\Omega_{\psi_i \psi_j}$. We assume the network G_A is sparse based on the observation that many empirical networks tend to have constant average degree relative to the network size. This sparsity implies that $m \sim O(n)$ and we can assume the matrix Ω has the form

$$\Omega = \frac{\mathbf{C}}{n} , \quad (17)$$

where \mathbf{C} is a matrix that is constant as we vary n .

A common variant of the SBM is the symmetric stochastic block model. The symmetric SBM assumes that all q communities have the same number of nodes and the matrix Ω is composed of two distinct probabilities: intra-community edge probability p_{in} and inter-community edge probability p_{out} . If nodes i and j belong to same community, $\psi_i = \psi_j$, then $\Omega_{\psi_i \psi_j} = p_{\text{in}}$, otherwise $\Omega_{\psi_i \psi_j} = p_{\text{out}}$. Similarly, the rescaled edge probability matrix $\mathbf{C} = n\Omega$ also has two distinct values: $c_{\text{in}} = np_{\text{in}}$, $c_{\text{out}} = np_{\text{out}}$.

A.2 Detectability limit of community structure in networks

The goal of community detection is to infer the community labels ψ based solely on observing the network G_A . A community structure is said to be detectable if there exists an algorithm that can infer the community labels better than random guessing. The detectability of community structure is related to the parameters of the SBM used to generate the network, specifically the differences in edge densities within and between communities. For instance, if $c_{\text{in}} = c_{\text{out}}$, the network is essentially an Erdős–Rényi random graph [35] without any community structure, making it impossible to detect communities. Conversely, when c_{in} is significantly larger than c_{out} , the communities are more densely connected internally than externally, making them easier to detect. If a community detection algorithm can detect ψ better than random guessing within polynomial time complexity, then the community structure is said to be detectable [23]. This detectability threshold coincides with the Kesten–Stigum threshold [6, 36]. Below the detectability threshold, no algorithm can perform better than random guessing, and the community structure is said to be undetectable.

For the symmetric SBM, the theoretical detectability threshold occurs when

$$|c_{\text{in}} - c_{\text{out}}| > q\sqrt{d} , \quad (18)$$

where the average degree $d = \frac{c_{\text{in}} + (q-1)c_{\text{out}}}{q}$. With a little transformation, we can obtain the threshold:

$$\text{SNR} := \frac{(c_{\text{in}} - c_{\text{out}})^2}{q^2 d} > 1 , \quad (19)$$

where SNR is the signal-to-noise ratio. So for any network G_A generated by the symmetric SBM, if $\text{SNR} > 1$, the community structure in G_A is considered detectable.

To see the SNR for general SBM [23], we first define the matrix \mathbf{N} which is a $(q \times q)$ -dimension diagonal matrix, with diagonal entries equal to the number of nodes in each community. Ordering the non-decreasing magnitude eigenvalues of matrix $\mathbf{N}\Omega$ as $\lambda_1, \lambda_2, \dots$, the general SNR is defined as

$$\text{SNR} = \frac{\lambda_2^2}{\lambda_1} , \quad (20)$$

which is equivalent to the SNR (19) above for the symmetric SBM.

A.3 The non-backtracking matrix and Bethe Hessian for dyadic networks

Spectral clustering using the non-backtracking matrix is an effective community detection method that is consistent with inference on the SBM. The non-backtracking matrix is a linearization of the belief propagation algorithm (BP), an approximate inference algorithm for the SBM. The BP can detect community structure with asymptotically optimal

accuracy [6]. The Bethe Hessian matrix is a compact formulation of the non-backtracking matrix that shares the same properties of detectability of the non-backtracking matrix [8].

The non-backtracking matrix \mathbf{NB} of a network is a matrix of dimension $2m \times 2m$ such that each row and column corresponds to a directed edge in the network. Note that the non-backtracking matrix is defined on directed edges, so in the case of an undirected network, each edge (i, j) is represented as two directed edges $i \rightarrow j$ and $j \rightarrow i$. Thus, for a network with m undirected edges, there are $2m$ directed edges in total. For the directed edges $i \rightarrow j$ and $k \rightarrow l$ in the network, the entry of the non-backtracking matrix $\mathbf{NB}_{i \rightarrow j, k \rightarrow l}$ is defined as

$$\mathbf{NB}_{i \rightarrow j, k \rightarrow l} = \begin{cases} 1 & j \neq k \text{ and } i = l \\ 0 & \text{otherwise} \end{cases}. \quad (21)$$

Following the standard approach to spectral clustering, we compute the first q eigenvectors $\mathbf{V}_q = [\boldsymbol{\nu}_{\cdot,1}, \boldsymbol{\nu}_{\cdot,2}, \dots, \boldsymbol{\nu}_{\cdot,q}]$ of the non-backtracking matrix \mathbf{NB} corresponding to the leading q eigenvalues. These eigenvectors are then used to cluster the nodes in the network into q communities. Since we are interested in clustering the n nodes of the network, rather than the $2m$ directed edges, the clustering is performed by first pooling the $2m$ -length eigenvectors of \mathbf{NB} into vectors of length n . This operation is performed using a pooling matrix which aggregate relevant components of the eigenvectors for each node. The pooling matrix \mathbf{P} is defined as follows:

$$\mathbf{P}_{i,k \rightarrow l} = \begin{cases} 1 & i = l \text{ and } k \in \partial i \\ 0 & \text{otherwise} \end{cases}, \quad (22)$$

where ∂i is the set of directed edges that point to node i . The pooling matrix \mathbf{P} effectively selects the components of the eigenvectors that correspond to the directed edges pointing to each node. The spectral clustering of the network is then performed by applying a clustering algorithm, such as k-means, to the rows of the pooled matrix $\mathbf{U}_q = \mathbf{P}\mathbf{V}_q$. The clustering algorithm groups the nodes based on the pooled eigenvectors, resulting in a partition of the nodes into q communities.

The construction and eigen-decomposition of the non-backtracking matrix can be expensive in terms of time and memory, especially for large networks. A better alternative is to construct the Bethe Hessian that has eigenvectors that correspond to the pooled eigenvectors $\mathbf{U} = [\boldsymbol{\mu}_{\cdot,1}, \boldsymbol{\mu}_{\cdot,2}, \dots, \boldsymbol{\mu}_{\cdot,n}]$. The Bethe Hessian is defined as

$$\mathbf{B}_\eta = (\eta^2 - 1)\mathbf{I} - \eta\mathbf{A} + \mathbf{D}, \quad (23)$$

where \mathbf{I} is identity matrix, \mathbf{D} is diagonal matrix of node degrees, η is a regularization parameter, which typically works well with the setting $\eta = \sqrt{d}$.

The Bethe Hessian can be derived from non-backtracking matrix [7, 37]. To see how, we start with the eigen decomposition of the non-backtracking matrix $\mathbf{NB} \cdot \mathbf{V} = \mathbf{\Lambda} \cdot \mathbf{V}$

(where Λ is the diagonal matrix of eigenvalues) and consider in terms of a specific directed edge $i \rightarrow j$:

$$\lambda \boldsymbol{\nu}_{i \rightarrow j} = \sum_{k \in \partial i / j} \boldsymbol{\nu}_{k \rightarrow i} , \quad (24)$$

and notice that the pooling operation $\boldsymbol{\mu} \mathbf{P} = \boldsymbol{\nu}$ can be expressed in terms of equation (24) and an additional term $\boldsymbol{\nu}_{j \rightarrow i}$,

$$\boldsymbol{\mu}_i = \sum_{k \in \partial i} \boldsymbol{\nu}_{k \rightarrow i} \quad (25)$$

$$= \sum_{k \in \partial i / j} \boldsymbol{\nu}_{k \rightarrow i} + \boldsymbol{\nu}_{j \rightarrow i} \quad (26)$$

$$= \lambda \boldsymbol{\nu}_{i \rightarrow j} + \boldsymbol{\nu}_{j \rightarrow i} . \quad (27)$$

Similarly for node j , we have:

$$\boldsymbol{\mu}_j = \lambda \boldsymbol{\nu}_{j \rightarrow i} + \boldsymbol{\nu}_{i \rightarrow j} , \quad (28)$$

then we can subtract $\boldsymbol{\mu}_i - \lambda \boldsymbol{\mu}_j$ to eliminate $\boldsymbol{\nu}_{i \rightarrow j}$:

$$\boldsymbol{\mu}_i - \lambda \boldsymbol{\mu}_j = \boldsymbol{\nu}_{j \rightarrow i} - \lambda^2 \boldsymbol{\nu}_{j \rightarrow i} , \quad (29)$$

and rearrange to get

$$\boldsymbol{\nu}_{j \rightarrow i} = \frac{\boldsymbol{\mu}_i - \lambda \boldsymbol{\mu}_j}{1 - \lambda^2} . \quad (30)$$

Substitute $\boldsymbol{\nu}_{j \rightarrow i}$ from equation (30) above into equation (25) and we get:

$$\boldsymbol{\mu}_i = \sum_{k \in \partial i} \frac{\boldsymbol{\mu}_i - \lambda \boldsymbol{\mu}_k}{1 - \lambda^2} \quad (31)$$

$$\boldsymbol{\mu}_i = d_i \frac{\boldsymbol{\mu}_i}{1 - \lambda^2} - \frac{\lambda}{1 - \lambda^2} \sum_{k \in \partial i} \boldsymbol{\mu}_k \quad (32)$$

$$(1 - \frac{d_i}{1 - \lambda^2}) \boldsymbol{\mu}_i + \frac{\lambda}{1 - \lambda^2} \sum_{k \in \partial i} \boldsymbol{\mu}_k = 0 \quad (33)$$

$$\frac{1}{\lambda^2 - 1} \left[(\lambda^2 - 1 + d_i) \boldsymbol{\mu}_i - \lambda \sum_{k \in \partial i} \boldsymbol{\mu}_k \right] = 0 . \quad (34)$$

Omitting the term $1/(\lambda^2 - 1)$, we have the matrix form:

$$[(\lambda^2 - 1) \mathbf{I} + \mathbf{D} - \lambda \mathbf{A}] \boldsymbol{\mu} = 0 \quad (35)$$

$$\mathbf{B}_\lambda \boldsymbol{\mu} = 0 , \quad (36)$$

where \mathbf{B}_λ is the Bethe Hessian matrix with regularization parameter $\eta = \lambda$.

From equation (35) we can conclude that $\boldsymbol{\mu}$ is related with null space of \mathbf{B}_λ . In other words, if we set the regularization parameter $\eta = \lambda$ to an eigenvalue of \mathbf{NB} , then $\boldsymbol{\mu}$ will be an eigenvector of \mathbf{B}_λ corresponding with eigenvalue 0. Note that although the above relationship does not hold when the parameter η is not an eigenvalue of \mathbf{NB} , the eigenvector of $\mathbf{B}_{\sqrt{d}}$ is still found to be a good approximation of $\boldsymbol{\mu}$ in practice [37].

Figure 8 gives an example spectrum of \mathbf{NB} and \mathbf{B}_η for a network generated by the symmetric SBM. The blue points in the plot above represent the eigenvalues of the non-backtracking matrix \mathbf{NB} and the light blue circle with radius \sqrt{d} indicates approximately the uninformative bulk within which most of the eigenvalues lie. The red to green points in the plot below represent the eigenvalues of the Bethe Hessian matrix \mathbf{B}_η for corresponding values of η . When η is set to one of the real informative eigenvalues of \mathbf{NB} , the corresponding eigenvector $\boldsymbol{\mu}$ can be used to optimally cluster the nodes in the network [34].

When the communities are detectable, there are a few informative real eigenvalues outside the bulk, which correspond to the number of communities in the network. We see that when η is sufficiently large, all eigenvalues of \mathbf{B}_η are positive. As η decreases, new negative eigenvalues appear each time η crosses a real informative eigenvalue of \mathbf{NB} . Consequently, when η is equal to the radius of the uninformative bulk, the number of negative eigenvalues of \mathbf{B}_η can also be used to determine the number of communities in the network. The eigenvectors corresponding with these negative eigenvalues can be used as a good approximation of $\boldsymbol{\mu}$ corresponding with the informative eigenvalues of \mathbf{NB} . The exact set of eigenvectors \mathbf{U}_q can be obtained by identifying the leading eigenvector of the Bethe Hessian matrix \mathbf{B}_η with η set to the each of the q informative eigenvalues of \mathbf{NB} .

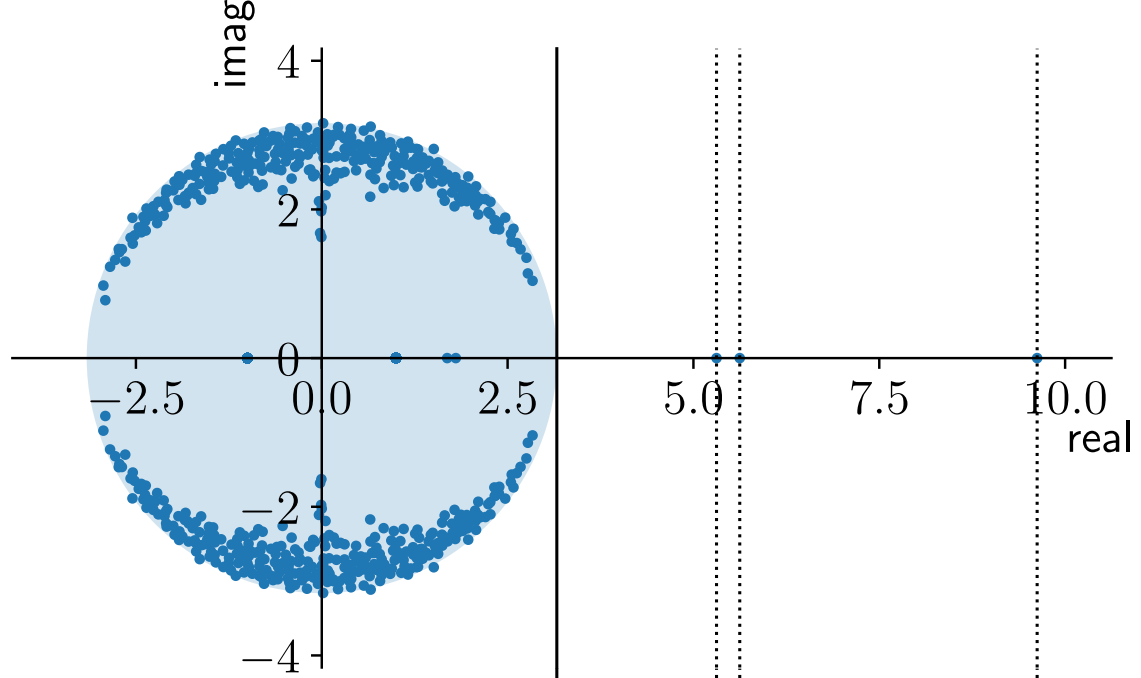
B Spectral clustering for hypergraphs

In this section, we first introduce the non-backtracking matrix for hypergraphs. Then we use this non-backtracking matrix to derive the Bethe Hessian for uniform hypergraphs and non-uniform hypergraphs.

B.1 The non-backtracking matrix for hypergraphs

The uniform hypergraph non-backtracking matrix [17] is a generalization of the non-backtracking matrix for dyadic networks [7]. Similar to the non-backtracking matrix for dyadic networks, the non-backtracking matrix for hypergraphs is defined on directed hyperedges. These directed hyperedges are simply defined from undirected hyperedges such that each node i in hyperedge e induces a directed hyperedge $i \rightarrow e$. Consequently, each undirected hyperedge of size κ induces κ directed hyperedges. The non-backtracking

(a) Spectrum of NB



(b) Spectrum of B_η

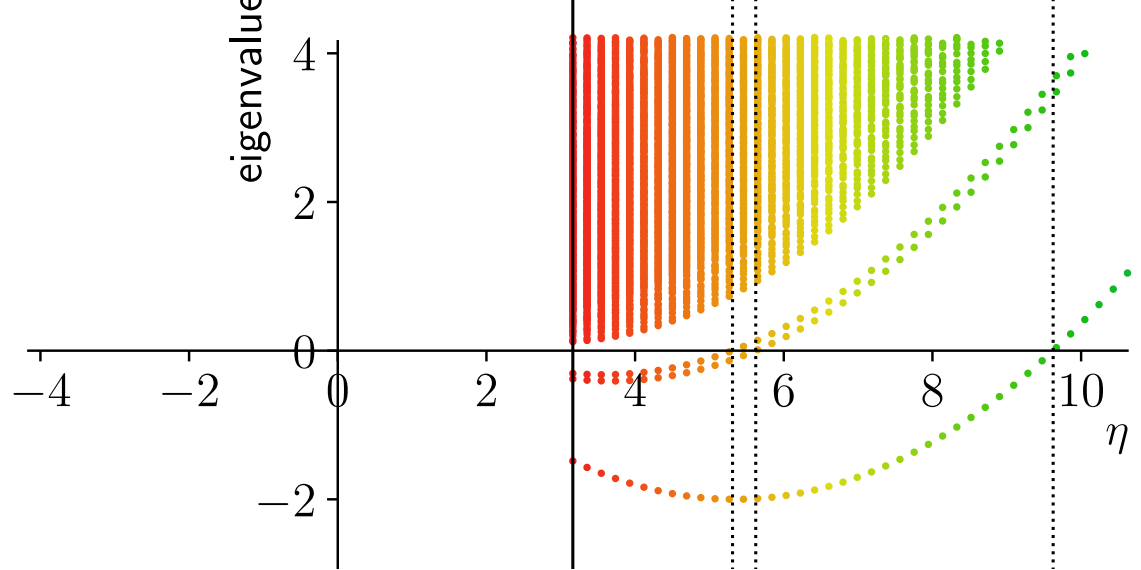


Figure 8: The spectrum of non-backtracking matrix (a) and Bethe Hessian matrix (b) for a network generate by symmetric SBM. The number of nodes $n = 300$, number of communities $q = 3$, average degree $d = 10$, edge probability ratio $p_{\text{out}}/p_{\text{in}} = 0.2$. The light blue circle is the bulk with radius \sqrt{d} . Each column of red to green points in (b) is the spectrum of B_η where η is x -axis value. Here the spectrum of B_η is scaled for better presenting.

matrix, $\mathbf{NB}^{(\kappa)}$, of a κ -uniform hypergraph is defined as follows. For two κ -hyperedges e_1 and e_2 , if $i \in e_1$ and $j \in e_2$, the non-backtracking matrix is given by

$$\mathbf{NB}_{i \rightarrow e_1, j \rightarrow e_2}^{(\kappa)} = \begin{cases} 1 & j \in e_1/i \text{ and } e_2 \neq e_1 \\ 0 & \text{otherwise} \end{cases}, \quad (37)$$

where $i \rightarrow e_1$ is a directed hyperedge [16] if node i is in hyperedge e_1 . Since each node in a hyperedge induces a directed hyperedge in the non-backtracking matrix, the dimension of the non-backtracking matrix is equal to the total sum of node-degrees, $\sum_i d_i$, which is equal to κm in the case of a κ -uniform hypergraph.

The non-backtracking matrix for a non-uniform hypergraph [16] is constructed in the same way, however, we can order the rows and columns by the order of the hyperedges,

$$\mathbf{NB}^{(\kappa)} = \begin{bmatrix} \mathbf{NB}^{(2 \rightarrow 2)} & \mathbf{NB}^{(2 \rightarrow 3)} & \dots & \mathbf{NB}^{(2 \rightarrow \kappa)} \\ \mathbf{NB}^{(3 \rightarrow 2)} & \mathbf{NB}^{(3 \rightarrow 3)} & \dots & \mathbf{NB}^{(3 \rightarrow \kappa)} \\ \dots & \dots & \dots & \dots \\ \mathbf{NB}^{(\kappa \rightarrow 2)} & \mathbf{NB}^{(\kappa \rightarrow 3)} & \dots & \mathbf{NB}^{(\kappa \rightarrow \kappa)} \end{bmatrix}, \quad (38)$$

where $\mathbf{NB}^{(\kappa' \rightarrow \kappa)}$ is the non-backtracking matrix from the κ' -hyperedges, $\mathcal{E}^{(\kappa')}$ to the κ -hyperedges, $\mathcal{E}^{(\kappa)}$. The dimension of each $\mathbf{NB}^{(\kappa' \rightarrow \kappa)}$ is $\kappa' m^{(\kappa')} \times \kappa m^{(\kappa)}$.

The leading q eigenvectors of the non-backtracking matrix can be used to perform spectral clustering. Since we are interested in clustering the nodes in the network, we can “pool” the eigenvectors to an n -dimensional vector $\boldsymbol{\mu}$,

$$\boldsymbol{\mu}_i = \sum_{\kappa \in \mathcal{K}} \sum_{e \in \partial_{\kappa} i} \boldsymbol{\nu}_{i \rightarrow e}, \quad (39)$$

and use the pooled vectors $\boldsymbol{\mu}$ as the input to a clustering algorithm, e.g., k-means.

B.2 The Bethe Hessian for hypergraphs

The construction and eigen decomposition of the non-backtracking matrix is computationally intensive in terms of time and space resources, especially for large hypergraphs. For dyadic networks, the Bethe Hessian [8] is a lower-dimensional symmetric matrix that captures the same desirable spectral properties of the non-backtracking matrix that makes it effective for spectral clustering. The Bethe Hessian has previously been extended for hypergraphs [19], but is only applicable if the hypergraph is uniform. Here we present a new version of the Bethe Hessian that is suitable for non-uniform hypergraphs, following a similar derivation as in the dyadic case (see Appendix A).

We consider an informative eigenvector $\boldsymbol{\nu}$ and corresponding eigenvalue λ of the non-backtracking matrix $\mathbf{NB}^{(\kappa)}$, such that $\mathbf{NB}^{(\kappa)} \boldsymbol{\nu} = \lambda \boldsymbol{\nu}$. For a given directed hyperedge $i \rightarrow e_1$, we expand the eigenvalue equation,

$$\lambda \boldsymbol{\nu}_{i \rightarrow e_1} = \sum_{\kappa \in \mathcal{K}} \sum_{j \in e_1 / i} \sum_{e_2 \in \partial_{\kappa} j / e_1} \boldsymbol{\nu}_{j \rightarrow e_2}, \quad (40)$$

where $\partial_\kappa j$ is all κ -hyperedges including j . We can reorder the sum in equation (40) and substitute in the pooled vector $\boldsymbol{\mu}$ from (39):

$$\lambda \boldsymbol{\nu}_{i \rightarrow e_1} = \sum_{j \in e_1 / i} \sum_{\kappa \in \mathcal{K}} \sum_{e_2 \in \partial_\kappa j / e_1} \boldsymbol{\nu}_{j \rightarrow e_2} \quad (41)$$

$$= \sum_{j \in e_1 / i} \left(\sum_{\kappa \in \mathcal{K}} \sum_{e_2 \in \partial_\kappa j} \boldsymbol{\nu}_{j \rightarrow e_2} - \boldsymbol{\nu}_{j \rightarrow e_1} \right) \quad (42)$$

$$= \sum_{j \in e_1 / i} (\boldsymbol{\mu}_j - \boldsymbol{\nu}_{j \rightarrow e_1}) \quad (43)$$

$$\lambda \boldsymbol{\nu}_{i \rightarrow e_1} + \sum_{j \in e_1 / i} \boldsymbol{\nu}_{j \rightarrow e_1} = \sum_{j \in e_1 / i} \boldsymbol{\mu}_j . \quad (44)$$

Note that equation (44) above repeats κ times, once for each node $i \in e_1$ if e_1 is a κ -hyperedge. Summing over all of nodes in e_1 , we get:

$$(\lambda + \kappa - 1) \sum_{i \in e_1} \boldsymbol{\nu}_{i \rightarrow e_1} = (\kappa - 1) \sum_{j \in e_1} \boldsymbol{\mu}_j , \quad (45)$$

then dividing by $(\lambda + \kappa - 1)$ and subtracting (44),

$$(1 - \lambda) \boldsymbol{\nu}_{i \rightarrow e_1} = \frac{\kappa - 1}{\lambda + \kappa - 1} \boldsymbol{\mu}_i - \frac{\lambda}{\lambda + \kappa - 1} \sum_{j \in e_1 / i} \boldsymbol{\mu}_j \quad (46)$$

$$\boldsymbol{\nu}_{i \rightarrow e_1} = \frac{\kappa - 1}{(1 - \lambda)(\lambda + \kappa - 1)} \boldsymbol{\mu}_i - \frac{\lambda}{(1 - \lambda)(\lambda + \kappa - 1)} \sum_{j \in e_1 / i} \boldsymbol{\mu}_j . \quad (47)$$

Now we substitute the above definition of $\boldsymbol{\nu}_{i \rightarrow e_1}$ into pooling equation (39),

$$\boldsymbol{\mu}_i = \sum_{\kappa \in \mathcal{K}} \sum_{e \in \partial_\kappa i} \left[\frac{\kappa - 1}{(1 - \lambda)(\lambda + \kappa - 1)} \boldsymbol{\mu}_i - \frac{\lambda}{(1 - \lambda)(\lambda + \kappa - 1)} \sum_{j \in e / i} \boldsymbol{\mu}_j \right] \quad (48)$$

$$= \sum_{\kappa \in \mathcal{K}} \frac{(\kappa - 1)d_i^{(\kappa)}}{(1 - \lambda)(\lambda + \kappa - 1)} \boldsymbol{\mu}_i - \lambda \sum_{\kappa \in \mathcal{K}} \sum_{e \in \partial_\kappa i} \sum_{j \in e / i} \frac{1}{(1 - \lambda)(\lambda + \kappa - 1)} \boldsymbol{\mu}_j , \quad (49)$$

where $d_i^{(\kappa)} = |\partial_\kappa i|$ is the κ -degree of i , i.e., the number of κ -hyperedges that i is included in. We can rearrange the above result to set the right-hand side to zero,

$$(1 - \sum_{\kappa \in \mathcal{K}} \frac{(\kappa - 1)d_i^{(\kappa)}}{(1 - \lambda)(\lambda + \kappa - 1)} \boldsymbol{\mu}_i + \lambda \sum_{\kappa \in \mathcal{K}} \sum_{e \in \partial_\kappa i} \sum_{j \in e / i} \frac{1}{(1 - \lambda)(\lambda + \kappa - 1)} \boldsymbol{\mu}_j) = 0 . \quad (50)$$

Finally, we can rewrite the above equation in matrix form, which is the Bethe Hessian matrix for non-uniform hypergraphs:

$$\mathbf{B}_\eta^{(\kappa)} = \mathbf{I} - \sum_{\kappa \in \mathcal{K}} \frac{(\kappa - 1)}{(1 - \eta)(\eta + \kappa - 1)} \mathbf{D}^{(\kappa)} + \sum_{\kappa \in \mathcal{K}} \frac{\eta}{(1 - \eta)(\eta + \kappa - 1)} \mathbf{A}^{(\kappa)} , \quad (51)$$

where η is a regularization parameter, $\mathbf{D}^{(\kappa)}$ is the diagonal degree matrix for κ -hyperedges, and $\mathbf{A}^{(\kappa)}$ is the one-mode projection matrix for κ -hyperedges, i.e.,

$$\mathbf{A}_{ij}^{(\kappa)} = \begin{cases} |\{e|i, j \in e, |e| = \kappa\}| & i \neq j \\ 0 & i = j \end{cases} . \quad (52)$$

Note that the matrix $\mathbf{A}^{(\kappa)}$ can also be expressed in terms of the κ -hyperedge incidence matrix $\mathbf{H}^{(\kappa)}$ as follows:

$$\mathbf{A}^{(\kappa)} = \mathbf{H}^{(\kappa)}(\mathbf{H}^{(\kappa)})^T - \text{diag}(\mathbf{H}^{(\kappa)}(\mathbf{H}^{(\kappa)})^T) . \quad (53)$$

B.3 The spectrum of Bethe Hessian matrix

The spectrum of Bethe Hessian relates to the spectrum of non-backtracking matrix such that the negative eigenvalues of Bethe Hessian correspond to the informative eigenvalues of non-backtracking matrix. Of particular importance to the task of detecting community structure is that we preserve the relationship between the eigenvectors. Specifically, when we take an informative eigenvalue λ and corresponding eigenvector $\boldsymbol{\nu}$ and set the regularization parameter $\eta = \lambda$, then the eigenvector associated with the eigenvalue 0 of the Bethe Hessian is the pooled vector $\boldsymbol{\mu}$.

Figure 9 provides an empirical demonstration of the relationship between the spectra of the non-backtracking matrix and the Bethe Hessian for two hypergraphs with $q = 2$ communities, generated using the HSBM described earlier. Figure 9(a, c) shows the κ -uniform case with $\kappa = 3$. The radius of the bulk of uninformative eigenvalues is $\sqrt{d(\kappa - 1)}$, where d is the average degree of the hypergraph. For the non-uniform case [Fig. 9(b, d)], we set $\mathcal{K} = \{2, 3, 4\}$. This time the radius of the bulk is $\sum_{\kappa \in \mathcal{K}} \sqrt{d^{(\kappa)}(\kappa - 1)}$, where $d^{(\kappa)}$ is the average degree of the κ -order hyperedges, $d^{(\kappa)} = \text{Tr}(\mathbf{D}^{(\kappa)})/n$.

Figure 9 shows the same relationship between the spectra of the non-backtracking matrix and Bethe Hessian that we see for dyadic networks in Figure 8. When parameter η is equal to the radius of uninformative bulk, then negative eigenvalues of \mathbf{B}_η correspond one-to-one with the real informative eigenvalues of $\mathbf{N}\mathbf{B}$. We can also use the eigenvectors corresponding with these negative eigenvalues of \mathbf{B}_η to perform spectral clustering, as described in Algorithm 1.

Algorithm 1 Spectral Clustering with Bethe Hessian

Input: incidence matrix \mathbf{H} , all possible hyperedge order \mathcal{K}
Output: communities labels $\vec{\psi}$

- 1: Compute $\eta = \sum_{\kappa \in \mathcal{K}} \sqrt{d^{(\kappa)}}(\kappa - 1)$
- 2: Compute \mathbf{B}_η by (2)
- 3: Compute spectral decomposition $\mathbf{B}_\eta = \mathbf{V} \Lambda \mathbf{V}^T$.
- 4: Compute $q = |\{\Lambda_{i,i} : \Lambda_{i,i} < 0\}|$.
- 5: Select first q eigenvectors of \mathbf{V} based on the increasing order of corresponding eigenvalues as \mathbf{W}_q .
- 6: Run k-means clustering on the rows of \mathbf{W}_q : $\vec{\psi} = k\text{-means}(\mathbf{W}_q^T, q)$
- 7: **return** $\vec{\psi}$

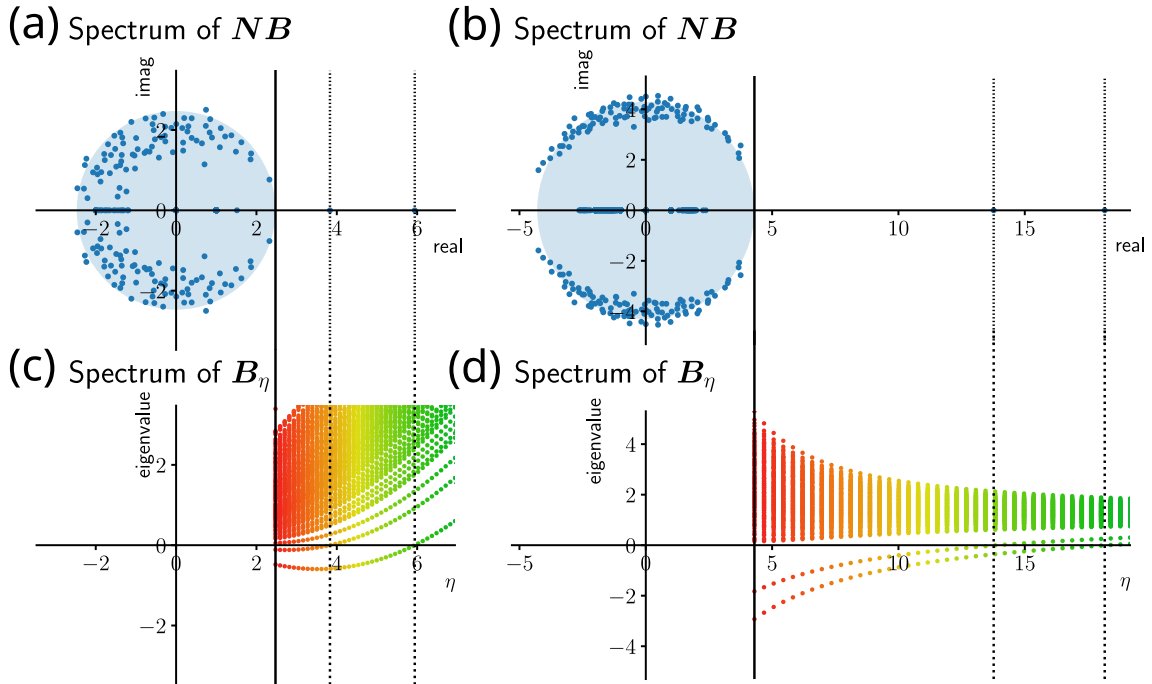


Figure 9: The spectrum of non-backtracking matrix (a, b) and Bethe Hessian matrix (c, d) for hypergraphs generated by $\kappa = 3$ uniform HSBM (a, c) and $\mathcal{K} = \{2, 3, 4\}$ nonuniform HSBM (b, d). In both settings, $n = 100$, $q = 2$ and degree parameters $d_{\text{in}} = 10$ and $d_{\text{out}} = 1$. The light blue circle is the uninformative bulk of \mathbf{NB} with radius $\sum_{\kappa \in \mathcal{K}} \sqrt{d^{(\kappa)}}(\kappa - 1)$.

C Time complexity comparison of spectral clustering operators

The computational cost of spectral clustering is primarily dominated by the eigen decomposition of the associated operator. For instance, when employing the Lanczos algorithm for eigen-decomposition [38], the time complexity is approximately $O(k(n + nnz))$, where $k \ll n$ is the number of Lanczos iterations, n is the size of the matrix and nnz is the number of non-zero entries. Crucially, the Lanczos algorithm operates more efficiently on symmetric matrices, giving the Bethe Hessian matrix a distinct advantage over the \mathbf{NB} .

Let us first consider the dyadic network case. For a network with n nodes and m edges, the dimension of its non-backtracking matrix \mathbf{NB} is $n_{\mathbf{NB}}^* = 2m$ and the number of non-zero entries is $nnz_{\mathbf{NB}} = \sum_{i \in \mathcal{V}} d_i(d_i - 1)$. For the Bethe Hessian matrix \mathbf{B} , the dimension is $n_{\mathbf{B}}^* = n$, and the number of non-zero entries is $nnz_{\mathbf{B}} = m + n$. Therefore, to compare the time complexity of \mathbf{NB} based and \mathbf{B} based spectral clustering, we compute

$$\begin{aligned}
n_{\mathbf{NB}}^* + nnz_{\mathbf{NB}} - n_{\mathbf{B}}^* - nnz_{\mathbf{B}} &= 2m + \sum_i d_i(d_i - 1) - n - n - m \\
&= \sum_i d_i(d_i - 1) + m - 2n \\
&= \sum_i d_i^2 - 2m + m - 2n \\
&= \sum_i d_i^2 - m - 2n \\
&\geq nd^2 - nd/2 - 2n \\
&= n(d^2 - d/2 - 2) ,
\end{aligned} \tag{54}$$

where d is the average degree. In a large connected network, $d > 2$, which makes (54) strictly greater than zero. Thus, the Bethe Hessian based spectral clustering has lower time complexity than the one based on non-backtracking matrix.

Now, consider a hypergraph containing hyperedges of all possible orders $\kappa \in \mathcal{K}$. Let $d_i^{(\kappa)}$ denote the order κ degree of node i . From the definition of the non-backtracking matrix (38), its dimension is equal to the total number of directed hyperedges:

$$n_{\mathbf{NB}}^* = \sum_i \sum_{\kappa} d_i^{(\kappa)} , \tag{55}$$

and the number of non-zero entries is

$$nnz_{\mathbf{NB}} = \sum_i \sum_{\kappa} d_i^{(\kappa)}(\kappa - 1)(d_i - 1) , \tag{56}$$

where the total degree of node i is $d_i = \sum_{\kappa \in \mathcal{K}} d_i^{(\kappa)}$. Based on the Hypergraph Bethe Hessian matrix (2), the dimension is $n_{\mathbf{B}}^* = n$. The number of non-zero entries in \mathbf{B} has

the form $nnz_{\mathbf{B}} = n + x$, where x is the number of non-zero entries in its off-diagonal part. Each order κ hyperedge contributes $\binom{\kappa}{2}$ non-zero entries in \mathbf{B} , but different hyperedges may overlap in their contributions. Therefore we can upper bound x as,

$$x < \sum_{\kappa} m^{(\kappa)} \binom{\kappa}{2} = \sum_{\kappa} \sum_i \frac{d_i^{(\kappa)}}{\kappa} \frac{\kappa(\kappa-1)}{2} = \sum_i \sum_{\kappa} d_i^{(\kappa)} \frac{(\kappa-1)}{2}. \quad (57)$$

We then have:

$$\begin{aligned} & n_{\mathbf{NB}}^* + nnz_{\mathbf{NB}} - n_{\mathbf{B}}^* - nnz_{\mathbf{B}} \\ & > \sum_i \sum_{\kappa} d_i^{(\kappa)} + \sum_i \sum_{\kappa} d_i^{(\kappa)} (\kappa-1)(d_i-1) - n - \sum_i \sum_{\kappa} d_i^{(\kappa)} \frac{(\kappa-1)}{2} \\ & = \sum_i \sum_{\kappa} \left[d_i^{(\kappa)} \left(1 + (\kappa-1)(d_i - \frac{3}{2}) \right) - \frac{1}{|\mathcal{K}|} \right]. \end{aligned} \quad (58)$$

For a large sparse hypergraph, $d_i^{(\kappa)} \sim O(n)$. Thus, as $n \rightarrow \infty$, the above expression remains positive, leading to the same conclusion: for both dyadic networks and hypergraphs, the eigen decomposition of the Bethe Hessian has lower time complexity than the non-backtracking operator.

D Generalizing the spectral detectability limit of symmetric HSBM

To introduce the detectability limit of symmetric HSBM in literature [16, 17], we need to introduce the definition appeared in both of them:

$$\hat{c}_a^{(\kappa)} = \frac{1}{(\kappa-1)!} \sum_{\{\vec{z} \mid \vec{z}_0=a, \vec{z}_{1:} \in [q]^{\kappa-1}\}} \mathbf{C}_{\vec{z}}^{(\kappa)} \prod_{l=1}^{\kappa-1} p_{\vec{z}_l}, \quad (59)$$

and

$$\hat{c}_{ab}^{(\kappa)} = \frac{1}{(\kappa-2)!} \sum_{\{\vec{z} \mid \vec{z}_0=a, \vec{z}_1=b, \vec{z}_{2:} \in [q]^{\kappa-2}\}} \mathbf{C}_{\vec{z}}^{(\kappa)} \prod_{l=2}^{\kappa-1} p_{\vec{z}_l}, \quad (60)$$

where $[q]^{\kappa}$ represent the cartesian product for κ sets $[q] = \{1, 2, \dots, q\}$, p_r is the normalized community size of community r . In the case that all communities have the same size, $p_r = \frac{1}{q}$ and we can replace the product with the factor $\frac{1}{q^{\kappa-1}}$ in (59) and with $\frac{1}{q^{\kappa-2}}$ in (60).

The relationship between $\hat{c}_a^{(\kappa)}$ and $\hat{c}_{ab}^{(\kappa)}$ is

$$\hat{c}_a^{(\kappa)} = \frac{1}{\kappa-1} \sum_{b \in [q]} \hat{c}_{ab}^{(\kappa)} n_b \quad (61)$$

Under the symmetric HSBM case, $p_r = \frac{1}{q}$ and \mathbf{C} satisfy (6) with parameters c_{in} and c_{out} , a node can be incident on a maximum of $\binom{n/q-1}{\kappa-1}$ possible κ -hyperedges within the same community. Then we define the average κ -in-degree $d_{\text{in}}^{(\kappa)}$ can be calculated as:

$$\begin{aligned}
d_{\text{in}}^{(\kappa)} &= \lim_{n \rightarrow \infty} \binom{n/q-1}{\kappa-1} \frac{c_{\text{in}}}{n^{\kappa-1}} \\
&= \lim_{n \rightarrow \infty} \frac{c_{\text{in}}}{n^{\kappa-1}} \frac{(n/q-1)!}{(\kappa-1)!(n/q-\kappa)!} \\
&= \lim_{n \rightarrow \infty} \frac{c_{\text{in}}}{n^{\kappa-1}} \frac{(n/q-1) \dots (n/q-\kappa+1)}{(\kappa-1)!} \\
&= \frac{c_{\text{in}}}{n^{\kappa-1}} \frac{(n/q)^{\kappa-1}}{(\kappa-1)!} \\
&= \frac{c_{\text{in}}}{q^{\kappa-1}(\kappa-1)!} .
\end{aligned} \tag{62}$$

A node can be connected to a maximum of $\binom{n-1}{\kappa-1} - \binom{n/q-1}{\kappa-1}$ possible κ -hyperedges that connect to at least one node in a different community. For each of the $q^{\kappa-1} - 1$ ordered community combination of other $\kappa - 1$ nodes, the out-community κ -degree of the node is

$$\begin{aligned}
d_{\text{out}}^{(\kappa)} &= \lim_{n \rightarrow \infty} \frac{\binom{n-1}{\kappa-1} - \binom{n/q-1}{\kappa-1}}{q^{\kappa-1} - 1} \frac{c_{\text{out}}}{n^{\kappa-1}} \\
&= \frac{c_{\text{out}}}{n^{\kappa-1}} \frac{n^{\kappa-1} - (n/q)^{\kappa-1}}{(\kappa-1)!(q^{\kappa-1} - 1)} \\
&= \frac{c_{\text{out}}}{q^{\kappa-1}(\kappa-1)!}
\end{aligned} \tag{63}$$

The average κ -degree for the node is

$$d^{(\kappa)} = d_{\text{in}}^{(\kappa)} + (q^{\kappa-1} - 1)d_{\text{out}}^{(\kappa)} . \tag{64}$$

With our definition of $d_{\text{in}}^{(\kappa)}$ and $d_{\text{out}}^{(\kappa)}$ above, we can represent the $\widehat{c}_{ab}^{(\kappa)}$ and $\widehat{c}_a^{(\kappa)}$ with notation $d_{\text{in}}^{(\kappa)}$ and $d_{\text{out}}^{(\kappa)}$:

$$\widehat{c}_{ab}^{(\kappa)} = \begin{cases} \widehat{c}_{\text{in}}^{(\kappa)} = \frac{c_{\text{in}} + (q^{\kappa-2} - 1)c_{\text{out}}}{q^{\kappa-2}(\kappa-2)!} = q(\kappa-1)(d_{\text{in}}^{(\kappa)} + (q^{\kappa-2} - 1)d_{\text{out}}^{(\kappa)}) & , a = b \\ \widehat{c}_{\text{out}}^{(\kappa)} = \frac{q^{\kappa-2}c_{\text{out}}}{q^{\kappa-2}(\kappa-2)!} = q(\kappa-1)q^{\kappa-2}d_{\text{out}}^{(\kappa)} & , a \neq b \end{cases} , \tag{65}$$

and with equation (61), we have

$$\begin{aligned}
\widehat{c}_a^{(\kappa)} &= \frac{\widehat{c}_{\text{in}}^{(\kappa)} + (q-1)\widehat{c}_{\text{out}}^{(\kappa)}}{q(\kappa-1)} \\
&= \frac{\frac{c_{\text{in}} + (q^{\kappa-2}-1)c_{\text{out}}}{q^{\kappa-2}(\kappa-2)!} + (q-1)\frac{q^{\kappa-2}c_{\text{out}}}{q^{\kappa-2}(\kappa-2)!}}{q(\kappa-1)} \\
&= \frac{c_{\text{in}} + (q^{\kappa-1}-1)c_{\text{out}}}{q^{\kappa-1}(\kappa-1)!} \\
&= d_{\text{in}}^{(\kappa)} + (q^{\kappa-1}-1)d_{\text{out}}^{(\kappa)} \\
&= d^{(\kappa)}
\end{aligned} \tag{66}$$

For the κ -uniform symmetric HSBM introduced in [17], the detectability threshold is

$$\begin{aligned}
\frac{(\widehat{c}_{\text{in}}^{(\kappa)} - \widehat{c}_{\text{out}}^{(\kappa)})^2}{q^2 d^{(\kappa)}(\kappa-1)} &= 1 \\
\frac{\left((\kappa-1)(d_{\text{in}}^{(\kappa)} - d_{\text{out}}^{(\kappa)})\right)^2}{(\kappa-1)d^{(\kappa)}} &= 1
\end{aligned} \tag{67}$$

which can degenerated from our format of detectability limit in (9) by restricting $\mathcal{K} = \{\kappa\}$.

For non-uniform symmetric HSBM with $q = 2$ considered in [16], they define:

$$\begin{aligned}
\alpha_\kappa &= d^{(\kappa)}(\kappa-1) \\
\beta_\kappa &= \frac{\widehat{c}_{\text{in}}^{(\kappa)} - \widehat{c}_{\text{out}}^{(\kappa)}}{2}
\end{aligned} \tag{68}$$

Then their conjectured detectability threshold of spectral clustering with non-backtracking matrix [16] (also for Bethe Hessian matrix since their relationship as shown in Appendix B) is $\text{SNR}_{\text{NB}} = 1$ where

$$\begin{aligned}
\text{SNR}_{\text{NB}} &:= \frac{\left(\sum_{\kappa \in \mathcal{K}} \beta_\kappa\right)^2}{\sum_{\kappa \in \mathcal{K}} \alpha_\kappa} \\
&= \frac{\left(\sum_{\kappa \in \mathcal{K}} \widehat{c}_{\text{in}}^{(\kappa)} - \widehat{c}_{\text{out}}^{(\kappa)}\right)^2}{2^2 \sum_{\kappa \in \mathcal{K}} d^{(\kappa)}(\kappa-1)} \\
&= \frac{\left(\sum_{\kappa \in \mathcal{K}} (\kappa-1)(d_{\text{in}}^{(\kappa)} - d_{\text{out}}^{(\kappa)})\right)^2}{\sum_{\kappa \in \mathcal{K}} (\kappa-1)d^{(\kappa)}}
\end{aligned} \tag{69}$$

By simple generalizing the β_κ in (68) into

$$\beta_{\kappa,q} = \frac{\widehat{c}_{\text{in}}^{(\kappa)} - \widehat{c}_{\text{out}}^{(\kappa)}}{q} \tag{70}$$

we can get the spectral detectability limit of non-uniform symmetric HSBM for any q :

$$\begin{aligned}
\text{SNR}_{\text{BH}} &:= \frac{(\sum_{\kappa \in \mathcal{K}} \beta_{\kappa})^2}{\sum_{\kappa \in \mathcal{K}} \alpha_{\kappa}} \\
&= \frac{\left(\sum_{\kappa \in \mathcal{K}} \hat{c}_{\text{in}}^{(\kappa)} - \hat{c}_{\text{out}}^{(\kappa)} \right)^2}{q^2 \sum_{\kappa \in \mathcal{K}} (\kappa - 1) d^{(\kappa)}} \\
&= \frac{\left(\sum_{\kappa \in \mathcal{K}} (\kappa - 1) (d_{\text{in}}^{(\kappa)} - d_{\text{out}}^{(\kappa)}) \right)^2}{\sum_{\kappa \in \mathcal{K}} (\kappa - 1) d^{(\kappa)}}.
\end{aligned} \tag{71}$$

E Belief propagation and detectability limit of symmetric HSBM

Similar with belief propagation in graph [6], the main process of belief propagation in hyper graph is to update the message $b_{\psi_i}^{i \rightarrow e}$ in all directed hyperedges, and then update the marginal probability $b_{\psi_i}^i$ that node i belong to community ψ_i for all nodes. Here $b_{\psi_i}^{i \rightarrow e}$ represent the marginal probability that node i belong to community ψ_i without hyperedge e . However, unlike graph, we need another intermediate hyperedge to node message $\hat{b}_{\psi_i}^{e \rightarrow i}$ when we update the node to hyperedge message $b_{\psi_i}^{i \rightarrow e}$. To make a distinction with all exist hyperedges \mathcal{E} , we use \mathbf{E} represent all possible hyperedges. Then the belief propagation can be formalized as

$$\begin{aligned}
\text{node to hyperedge message} : b_{\psi_i}^{i \rightarrow e} &\propto n_{\psi_i} \prod_{f \in \partial i / e \cap \mathbf{E}} \hat{b}_{\psi_i}^{f \rightarrow i} \\
\text{hyperedge to node message} : \hat{b}_{\psi_i}^{e \rightarrow i} &\propto \sum_{\overrightarrow{\psi_{e/i}} \in [q]^{|e|-1}} \left(\Omega_{\overrightarrow{\psi_e}} \right)^{A_e} \left(1 - \Omega_{\overrightarrow{\psi_e}} \right)^{1-A_e} \prod_{j \in e / i} b_{\psi_j}^{j \rightarrow e} \\
\text{node marginal} : b_{\psi_i}^i &\propto n_{\psi_i} \prod_{f \in \partial i \cap \mathbf{E}} \hat{b}_{\psi_i}^{f \rightarrow i}
\end{aligned} \tag{72}$$

where $A_e = 1$ only if $e \in \mathcal{E}$, otherwise $A_e = 0$. $\overrightarrow{\psi_{e/i}}$ means the community assignment for the nodes in hyperedge e except node i , n_{ψ_i} means number of nodes in community ψ_i by percentage. We illustrate $b^{i \rightarrow e}$, $\hat{b}^{e \rightarrow i}$ and b^i with factor graph [39] in Figure 10.

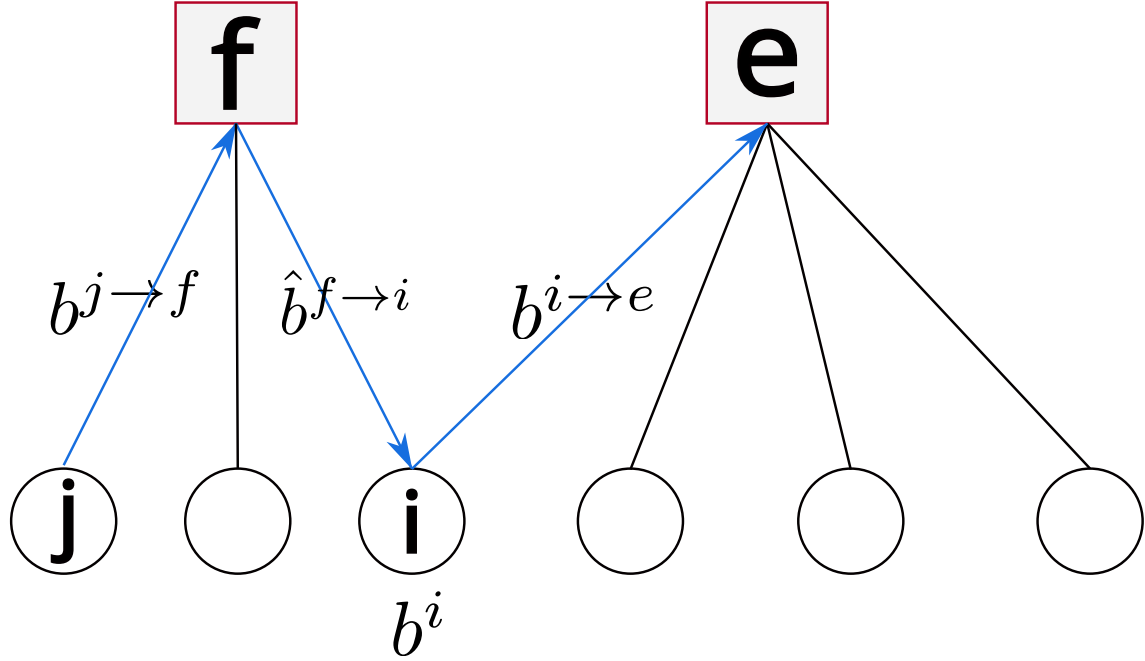


Figure 10: The factor graph representation of hypergraph. The red square represent the hyperedge, the circle represent the node. The message and marginal probability on directed hyperedge and node are also shown as $b^{j \rightarrow f}$, $b^{i \rightarrow e}$, $\hat{b}^{f \rightarrow i}$ and b^i . The blue directed hyperedge form a non-backtracking path $b^{j \rightarrow f} \rightarrow \hat{b}^{f \rightarrow i} \rightarrow b^{i \rightarrow e}$.

Next we discuss the $\hat{b}_{\psi_i}^{e \rightarrow i}$ based on existence of hyperedge e .

E.1 Discussion on hyperedge to node message

When hyperedge e exist, $A_e = 1$, we have

$$\begin{aligned} \hat{b}_{\psi_i}^{e \rightarrow i} &\propto \sum_{\overrightarrow{\psi_{e/i}} \in [q]^{|e|-1}} \Omega_{\overrightarrow{\psi_e}} \prod_{j \in e/i} b_{\psi_j}^{j \rightarrow e} \\ &\propto \sum_{\overrightarrow{\psi_{e/i}} \in [q]^{|e|-1}} C_{\overrightarrow{\psi_e}} \prod_{j \in e/i} b_{\psi_j}^{j \rightarrow e}. \end{aligned} \quad (73)$$

However if $A_e = 0$, then

$$\begin{aligned}
\hat{b}_{\psi_i}^{e \rightarrow i} &\propto \sum_{\overrightarrow{\psi_{e/i}} \in [q]^{|e|-1}} \left(1 - \Omega_{\overrightarrow{\psi_e}}\right) \prod_{j \in e/i} b_{\psi_j}^{j \rightarrow e} \\
&= \sum_{\overrightarrow{\psi_{e/i}} \in [q]^{|e|-1}} \left(1 - \frac{C_{\overrightarrow{\psi_e}}}{n^{|e|-1}}\right) \prod_{j \in e/i} b_{\psi_j}^{j \rightarrow e} \\
&= \sum_{\overrightarrow{\psi_{e/i}} \in [q]^{|e|-1}} \prod_{j \in e/i} b_{\psi_j}^{j \rightarrow e} - \sum_{\overrightarrow{\psi_{e/i}} \in [q]^{|e|-1}} \frac{C_{\overrightarrow{\psi_e}}}{n^{|e|-1}} \prod_{j \in e/i} b_{\psi_j}^{j \rightarrow e}, \\
&= \prod_{j \in e/i} \sum_{\psi_j \in [q]} b_{\psi_j}^{j \rightarrow e} - \sum_{\overrightarrow{\psi_{e/i}} \in [q]^{|e|-1}} \frac{C_{\overrightarrow{\psi_e}}}{n^{|e|-1}} \prod_{j \in e/i} b_{\psi_j}^{j \rightarrow e} \\
&= 1 - \sum_{\overrightarrow{\psi_{e/i}} \in [q]^{|e|-1}} \frac{C_{\overrightarrow{\psi_e}}}{n^{|e|-1}} \prod_{j \in e/i} b_{\psi_j}^{j \rightarrow e}
\end{aligned} \tag{74}$$

where the last line use $\sum_{\psi_j \in [q]} b_{\psi_j}^{j \rightarrow e} = 1$. According to sparse assumption, $C_{\overrightarrow{\psi_e}}$ is a constant compared to n , so

$$\lim_{n \rightarrow \infty} \hat{b}_{\psi_i}^{e \rightarrow i} = \frac{1}{q} \ . \tag{75}$$

According to (72), we have

$$\begin{aligned}
b_{\psi_j}^{j \rightarrow e} &\propto n_{\psi_j} \prod_{f \in \partial j/e} \hat{b}_{\psi_j}^{f \rightarrow j} \\
&= \frac{n_{\psi_j}}{\hat{b}_{\psi_j}^{e \rightarrow j}} \prod_{f \in \partial j} \hat{b}_{\psi_j}^{f \rightarrow j} \\
&= \frac{b_{\psi_j}^j}{\hat{b}_{\psi_j}^{e \rightarrow j}}
\end{aligned} \tag{76}$$

Based on (75) and (76), we have

$$\lim_{n \rightarrow \infty} b_{\psi_j}^{j \rightarrow e} = b_{\psi_j}^j \ . \tag{77}$$

We substitute (77) into (74) and consider $1 + x \approx \exp(x)$ when $x \rightarrow 0$, then when $n \rightarrow \infty$

$$\hat{b}_{\psi_i}^{e \rightarrow i} = \exp \left(-\frac{1}{n^{|e|-1}} \sum_{\overrightarrow{\psi_{e/i}} \in [q]^{|e|-1}} C_{\overrightarrow{\psi_e}} \prod_{j \in e/i} b_{\psi_j}^j \right) \ . \tag{78}$$

E.2 Update of node to hyperedge message and external field

Based on $\hat{b}_{\psi_i}^{e \rightarrow i}$ in different case (73) and (78), we can update node to hyperedge message as

$$\begin{aligned}
b_{\psi_i}^{i \rightarrow e} &\propto n_{\psi_i} \prod_{f \in \partial i / e \cap \mathbf{E}} \hat{b}_{\psi_i}^{f \rightarrow i} \\
&= n_{\psi_i} \prod_{f \in \partial i / e \cap E} \hat{b}_{\psi_i}^{f \rightarrow i} \prod_{f \in \partial i / e \cap \mathbf{E} / E} \hat{b}_{\psi_i}^{f \rightarrow i} \\
&= n_{\psi_i} \prod_{f \in \partial i / e \cap E} \hat{b}_{\psi_i}^{f \rightarrow i} \prod_{f \in \partial i / e \cap \mathbf{E} / E} \exp \left(-\frac{1}{n^{|f|-1}} \sum_{\overrightarrow{\psi_{f/i}} \in [q]^{|f|-1}} \mathbf{C}_{\overrightarrow{\psi_f}} \prod_{j \in f/i} b_{\psi_j}^j \right) . \quad (79) \\
&= n_{\psi_i} \prod_{f \in \partial i / e \cap E} \hat{b}_{\psi_i}^{f \rightarrow i} \exp \left(-\sum_{f \in \partial i / e \cap \mathbf{E} / E} \frac{1}{n^{|f|-1}} \sum_{\overrightarrow{\psi_{f/i}} \in [q]^{|f|-1}} \mathbf{C}_{\overrightarrow{\psi_f}} \prod_{j \in f/i} b_{\psi_j}^j \right) \\
&= n_{\psi_i} \prod_{f \in \partial i / e \cap E} \hat{b}_{\psi_i}^{f \rightarrow i} \exp(-h_{\psi_i}^{i \rightarrow e})
\end{aligned}$$

Because of $e \in E$ and the existed hyperedge set E is far smaller than all possible hyperedge set \mathbf{E} in sparse regime, so

$$h_{\psi_i}^{i \rightarrow e} = h_{\psi_i}^i = \sum_{f \in \partial i \cap \mathbf{E}} \frac{1}{n^{|f|-1}} \sum_{\overrightarrow{\psi_{f/i}} \in [q]^{|f|-1}} \mathbf{C}_{\overrightarrow{\psi_f}} \prod_{j \in f/i} b_{\psi_j}^j . \quad (80)$$

We call the $h_{\psi_i}^i$ as external field. The external field can not be reduced anymore for general tensor \mathbf{C} . However, considering the specific form of \mathbf{C} (6) in symmetric HSBM,

we can reduce $h_{\psi_i}^i$ to h_{ψ_i}

$$\begin{aligned}
h_{\psi_i}^i &= \sum_{f \in \partial i \cap \mathbf{E}} \frac{1}{n^{|f|-1}} \left(c_{\text{in}} \prod_{j \in f/i} b_{\psi_i}^j + c_{\text{out}} \sum_{\substack{\overrightarrow{\psi_f/i} \in [q]^{|f|-1} / [\psi_i] \\ |f|-1}} \prod_{j \in f/i} b_{\psi_j}^j \right) \\
&= \sum_{\kappa \in \mathcal{K}} \frac{1}{n^{\kappa-1}} \sum_{f \in \mathbf{E}^{(\kappa-1)}} \left(c_{\text{in}} \prod_{j \in f} b_{\psi_i}^j + c_{\text{out}} \sum_{\substack{\overrightarrow{\psi_f} \in [q]^{\kappa-1} / [\psi_i] \\ \kappa-1}} \prod_{j \in f} b_{\psi_j}^j \right) , \quad (81) \\
&= \sum_{\kappa \in \mathcal{K}} \frac{1}{n^{\kappa-1}} \sum_{f \in \mathbf{E}^{(\kappa-1)}} \left(c_{\text{out}} + (c_{\text{in}} - c_{\text{out}}) \prod_{j \in f} b_{\psi_i}^j \right) \\
&\approx \sum_{\kappa \in \mathcal{K}} \left[c_{\text{out}} + \frac{c_{\text{in}} - c_{\text{out}}}{n^{\kappa-1}(\kappa-1)!} \left(\sum_{j \in [n]} b_{\psi_i}^j \right)^{\kappa-1} \right] = h_{\psi_i}
\end{aligned}$$

where the second last line is derived based on $\sum_{\overrightarrow{\psi_f} \in [q]^{\kappa-1}} \prod_{j \in f} b_{\psi_j}^j = 1$. The last line is derived with similar idea in paper [17].

E.3 Update of node marginal and summary

The node marginal $b_{\psi_i}^i$ is updated similarly to $b_{\psi_i}^{i \rightarrow e}$,

$$\begin{aligned}
b_{\psi_i}^i &\propto n_{\psi_i} \prod_{f \in \partial i} \hat{b}_{\psi_i}^{f \rightarrow i} \\
&= n_{\psi_i} \prod_{f \in \partial i \cap E} \hat{b}_{\psi_i}^{f \rightarrow i} \prod_{f \in \partial i \cap \mathbf{E}/E} \hat{b}_{\psi_i}^{f \rightarrow i} . \quad (82) \\
&= n_{\psi_i} \exp(-h_{\psi_i}^i) \prod_{f \in \partial i \cap E} \hat{b}_{\psi_i}^{f \rightarrow i}
\end{aligned}$$

Based on above derivation, we can summary the belief propagation as

$$\begin{aligned}
\text{node to hyperedge message : } & b_{\psi_i}^{i \rightarrow e} \propto n_{\psi_i} \exp(-h_{\psi_i}^i) \prod_{f \in \partial i / e \cap E} \hat{b}_{\psi_i}^{f \rightarrow i} \\
\text{hyperedge to node message : } & \hat{b}_{\psi_i}^{e \rightarrow i} \propto \sum_{\overrightarrow{\psi_e / i} \in [q]^{|e|-1}} C_{\overrightarrow{\psi_e}} \prod_{j \in e / i} b_{\psi_j}^{j \rightarrow e} \\
\text{external field : } & h_{\psi_i}^i = \sum_{f \in \partial i \cap E} \frac{1}{n^{|f|-1}} \sum_{\overrightarrow{\psi_f / i} \in [q]^{|f|-1}} C_{\overrightarrow{\psi_f}} \prod_{j \in f / i} b_{\psi_j}^j \\
\text{node marginal : } & b_{\psi_i}^i \propto n_{\psi_i} \exp(-h_{\psi_i}^i) \prod_{f \in \partial i \cap E} \hat{b}_{\psi_i}^{f \rightarrow i}
\end{aligned} \tag{83}$$

E.4 The detectability of belief propagation

Similarly with paper [6] and [18], we get the detectability by deriving the stability of trivial fixed point in belief propagation. We will focus on symmetric HSBM case (6). In this case, $n_{\psi_i} = \frac{1}{q}$ and we can verify that there is a trivial fixed point of belief propagation based on (83) and external field (81)

$$\begin{aligned}
b_{\psi_i}^{i \rightarrow e} &= \frac{1}{q} \\
\hat{b}_{\psi_i}^{e \rightarrow i} &= \frac{1}{q} \\
b_{\psi_i}^i &= \frac{1}{q}
\end{aligned} \tag{84}$$

This trivial fixed point means nothing but any node belong to any community with same probability, so we need this trivial fixed point should be unstable. One way to discuss the stability of the fixed point is to get the largest modular eigenvalue of Jacobian Matrix of belief propagation [36]. Here we use another approach which is inherited from [6] and [18].

We assume the message passing as a tree with depth s , as shown in Figure 11. We will check if the node to hyperedge message perturbation around trivial fixed point will be amplified or reduced during its propagation from all the leaves to root. First, we need to know how the perturbation propagate between adjacent node to hyperedge message, such as $b^{i_s \rightarrow f_s}$ and $b^{i_{s-1} \rightarrow f_{s-1}}$ in Figure 11. This propagation progress can be formalized as transition matrix \hat{T} with dimension $q \times q$, defined as

$$\hat{T}_{x,y}^{i \rightarrow e; j \rightarrow f} = \frac{\partial b_x^{i \rightarrow e}}{\partial b_y^{j \rightarrow f}} , \tag{85}$$

where $e \neq f$ and $i \in f / j$, as this short message passing path is $b^{j \rightarrow f} \rightarrow \hat{b}^{f \rightarrow i} \rightarrow b^{i \rightarrow e}$. Next we will derive this transition matrix at trivial fixed point.

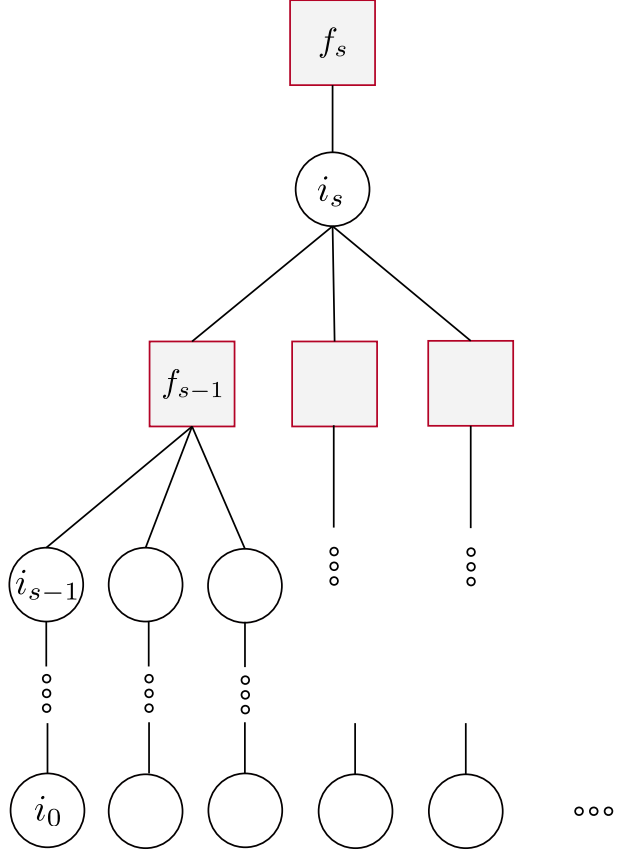


Figure 11: *The approximate message passing tree in belief propagation.*

E.4.1 Transition matrix at trivial fixed point

Based on belief propagation (83), we can write the full update function of $b_x^{i \rightarrow e}$ without hyperedge to node message as

$$b_x^{i \rightarrow e} = \frac{1}{Z^{i \rightarrow e}} n_x \exp(-h_x^i) \prod_{g \in \partial i / e \cap E} \sum_{\substack{\psi_g \in [q]^{|g|-1}, \psi_i = x}} C_{\psi_g} \prod_{l \in g / i} b_{\psi_l}^{j \rightarrow g}, \quad (86)$$

where $Z^{i \rightarrow e}$ is normalization term over community label x . We define the numerator part of (86) as $\beta_x^{i \rightarrow e}$, then the transition matrix can be transformed as

$$\begin{aligned} \hat{T}_{x;y}^{i \rightarrow e; j \rightarrow f} &= \frac{\partial b_x^{i \rightarrow e}}{\partial b_y^{j \rightarrow f}} \\ &= \frac{1}{Z^{i \rightarrow e}} \frac{\partial \beta_x^{i \rightarrow e}}{\partial b_y^{j \rightarrow f}} - \frac{1}{(Z^{i \rightarrow e})^2} \frac{\partial Z^{i \rightarrow e}}{\partial b_y^{j \rightarrow f}} \beta_x^{i \rightarrow e} \end{aligned} \quad (87)$$

In symmetric HSBM case, the external field $h_{\psi_i}^i$ is a constant at trivial fixed point based on (81)

$$\begin{aligned} h_{\psi_i}^i = h_{\psi_i} &= \sum_{\kappa \in \mathcal{K}} \left[c_{\text{out}} + \frac{c_{\text{in}} - c_{\text{out}}}{n^{\kappa-1}(\kappa-1)!} \left(\sum_{j \in [n]} \frac{1}{q} \right)^{\kappa-1} \right] . \\ &= \sum_{\kappa \in \mathcal{K}} \left[c_{\text{out}} + \frac{c_{\text{in}} - c_{\text{out}}}{q^{\kappa-1}(\kappa-1)!} \right] = h \end{aligned} \quad (88)$$

The average κ -order degree (66) is also a constant. Based on (59), we have

$$\sum_{\overrightarrow{\psi_{g/i}} \in [q]^{|g|-1}, \overrightarrow{\psi_i} = x} C_{\overrightarrow{\psi_g}} \prod_{l \in g/i} \frac{1}{q} = d^{(|g|)} (|g| - 1)! . \quad (89)$$

Then at trivial fixed point, $\beta_x^{i \rightarrow e}$ is

$$\begin{aligned} \beta_x^{i \rightarrow e} &= n_x \exp(-h_x^i) \prod_{g \in \partial i/e \cap E} \sum_{\overrightarrow{\psi_{g/i}} \in [q]^{|g|-1}, \overrightarrow{\psi_i} = x} C_{\overrightarrow{\psi_g}} \prod_{l \in g/i} \frac{1}{q} \\ &= \frac{\exp(-h)}{q} \prod_{g \in \partial i/e \cap E} d^{(|g|)} (|g| - 1)! \end{aligned} , \quad (90)$$

and $Z^{i \rightarrow e}$ is

$$\begin{aligned} Z^{i \rightarrow e} &= \sum_{x \in [q]} \beta_x^{i \rightarrow e} \\ &= \sum_{x \in [q]} \frac{\exp(-h)}{q} \prod_{g \in \partial i/e \cap E} d^{(|g|)} (|g| - 1)! . \\ &= \exp(-h) \prod_{g \in \partial i/e \cap E} d^{(|g|)} (|g| - 1)! \end{aligned} \quad (91)$$

Next the partial derivative $\frac{\partial \beta_x^{i \rightarrow e}}{\partial b_y^{j \rightarrow f}}$ is

$$\begin{aligned}
\frac{\partial \beta_x^{i \rightarrow e}}{\partial b_y^{j \rightarrow f}} &= \frac{\partial \left\{ n_x \exp(-h_x^i) \prod_{g \in \partial i/e \cap E} \sum_{\overrightarrow{\psi}_{g/i} \in [q]^{|g|-1}, \overrightarrow{\psi}_i = x} \mathbf{C}_{\overrightarrow{\psi}_g} \prod_{l \in g/i} b_{\psi_l}^{l \rightarrow g} \right\}}{\partial b_y^{j \rightarrow f}} \\
&= \frac{\exp(-h)}{q} \left(\prod_{g \in \partial i/e, f \cap E} \sum_{\overrightarrow{\psi}_{g/i} \in [q]^{|g|-1}, \overrightarrow{\psi}_i = x} \mathbf{C}_{\overrightarrow{\psi}_g} \prod_{l \in g/i} b_{\psi_l}^{l \rightarrow g} \right) \\
&\quad \times \sum_{\overrightarrow{\psi}_{f/i,j} \in [q]^{|f|-2}, \overrightarrow{\psi}_i = x, \overrightarrow{\psi}_j = y} \mathbf{C}_{\overrightarrow{\psi}_f} \prod_{l \in f/i,j} b_{\psi_l}^{l \rightarrow f} \\
&= \frac{\exp(-h)}{q} \left(\prod_{g \in \partial i/e, f \cap E} d^{(|g|)}(|g|-1)! \right) \sum_{\overrightarrow{\psi}_{f/i,j} \in [q]^{|f|-2}, \overrightarrow{\psi}_i = x, \overrightarrow{\psi}_j = y} \mathbf{C}_{\overrightarrow{\psi}_f} \prod_{l \in f/i,j} \frac{1}{q} \\
&= \frac{\exp(-h)}{q} \left(\prod_{g \in \partial i/e, f \cap E} d^{(|g|)}(|g|-1)! \right) \hat{c}_{xy}^{(|f|)}(|f|-2)!
\end{aligned} \tag{92}$$

where the last line is based on definition (60). In symmetric HSBM case, $\hat{c}_{xy}^{(|f|)}$ is follow (65), so we have

$$\frac{\partial \beta_x^{i \rightarrow e}}{\partial b_y^{j \rightarrow f}} = \frac{\exp(-h)}{q} \left(\prod_{g \in \partial i/e, f \cap E} d^{(|g|)}(|g|-1)! \right) \frac{c_{\text{in}} \delta_{x,y} + c_{\text{out}} (1 - \delta_{x,y}) + (q^{|f|-2} - 1) c_{\text{out}}}{q^{|f|-2}} \tag{93}$$

where $\delta_{x,y} = 1$ if $x = y$. Then we have

$$\begin{aligned}
\frac{\partial Z^{i \rightarrow e}}{\partial b_y^{j \rightarrow f}} &= \sum_{x \in [q]} \frac{\partial \beta_x^{i \rightarrow e}}{\partial b_y^{j \rightarrow f}} \\
&= \exp(-h) \left(\prod_{g \in \partial i/e, f \cap E} d^{(|g|)}(|g|-1)! \right) \left(\frac{c_{\text{in}} + (q^{|f|-2} - 1) c_{\text{out}}}{q^{|f|-1}} + \frac{c_{\text{out}}}{q} (q-1) \right) \\
&= \exp(-h) \left(\prod_{g \in \partial i/e, f \cap E} d^{(|g|)}(|g|-1)! \right) \left(\frac{c_{\text{in}} + (q^{|f|-1} - 1) c_{\text{out}}}{q^{|f|-1}} \right)
\end{aligned} \tag{94}$$

Finally substitute (90), (91), (93), (94) into (87), we get the transition matrix at trivial fixed point

$$\begin{aligned}
\hat{T}_{x;y}^{i \rightarrow e; j \rightarrow f} &= \frac{1}{Z^{i \rightarrow e}} \frac{\partial \beta_x^{i \rightarrow e}}{\partial b_y^{j \rightarrow f}} - \frac{1}{(Z^{i \rightarrow e})^2} \frac{\partial Z^{i \rightarrow e}}{\partial b_y^{j \rightarrow f}} \beta_x^{i \rightarrow e} \\
&= \frac{\frac{\exp(-h)}{q} \left(\prod_{g \in \partial i/e, f \cap E} d^{(|g|)} (|g| - 1)! \right) \frac{c_{\text{in}} \delta_{x,y} + c_{\text{out}} (1 - \delta_{x,y}) + (q^{|f|-2} - 1) c_{\text{out}}}{q^{|f|-2}}}{\exp(-h) \prod_{g \in \partial i/e \cap E} d^{(|g|)} (|g| - 1)!} \\
&\quad - \frac{\exp(-h) \left(\prod_{g \in \partial i/e, f \cap E} d^{(|g|)} (|g| - 1)! \right) \left(\frac{c_{\text{in}} + (q^{|f|-1} - 1) c_{\text{out}}}{q^{|f|-1}} \right)}{q \exp(-h) \prod_{g \in \partial i/e \cap E} d^{(|g|)} (|g| - 1)!} \\
&= \frac{1}{qd^{(|f|)} (|f| - 1)!} \frac{c_{\text{in}} \delta_{x,y} + c_{\text{out}} (1 - \delta_{x,y}) + (q^{|f|-2} - 1) c_{\text{out}}}{q^{|f|-2}} \\
&\quad - \frac{1}{qd^{(|f|)} (|f| - 1)!} \frac{c_{\text{in}} + (q^{|f|-1} - 1) c_{\text{out}}}{q^{|f|-1}} \\
&= \frac{1}{d^{(|f|)} (|f| - 1)!} \frac{qc_{\text{in}} \delta_{x,y} + qc_{\text{out}} (1 - \delta_{x,y}) + q(q^{|f|-2} - 1) c_{\text{out}} - c_{\text{in}} - (q^{|f|-1} - 1) c_{\text{out}}}{q^{|f|}} \\
&= \frac{1}{d^{(|f|)} (|f| - 1)!} \frac{c_{\text{in}} (q \delta_{x,y} - 1) + c_{\text{out}} (1 - q \delta_{x,y})}{q^{|f|}} \\
&= \frac{1}{d^{(|f|)} (|f| - 1)!} \frac{(q \delta_{x,y} - 1)(c_{\text{in}} - c_{\text{out}})}{q^{|f|}}
\end{aligned} \tag{95}$$

We define \mathbf{J} is all ones matrix, then the transition matrix $\hat{\mathbf{T}}$ is

$$\begin{aligned}
\hat{\mathbf{T}}^{i \rightarrow e; j \rightarrow f} &= \frac{1}{d^{(|f|)} (|f| - 1)! q^{|f|}} [q(c_{\text{in}} - c_{\text{out}}) \mathbf{I} + (c_{\text{out}} - c_{\text{in}}) \mathbf{J}] \\
&= \frac{1}{d^{(|f|)} (|f| - 1)! q^{|f|}} \mathbf{T}
\end{aligned} \tag{96}$$

E.4.2 Stability of trivial fixed point

We first focus on the message passing path in Figure 11 from i_0 to f_s . We define ε^r as the perturbation of message $b^{i_r \rightarrow f_r}$ around trivial fixed point, as $b^{i_r \rightarrow f_r} = \frac{1}{q} + \varepsilon^r$. Then we have

$$\begin{aligned}
\varepsilon^{r+1} &= \hat{\mathbf{T}}^{i_{r+1} \rightarrow f_{r+1}; i_r \rightarrow f_r} \varepsilon^r \\
&= \frac{1}{d^{(|f_r|)} (|f_r| - 1)! q^{|f_r|}} \mathbf{T} \varepsilon^r
\end{aligned} \tag{97}$$

The perturbation ε^0 in the leaf will propagate s times to the ε^s , so

$$\varepsilon^s = \left(\prod_{r=0}^{s-1} \frac{1}{d^{(|f_r|)} (|f_r| - 1)! q^{|f_r|}} \right) \mathbf{T}^s \varepsilon^0 \tag{98}$$

When $s \rightarrow \infty$, we define

$$\begin{aligned}
\mu &= \lim_{s \rightarrow \infty} \prod_{r=0}^{s-1} \frac{1}{d^{|f_r|} (|f_r| - 1)! q^{|f_r|}} \\
&= \exp \left(\lim_{s \rightarrow \infty} \sum_{r=0}^{s-1} \log \frac{1}{d^{|f_r|} (|f_r| - 1)! q^{|f_r|}} \right) , \\
&\approx \exp \left(s \mathbb{E}_f \left(\log \frac{1}{d^{|f|} (|f| - 1)! q^{|f|}} \right) \right)
\end{aligned} \tag{99}$$

where \mathbb{E}_f is the expectation over randomly drawn hyperedges $f \in E$. On the other hand, the leading eigenvalue of \mathbf{T} is $\lambda = q(c_{\text{in}} - c_{\text{out}})$. So the equation (98) is approximated as

$$\varepsilon^s = \mu \lambda^s \varepsilon^0 . \tag{100}$$

Before proceeding with the following derivation, we observe that the perturbation of node marginal b^i follow the same transition as perturbation of $b^{i \rightarrow e}$. That is equal to say the $\hat{\mathbf{T}}^{i;j \rightarrow f} = \hat{\mathbf{T}}^{i \rightarrow e;j \rightarrow f}$, where

$$\hat{\mathbf{T}}_{x;y}^{i;j \rightarrow f} = \frac{\partial b_x^i}{\partial b_y^{j \rightarrow f}} . \tag{101}$$

This can be derived with similar way in section E.4.1, just remove e in each equation. So now, we can define ε^r also to be the perturbation of b^{i_r} except $r = 0$, and the equation (100) still holds. However in this case, each node can average has d hyperedges as its son nodes in message passing tree, each hyperedge still average has $\hat{\kappa} - 1$ nodes as its son nodes in message passing tree. Then there are totally $[d(\hat{\kappa} - 1)]^s$ leave nodes whose perturbation will finally affect ε^s in root node i_s . Here, the $\hat{\kappa}$ is the average order of hyperedges. To derive $\hat{\kappa}$, we first estimate the expected number of order- κ hyperedges $m^{(\kappa)}$ under the symmetric HSBM. As $n \rightarrow \infty$, this estimation yields:

$$\begin{aligned}
m^{(\kappa)} &= \lim_{n \rightarrow \infty} q \binom{\frac{n}{q}}{\kappa} \frac{c_{\text{in}}}{n^{\kappa-1}} + \left(\binom{n}{\kappa} - q \binom{\frac{n}{q}}{\kappa} \right) \frac{c_{\text{out}}}{n^{\kappa-1}} \\
&= \frac{n}{\kappa! q^{\kappa-1}} c_{\text{in}} + \frac{n(q^{\kappa-1} - 1)}{\kappa! q^{\kappa-1}} c_{\text{out}} , \\
&= \frac{n}{\kappa} d^{(\kappa)}
\end{aligned} \tag{102}$$

where $d^{(\kappa)}$ is from (8) and the asymptotic limits of the combinatorial parts are given by:

$$\begin{aligned}
\lim_{n \rightarrow \infty} q \binom{\frac{n}{q}}{\kappa} \frac{1}{n^{\kappa-1}} &= \lim_{n \rightarrow \infty} \frac{(n/q)!}{\kappa! (n/q - \kappa)!} \frac{q}{n^{\kappa-1}} = \frac{1}{(\kappa)!} \frac{(n/q)^\kappa q}{n^{\kappa-1}} = \frac{n}{\kappa! q^{\kappa-1}} \\
\lim_{n \rightarrow \infty} \left(\binom{n}{\kappa} - q \binom{\frac{n}{q}}{\kappa} \right) \frac{1}{n^{\kappa-1}} &= \frac{n}{(\kappa)!} - \frac{n}{(\kappa)! q^{\kappa-1}} = \frac{n(q^{\kappa-1} - 1)}{\kappa! q^{\kappa-1}}
\end{aligned} . \tag{103}$$

Then the average order $\hat{\kappa}$ is then calculated as the ratio of the total order of hyperedges to the total number of hyperedges:

$$\begin{aligned}\hat{\kappa} &= \frac{\sum_{\kappa \in \mathcal{K}} \kappa m^{(\kappa)}}{\sum_{\kappa \in \mathcal{K}} m^{(\kappa)}} \\ &= \frac{\sum_{\kappa \in \mathcal{K}} n d^{(\kappa)}}{\sum_{\kappa \in \mathcal{K}} \frac{n}{\kappa} d^{(\kappa)}} \\ &= \frac{d}{\sum_{\kappa \in \mathcal{K}} \frac{d^{(\kappa)}}{\kappa}}.\end{aligned}\quad (104)$$

Next we aggregate perturbations in all leaves in the tree. Because the expectation of any perturbation ε is 0, we consider its variance

$$\begin{aligned}\mathbb{E}((\varepsilon^s)^2) &= \mathbb{E}\left(\left(\sum_{i=1}^{[d(\hat{\kappa}-1)]^s} \mu \lambda^s \varepsilon^{0;i}\right)^2\right) \\ &\approx \mu^2 \lambda^{2s} [d(\hat{\kappa}-1)]^s \mathbb{E}((\varepsilon^0)^2)\end{aligned}\quad (105)$$

The stability of trivial fixed point is decided by

$$\begin{aligned}\sqrt[s]{\mu^2 \lambda^{2s} [d(\hat{\kappa}-1)]^s} &< 1 \\ \exp\left(2\mathbb{E}\left(\log\left(\frac{1}{d^{|f|}(|f|-1)!q^{|f|}}\right)\right)\right) q^2 (c_{\text{in}} - c_{\text{out}})^2 [d(\hat{\kappa}-1)] &< 1\end{aligned}, \quad (106)$$

where

$$\begin{aligned}\mathbb{E}\left(\log\left(\frac{1}{d^{|f|}(|f|-1)!q^{|f|}}\right)\right) &= \sum_{\kappa \in \mathcal{K}} \frac{m^{(\kappa)}}{\sum_{\kappa' \in \mathcal{K}} m^{(\kappa')}} \log\left(\frac{1}{d^{(\kappa)}(\kappa-1)!q^\kappa}\right) \\ &= \sum_{\kappa \in \mathcal{K}} \frac{\frac{n}{\kappa} d^{(\kappa)}}{\sum_{\kappa' \in \mathcal{K}} \frac{n}{\kappa'} d^{(\kappa')}} \log\left(\frac{1}{d^{(\kappa)}(\kappa-1)!q^\kappa}\right) \\ &= \sum_{\kappa \in \mathcal{K}} \frac{d^{(\kappa)}/\kappa}{\sum_{\kappa' \in \mathcal{K}} \frac{d^{(\kappa')}}{\kappa'}} \log\left(\frac{1}{d^{(\kappa)}(\kappa-1)!q^\kappa}\right) \\ &= \sum_{\kappa \in \mathcal{K}} \frac{\hat{\kappa} d^{(\kappa)}}{d \kappa} \log\left(\frac{1}{d^{(\kappa)}(\kappa-1)!q^\kappa}\right)\end{aligned}. \quad (107)$$

Here number of order- κ hyperedge $m^{(\kappa)}$ is from equation (102), average order (104) $\hat{\kappa} = \frac{d}{\sum_{\kappa \in \mathcal{K}} \frac{d^{(\kappa)}}{\kappa}}$ and average degree (10) $d = \sum_{\kappa \in \mathcal{K}} d^{(\kappa)}$. Because the detectability is equal to instability of trivial fixed point, so based on equation (106) and (107), the detectability

threshold of belief propagation is

$$\begin{aligned}
& q^2(c_{\text{in}} - c_{\text{out}})^2[d(\hat{\kappa} - 1)] \prod_{\kappa \in \mathcal{K}} \left(\frac{1}{d^{(\kappa)}(\kappa - 1)!q^\kappa} \right)^{2\frac{\hat{\kappa}d^{(\kappa)}}{d\kappa}} > 1 \\
& d(\hat{\kappa} - 1) \prod_{\kappa \in \mathcal{K}} \left(\frac{q(c_{\text{in}} - c_{\text{out}})}{d^{(\kappa)}(\kappa - 1)!q^\kappa} \right)^{2\frac{\hat{\kappa}d^{(\kappa)}}{d\kappa}} > 1 \\
& d(\hat{\kappa} - 1) \prod_{\kappa \in \mathcal{K}} \left(\frac{(c_{\text{in}} - c_{\text{out}})}{d^{(\kappa)}(\kappa - 1)!q^{\kappa-1}} \right)^{2\frac{\hat{\kappa}d^{(\kappa)}}{d\kappa}} > 1 \\
& d(\hat{\kappa} - 1) \prod_{\kappa \in \mathcal{K}} \left(\frac{d_{\text{in}}^{(\kappa)} - d_{\text{out}}^{(\kappa)}}{d^{(\kappa)}} \right)^{2\frac{\hat{\kappa}d^{(\kappa)}}{d\kappa}} > 1
\end{aligned} \tag{108}$$

where the simplification leading to the second line relies on:

$$\sum_{\kappa \in \mathcal{K}} \frac{\hat{\kappa}d^{(\kappa)}}{d\kappa} = 1 \tag{109}$$

while the last line is a direct result of substituting the explicit expressions for $d_{\text{in}}^{(\kappa)}$ and $d_{\text{out}}^{(\kappa)}$ as defined in (7). We denote the left formula of inequality (108) as

$$\text{SNR}_{\text{BP}} := d(\hat{\kappa} - 1) \prod_{\kappa \in \mathcal{K}} \left(\frac{d_{\text{in}}^{(\kappa)} - d_{\text{out}}^{(\kappa)}}{d^{(\kappa)}} \right)^{2\frac{\hat{\kappa}d^{(\kappa)}}{d\kappa}} \tag{110}$$

F Supplementary experiment: detectability limits of symmetric HSBM

We use numeric experiment to verify the detectability limit of Bethe Hessian-based spectral clustering (9) and belief propagation (12). First, we run experiment on κ -uniform hyper graph to verify the detectability limit (67) in literature [17]. Then we run experiment on nonuniform hyper graph with $q = 2$ to verify the SNR_{BH} (9) in literature [16] and SNR_{BP} (12) in this paper.

We use AMI [24] to evaluate the community detection result. Assume ψ^* is the real community label vector and ψ is detected community label vector. Then AMI is defined by

$$\text{AMI}(\psi, \psi^*) = \frac{\text{MI}(\psi, \psi^*) - \mathbb{E}(\text{MI}(\psi, \psi^*))}{\frac{1}{2}(H(\psi) + H(\psi^*)) - \mathbb{E}(\text{MI}(\psi, \psi^*))} \tag{111}$$

where MI represent mutual information, \mathbb{E} means the expectation. The AMI score lies in range $[0, 1]$, with 0 means the detected communities have no difference to randomly detection, 1 means the detected communities is perfect fit the true communities.

For each of our experiments in this chapter, we fix the average degree d of hyper graph. Assume a hyper graph generated by nonuniform symmetric HSBM has average degree d , then

$$\begin{aligned} d &= \frac{\sum_{\kappa \in \mathcal{K}} q\left(\frac{n}{\kappa}\right) \kappa \frac{c_{\text{in}}}{n^{\kappa-1}} + \left(\binom{n}{\kappa} - q\left(\frac{n}{\kappa}\right)\right) \kappa \frac{c_{\text{out}}}{n^{\kappa-1}}}{n} \\ &= \sum_{\kappa \in \mathcal{K}} q\left(\frac{n}{\kappa}\right) \frac{\kappa}{n^\kappa} c_{\text{in}} + \left(\binom{n}{\kappa} - q\left(\frac{n}{\kappa}\right)\right) \frac{\kappa}{n^\kappa} c_{\text{out}} \end{aligned} \quad (112)$$

After given d and setting $\epsilon = \frac{c_{\text{out}}}{c_{\text{in}}}$, we have

$$\begin{aligned} c_{\text{in}} &= \frac{d}{\sum_{\kappa \in \mathcal{K}} q\left(\frac{n}{\kappa}\right) \frac{\kappa}{n^\kappa} + \epsilon \left(\binom{n}{\kappa} - q\left(\frac{n}{\kappa}\right)\right) \frac{\kappa}{n^\kappa}} \\ c_{\text{out}} &= \frac{d\epsilon}{\sum_{\kappa \in \mathcal{K}} q\left(\frac{n}{\kappa}\right) \frac{\kappa}{n^\kappa} + \epsilon \left(\binom{n}{\kappa} - q\left(\frac{n}{\kappa}\right)\right) \frac{\kappa}{n^\kappa}} \end{aligned} \quad (113)$$

We can generate a hyper graph by sample from Bernoulli distribution with probability $c_{\text{in}}/n^{\kappa-1}$ or $c_{\text{out}}/n^{\kappa-1}$ for each of $\binom{n}{\kappa}$ possible hyperedges and $\kappa \in \mathcal{K}$. When n is large enough, the high time complexity $O(n^{\max(\mathcal{K})})$ of this method makes it difficult to apply. So we use another more efficient approach to generate hyper graph with HSBM. The details of the approach is presented in Appendix G.1.

Beyond the Bethe Hessian spectral clustering Algorithm 1, we also implement the belief propagation with the assumption of symmetric HSBM based on the code in paper [18]. The main difference is the calculation of external field (81) shown in Appendix E.2 and the update of hyperedge to node message shown in Appendix G.2.

F.1 Experiment on uniform hyper graph

For a κ -uniform hyper graph generated by κ -uniform symmetric HSBM, we can get the critical ϵ^* at detectability threshold $\text{SNR}_{\text{BH}} = 1$ (9) when $\mathcal{K} = \{\kappa\}$. Considering assortative case $d_{\text{in}}^{(\kappa)} > d_{\text{out}}^{(\kappa)}$, then at the detectability threshold, we have

$$(\kappa - 1)(d_{\text{in}}^{(\kappa)} - d_{\text{out}}^{(\kappa)}) = \sqrt{(\kappa - 1)d^{(\kappa)}} \quad (114)$$

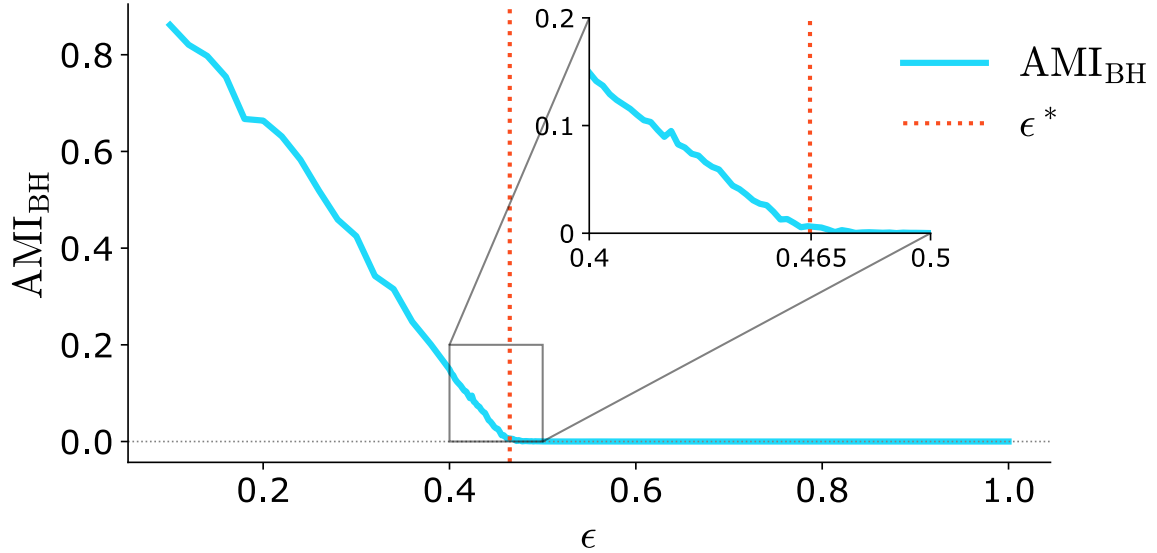


Figure 12: The experiment run on 3-uniform hyper graph. The blue line is the AMI_{BH} at different ϵ . For each point, we run experiment for 50 times. The orange vertical dash line is the critical ϵ^* where the detectability phase transition happen.

Combined with average κ -degree (8), we can get the $d_{\text{in}}^{(\kappa)}, d_{\text{out}}^{(\kappa)}$ at the detectability threshold:

$$\begin{aligned} d_{\text{in}}^{(\kappa)} &= \frac{1}{q^{\kappa-1}} \left(d^{(\kappa)} + (q^{\kappa-1} - 1) \sqrt{\frac{d^{(\kappa)}}{\kappa-1}} \right) \\ d_{\text{out}}^{(\kappa)} &= \frac{1}{q^{\kappa-1}} \left(d^{(\kappa)} - \sqrt{\frac{d^{(\kappa)}}{\kappa-1}} \right) \end{aligned} \quad (115)$$

With setting $\epsilon = \frac{c_{\text{out}}}{c_{\text{in}}}$ and relation between $d_{\text{in}}^{(\kappa)}, d_{\text{out}}^{(\kappa)}$ and $c_{\text{in}}, c_{\text{out}}$ (7), the critical ϵ^* is

$$\epsilon^* = \frac{d_{\text{out}}^{(\kappa)}}{d_{\text{in}}^{(\kappa)}} = \frac{\sqrt{d^{(\kappa)}(\kappa-1)} - 1}{\sqrt{d^{(\kappa)}(\kappa-1)} + q^{\kappa-1} - 1} \quad (116)$$

which is also shown in paper [17].

We fix the κ -uniform hyper graph size $n = 30000$, number of communities $q = 2$, order $\kappa = 3$ and average degree $d = 10$. For different ϵ , we calculate the c_{in} and c_{out} with equation (113) and generate a hyper graph with κ -uniform symmetric HSBM. Then we use Bethe Hessian method to detect communities of the hyper graph. As the result shown in Figure 12, the critical ϵ^* is close to the point that AMI_{BH} start to be 0. In this experiment, the $\epsilon^* = 0.465$.

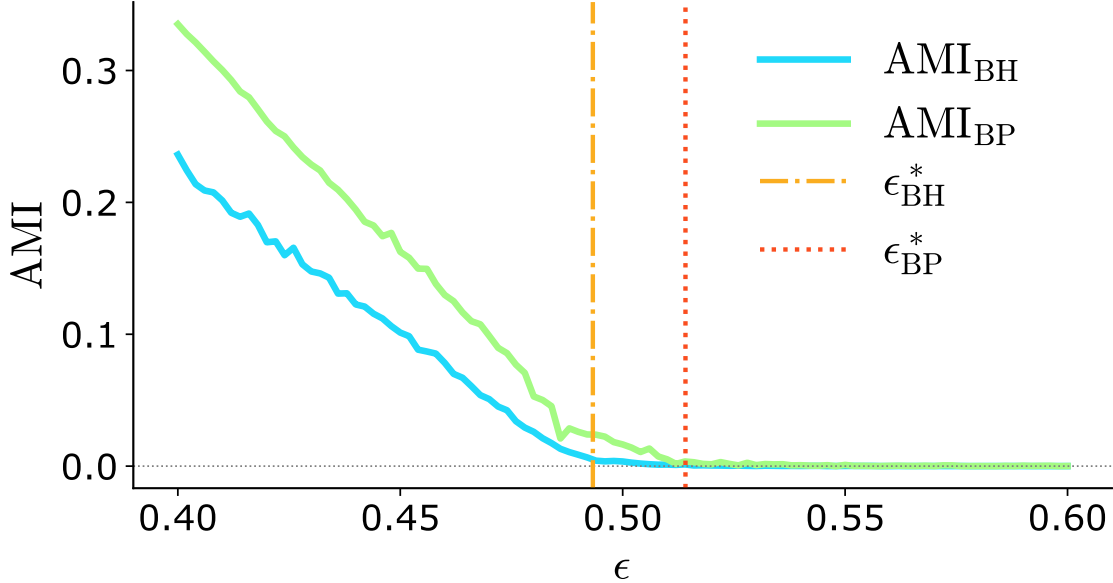


Figure 13: The experiment run on nonuniform hyper graph with 2 communities. For each ϵ , we run bethe hessian method 100 times and belief propagation for 10 times.

F.2 Experiment on nonuniform hyper graph

We fix the nonuniform hyper graph size $n = 30000$, number of communities $q = 2$, $\mathcal{K} = \{2, 3\}$ and average degree $d = 10$. For different ϵ , we calculate the c_{in} and c_{out} with equation (113) and generate a hyper graph with nonuniform symmetric HSBM. Then we use Bethe Hessian spectral clustering and belief propagation to detect communities of the hyper graph, the result is recorded as AMI_{BH} and AMI_{BP} .

We define the critical ϵ_{BH}^* and ϵ_{BP}^* corresponding with $\text{SNR}_{\text{BH}} = 1$ (9) and $\text{SNR}_{\text{BP}} = 1$ (12). As the result shown in Figure 13, the ϵ_{BH}^* is close to the point that AMI_{BH} start to be 0, the ϵ_{BP}^* is close to the point that AMI_{BP} start to be 0. These results verify that the detectability SNR_{BH} (9) of spectral clustering with Bethe Hessian is same as the non-backtracking matrix. And SNR_{BH} is weaker than detectability SNR_{BP} (12) of belief propagation, which we believe is the theoretical detectability limit.

G Implementation details of Experiment

G.1 Efficient approach to generate hyper graph with HSBM

The main idea for efficiently generating hyper graph with HSBM is to sample κ -order hyperedges for each possible combination of community assignment of the κ nodes and $\kappa \in \mathcal{K}$. We first need to find all possible ordered combination of q communities that

each community can exist multiple times. For example, if $q = 2$, then the combination of community assignment for a 3-order hyperedge could be $\{0, 0, 0\}$, $\{0, 0, 1\}$, $\{0, 1, 1\}$, $\{1, 1, 1\}$.

Then, for each of community assignment $\vec{\psi}$, we calculate the expected number of generated hyperedge as

$$m_{\vec{\psi}} = \sum_{\psi \in [q]} \binom{n \times n_{\psi}}{\#\{\psi \text{ in } \vec{\psi}\}} \mathbf{\Omega}_{\vec{\psi}} , \quad (117)$$

where $\#\{\psi \text{ in } \vec{\psi}\}$ means the occurrence count of ψ in the $\vec{\psi}$.

Finally, for each of community assignment $\vec{\psi}$, we sample hyperedges $m_{\vec{\psi}}$ times. Each sampling we random select $\#\{\psi \text{ in } \vec{\psi}\}$ nodes in community ψ for each $\psi \in \vec{\psi}$. With this approach, we reduced the time wasted on hyperedges that will not be generated.

G.2 Dynamic programming for updating hyperedge to node message

The update of hyperedge to node message can be represented as

$$\log(\hat{b}_{\psi_i}^{e \rightarrow i}) = -\log Z^{e \rightarrow i} + \log \underbrace{\sum_{\substack{\vec{\psi}_e \in [q]^{|e|-1} \\ \eta(e, i, \psi_i)}} \mathbf{C}_{\vec{\psi}_e} \prod_{j \in e/i} b_{\psi_j}^{j \rightarrow e}}_{\eta(e, i, \psi_i)} , \quad (118)$$

where $Z^{e \rightarrow i}$ is the normalization term. For simplicity, we assume $e = \{1, 2, \dots, \kappa\}$, $i = 1$, then another term $\eta(e, i, \psi_i)$ can be expand as

$$\exp(\eta(e, 1, \psi_1)) = \sum_{\psi_2 \in [q]} \sum_{\psi_3 \in [q]} \dots \sum_{\psi_{\kappa} \in [q]} \mathbf{C}_{\vec{\psi}_e} b_{\psi_2}^{2 \rightarrow e} b_{\psi_3}^{3 \rightarrow e} \dots b_{\psi_{\kappa}}^{\kappa \rightarrow e} . \quad (119)$$

There are $(\kappa - 1)q^{\kappa-1}$ times of multiplication if we directly calculate $\eta(e, 1, \psi_1)$, which is unacceptable for high order κ . However, based on the specific \mathbf{C} (6) in the symmetric

HSBM, we can calculate $\eta(e, i, \psi_i)$ with dynamic programming

$$\begin{aligned}
\exp(\eta(e, 1, \psi_1)) &= \sum_{\psi_\kappa \in [q]} b_{\psi_\kappa}^{\kappa \rightarrow e} \sum_{\psi_2 \in [q]} \sum_{\psi_3 \in [q]} \dots \sum_{\psi_{\kappa-1} \in [q]} C_{\psi_e} b_{\psi_2}^{2 \rightarrow e} b_{\psi_3}^{3 \rightarrow e} \dots b_{\psi_{\kappa-1}}^{\kappa-1 \rightarrow e} \\
&= \sum_{\psi_\kappa \in [q]/\psi_1} b_{\psi_\kappa}^{\kappa \rightarrow e} \sum_{\psi_2 \in [q]} \sum_{\psi_3 \in [q]} \dots \sum_{\psi_{\kappa-1} \in [q]} c_{\text{out}} b_{\psi_2}^{2 \rightarrow e} b_{\psi_3}^{3 \rightarrow e} \dots b_{\psi_{\kappa-1}}^{\kappa-1 \rightarrow e} \\
&\quad \underbrace{\exp(\eta(e/\kappa, 1, \psi_1)) + (c_{\text{out}} - c_{\text{in}}) b_{\psi_1}^{2 \rightarrow e} b_{\psi_1}^{3 \rightarrow e} \dots b_{\psi_1}^{\kappa-1 \rightarrow e}}_{\exp(\eta(e/\kappa, 1, \psi_1))} \\
&\quad + b_{\psi_1}^{\kappa \rightarrow e} \sum_{\psi_2 \in [q]} \sum_{\psi_3 \in [q]} \dots \sum_{\psi_{\kappa-1} \in [q]} C_{\psi_e} b_{\psi_2}^{2 \rightarrow e} b_{\psi_3}^{3 \rightarrow e} \dots b_{\psi_{\kappa-1}}^{\kappa-1 \rightarrow e} \\
&\quad \underbrace{\exp(\eta(e/\kappa, 1, \psi_1))}_{\exp(\eta(e/\kappa, 1, \psi_1))} \\
&= \sum_{\psi_\kappa \in [q]} b_{\psi_\kappa}^{\kappa \rightarrow e} \exp(\eta(e/\kappa, 1, \psi_1)) + (c_{\text{out}} - c_{\text{in}}) \sum_{\psi_\kappa \in [q]/\psi_1} b_{\psi_\kappa}^{\kappa \rightarrow e} b_{\psi_1}^{2 \rightarrow e} b_{\psi_1}^{3 \rightarrow e} \dots b_{\psi_1}^{\kappa-1 \rightarrow e} \\
&= \exp(\eta(e/\kappa, 1, \psi_1)) + (c_{\text{out}} - c_{\text{in}}) \sum_{\psi_\kappa \in [q]/\psi_1} b_{\psi_\kappa}^{\kappa \rightarrow e} b_{\psi_1}^{2 \rightarrow e} b_{\psi_1}^{3 \rightarrow e} \dots b_{\psi_1}^{\kappa-1 \rightarrow e}
\end{aligned} \tag{120}$$

By removing nodes of e one by one from κ , finally we can get

$$\begin{aligned}
\exp(\eta(\{1, 2\}, 1, \psi_1)) &= c_{\text{in}} b_{\psi_1}^{2 \rightarrow \{1, 2\}} + c_{\text{out}} \sum_{\psi_2 \in [q]/\psi_1} b_{\psi_2}^{2 \rightarrow \{1, 2\}} \\
&= c_{\text{in}} + (c_{\text{out}} - c_{\text{in}}) \sum_{\psi_2 \in [q]/\psi_1} b_{\psi_2}^{2 \rightarrow \{1, 2\}}
\end{aligned} \tag{121}$$

The number of multiplication of (121) is $\kappa + \kappa - 1 + \dots + 2 = O(\kappa^2)$ which is smaller than directly calculation of (119) for high order κ .

H Supplementary analysis: community structure dominated by hyperedge order and shape.

We designed a supplementary experiment to investigate how the dominance of different hyperedge orders influences the detected community structure using Bethe Hessian-based Spectral Clustering. We consider a hypergraph of n nodes equally partitioned into $q = 4$ communities, $\{0, 1, 2, 3\}$. The structure is designed to favor two competing community patterns: all the κ -hyperedges are placed between nodes in communities $\{0, 2\}$ or $\{1, 3\}$, all the κ^* -hyperedges are placed between communities $\{0, 1\}$ or $\{2, 3\}$, as illustrated in Figure 14.

If we apply Bethe Hessian-based spectral clustering algorithm 1 to detect 2 communities in this hypergraph considering only the assortative case, two distinct, coarse-grained community structures could be detected:

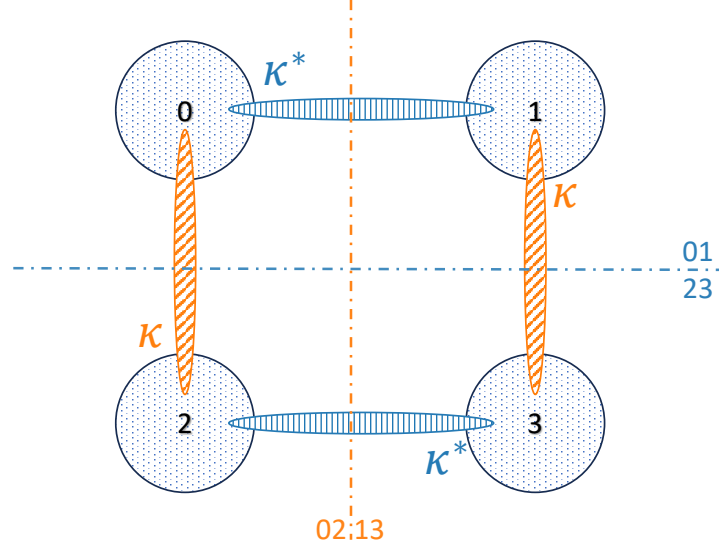


Figure 14: *Illustration of community structure of hypergraph used in experiment for exploring the effect of order to detectability.*

- κ^* -dominated structure with communities $\{0, 1\}$ are merged into one community, $\{2, 3\}$ are merged into the second.
- κ -dominated structure with communities $\{0, 2\}$ are merged into one community, $\{1, 3\}$ are merged into the second.

Intuitively, if the number of κ -order hyperedges $|\mathcal{E}^{(\kappa)}|$ significantly outweighs $|\mathcal{E}^{(\kappa^*)}|$, the κ -dominated community structure should prevail. Our objective is to determine the critical switching ratio of $|\mathcal{E}^{(\kappa)}|$ and $|\mathcal{E}^{(\kappa^*)}|$, at which the detected community structure transitions from the κ^* -dominated structure to the κ -dominated one.

H.1 Simple case with $\kappa = 2, \kappa^* = 3$

We first consider a simplified scenario with $\kappa = 2, \kappa^* = 3$. To generate the hypergraph shown in Figure 14 using the HSBM, we define the affinity tensors as follows:

$$\begin{aligned} \mathbf{C}_z^{(2)} &= \begin{cases} a, & z \in \{(0, 2), (2, 0), (1, 3), (3, 1)\} \\ 0, & \text{otherwise} \end{cases} \\ \mathbf{C}_z^{(3)} &= \begin{cases} a^*, & z \in \{(0, 0, 1), (0, 1, 0), (1, 0, 1), \\ & (0, 1, 1), (1, 0, 1), (1, 1, 0), \\ & (2, 2, 3), (2, 3, 2), (3, 2, 2), \\ & (2, 3, 3), (3, 2, 3), (3, 3, 2)\} \\ 0, & \text{otherwise} \end{cases}, \end{aligned} \quad (122)$$

where a and a^* are adjusted parameters. By observing the definition of $\widehat{c}_{ab}^{(\kappa)}$ in Appendix D, we can construct the matrix $\widehat{\mathbf{C}}^{(\kappa)}$ by fixing two dimensions and aggregating the remaining $\kappa - 2$ dimension of scaled affinity tensor $\frac{1}{q^{\kappa-2}(\kappa-2)!} \mathbf{C}^{(\kappa)}$. In this scenario, we calculate the corresponding 4×4 matrices $\widehat{\mathbf{C}}^{(2)}$ and $\widehat{\mathbf{C}}^{(3)}$:

$$\begin{aligned} \widehat{\mathbf{C}}^{(2)} &= \frac{1}{4^{2-2}(2-2)!} \begin{bmatrix} 0, & 0, & a, & 0 \\ 0, & 0, & 0, & a \\ a, & 0, & 0, & 0 \\ 0, & a, & 0, & 0 \end{bmatrix} \\ \widehat{\mathbf{C}}^{(3)} &= \frac{1}{4^{3-2}(3-2)!} \begin{bmatrix} a^*, & 2a^*, & 0, & 0 \\ 2a^*, & a^*, & 0, & 0 \\ 0, & 0, & a^*, & 2a^* \\ 0, & 0, & 2a^*, & a^* \end{bmatrix}. \end{aligned} \quad (123)$$

We utilize the SNR_{BH} based on $\widehat{\mathbf{C}}^{(\kappa)}$ as shown in (71), as

$$\text{SNR}_{\text{BH}} := \frac{\left(\sum_{\kappa \in \mathcal{K}} \widehat{c}_{\text{in}}^{(\kappa)} - \widehat{c}_{\text{out}}^{(\kappa)} \right)^2}{q^2 \sum_{\kappa \in \mathcal{K}} (\kappa - 1) d^{(\kappa)}}, \quad (124)$$

where $d^{(\kappa)} = \frac{\widehat{c}_{\text{in}}^{(\kappa)} + (q-1)\widehat{c}_{\text{out}}^{(\kappa)}}{q(\kappa-1)}$. This formulation allows us to leverage techniques from the detectability analysis of hierarchical community structures on network [25]. The finest 4 communities $\{0, 1, 2, 3\}$ and two coarse-grained community structure, the κ -dominated $\{\{0, 2\}, \{1, 3\}\}$, the κ^* -dominated $\{\{0, 1\}, \{2, 3\}\}$, form two hierarchical community structure. We can aggregate the matrix $\widehat{\mathbf{C}}^{(2)}$ and $\widehat{\mathbf{C}}^{(3)}$ by different coarser communities to form 2×2 matrices, and then derive their corresponding $\text{SNR}_{\text{BH} 02;13}$ and $\text{SNR}_{\text{BH} 01;23}$ based on (124). Although $\text{SNR}_{\text{BH} 02;13} = 1$ or $\text{SNR}_{\text{BH} 01;23} = 1$ can not rigorously be the detectability limit for κ or κ^* dominated community structure, the switching point between

the these two competing community structure can be approximated by solving for the equality $\text{SNR}_{\text{BH } 02;13} = \text{SNR}_{\text{BH } 01;23}$.

For the κ^* dominated community structure, the aggregation process of $\hat{\mathbf{C}}$ is by averaging each block defined by the community partition $\{\{0, 1\}, \{2, 3\}\}$. Using the matrices in (123), the aggregated matrices $\hat{\mathbf{C}}_{(\kappa^*)}$ are thus calculated as:

$$\begin{aligned}\hat{\mathbf{C}}_{(\kappa^*)}^{(2)} &= \begin{bmatrix} 0, & a/2 \\ a/2, & 0 \end{bmatrix} \\ \hat{\mathbf{C}}_{(\kappa^*)}^{(3)} &= \frac{1}{4} \begin{bmatrix} \frac{3}{2}a^*, & 0 \\ 0, & \frac{3}{2}a^* \end{bmatrix}.\end{aligned}\quad (125)$$

The average κ -degree $d^{(\kappa)}$ can be calculated by the average of one row of $\frac{1}{\kappa-1}\hat{\mathbf{C}}^{(\kappa)}$, which remains constant regardless of the aggregation process above:

$$\begin{aligned}d^{(2)} &= \frac{a}{4} \\ d^{(3)} &= \frac{3a^*}{32}.\end{aligned}\quad (126)$$

Then based on (124), we have

$$\text{SNR}_{\text{BH } 01;23} = \frac{(-\frac{a}{2} + \frac{3}{8}a^*)^2}{2^2[(2-1)d^{(2)} + (3-1)d^{(3)}]}.\quad (127)$$

Similarly, for the κ -dominated community structure $\{\{0, 2\}, \{1, 3\}\}$, the aggregated matrices are:

$$\begin{aligned}\hat{\mathbf{C}}_{(\kappa)}^{(2)} &= \begin{bmatrix} a/2, & 0 \\ 0, & a/2 \end{bmatrix} \\ \hat{\mathbf{C}}_{(\kappa)}^{(3)} &= \frac{1}{4} \begin{bmatrix} \frac{1}{2}a^*, & a^* \\ a^*, & \frac{1}{2}a^* \end{bmatrix},\end{aligned}\quad (128)$$

leading to

$$\text{SNR}_{\text{BH } 02;13} = \frac{(\frac{a}{2} + \frac{1}{8}a^* - \frac{1}{4}a^*)^2}{2^2[(2-1)d^{(2)} + (3-1)d^{(3)}]}.\quad (129)$$

Solving for the switching point $\text{SNR}_{\text{BH } 01;23} = \text{SNR}_{\text{BH } 02;13}$:

$$\begin{aligned}(-\frac{a}{2} + \frac{3}{8}a^*)^2 &= (\frac{a}{2} + \frac{a^*}{8} - \frac{a^*}{4})^2 \\ (\frac{3a^*}{8})^2 - \frac{3}{8}aa^* &= (\frac{a^*}{8})^2 - \frac{1}{8}aa^* \\ \frac{1}{8}(a^*)^2 - \frac{1}{4}aa^* &= 0 \\ \frac{a}{a^*} &= \frac{1}{2}\end{aligned}\quad (130)$$

Thus, the theoretical switching condition for the affinity tensor parameters is $\frac{a}{a^*} = \frac{1}{2}$.

To determine the corresponding hyperedge ratio $\rho = |\mathcal{E}^{(2)}|/|\mathcal{E}^{(3)}|$, we estimate $|\mathcal{E}^{(\kappa)}|$ using the approximate formula:

$$\begin{aligned} |\mathcal{E}^{(\kappa)}| &= 2 \left[\binom{2n/q}{\kappa} - 2 \binom{n/q}{\kappa} \right] \frac{a}{n^{\kappa-1}} \\ &\approx \frac{2a}{n^{\kappa-1} \kappa!} [(2n/q)^\kappa - 2(n/q)^\kappa] \quad . \\ &= \frac{2an}{q^\kappa \kappa!} (2^\kappa - 2) \end{aligned} \quad (131)$$

Substituting $\kappa = 2$, $\kappa^* = 3$ and $q = 4$, we have

$$\rho_{theo}^* = \frac{|\mathcal{E}^{(2)}|}{|\mathcal{E}^{(3)}|} = \frac{2a/(4^2 2!)}{6a^*/(4^3 3!)} = 4 \frac{a}{a^*} = 2 \quad . \quad (132)$$

The theoretical switching point in terms of the hyperedge ratio is $\rho_{theo}^* = 2$.

To experimentally observe the transition, we conducted a simulation using Bethe Hessian based-spectral clustering to detect 2 communities on hypergraphs generated by fixing the total average degree d and varying the ratio ρ . By definition:

$$\begin{aligned} d &= \frac{\kappa |\mathcal{E}^{(\kappa)}| + \kappa^* |\mathcal{E}^{(\kappa^*)}|}{n} \\ \rho &= \frac{|\mathcal{E}^{(\kappa)}|}{|\mathcal{E}^{(\kappa^*)}|} \end{aligned} \quad . \quad (133)$$

Solving these relations for the hyperedge counts, we get:

$$\begin{aligned} |\mathcal{E}^{(\kappa^*)}| &= \frac{nd}{\kappa\rho + \kappa^*} \\ |\mathcal{E}^{(\kappa)}| &= \frac{nd\rho}{\kappa\rho + \kappa^*} \end{aligned} \quad . \quad (134)$$

Using the estimation of $|\mathcal{E}^{(\kappa)}|$ in (131), we derive the affinity tensor parameters a and a^* :

$$\begin{aligned} a &= \frac{4^\kappa \kappa! d \rho}{2(2^\kappa - 2)(\kappa\rho + \kappa^*)} \\ a^* &= \frac{4^{\kappa^*} \kappa^*! d}{2(2^{\kappa^*} - 2)(\kappa\rho + \kappa^*)} \end{aligned} \quad . \quad (135)$$

Based on these derived values for a and a^* , we set up the affinity tensor and generated the hypergraph for community detection. The results are shown in Figure 15.

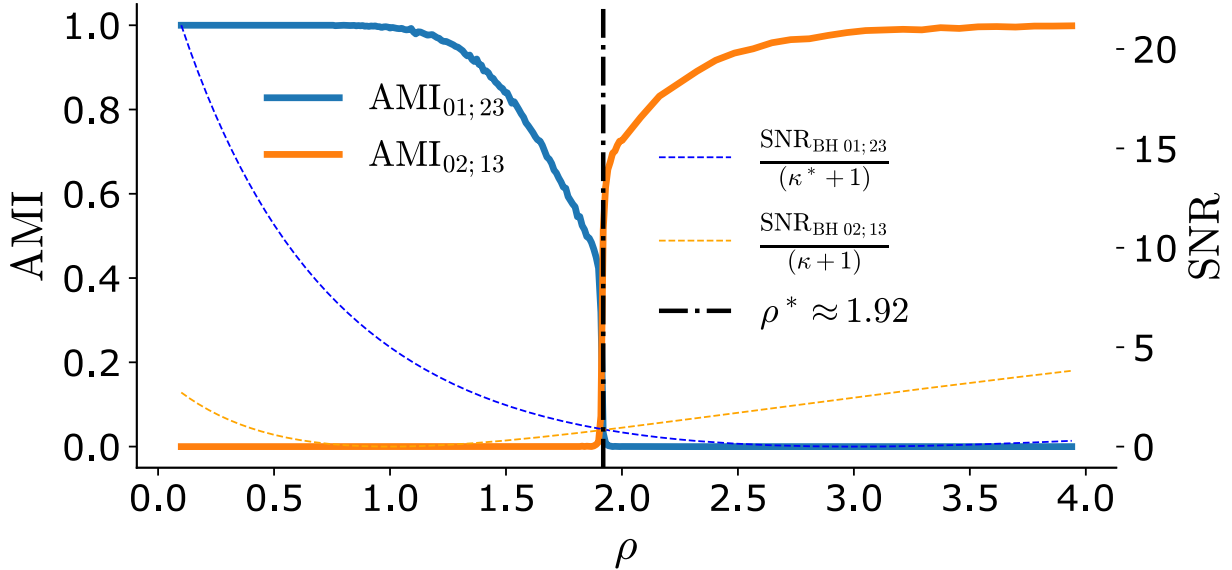


Figure 15: *Experimental results with $n = 8000$, $d = 50$, $\kappa = 2$ and $\kappa^* = 3$. We show the $\text{AMI}_{01;23}$ and $\text{AMI}_{02;13}$ as the AMI of detected communities by Bethe Hessian based-spectral clustering to the κ^* and κ dominated community structure.*

We observed that the derived ρ_{theo}^* has a little bias to the sharp transition point. Instead, the transition point ρ^* can be better aligned by the cross point of two manually modified $\text{SNR}_{\text{BH } 01;23}$ and $\text{SNR}_{\text{BH } 02;13}$:

$$\frac{\text{SNR}_{\text{BH } 01;23}}{\kappa^* + 1} = \frac{\text{SNR}_{\text{BH } 02;13}}{\kappa + 1} . \quad (136)$$

Next, we proceed to consider a more general case with arbitrary κ and κ^* .

H.2 General case with arbitrary κ , κ^*

Similar as last section, we first define the affinity tensor under scenario of arbitrary κ , κ^* :

$$\begin{aligned} C_z^{(\kappa)} &= \begin{cases} a, & z \in \{\{(0, 2)^\kappa / (0)^\kappa, (2)^\kappa\}, \{(1, 3)^\kappa / (1)^\kappa, (3)^\kappa\}\} \\ 0, & \text{otherwise} \end{cases} \\ C_z^{(\kappa^*)} &= \begin{cases} a^*, & z \in \{\{(0, 1)^{\kappa^*} / (0)^{\kappa^*}, (1)^{\kappa^*}\}, \{(2, 3)^{\kappa^*} / (2)^{\kappa^*}, (3)^{\kappa^*}\}\} \\ 0, & \text{otherwise} \end{cases} \end{aligned} , \quad (137)$$

where $(\dots)^\kappa$ means all κ -length permutations of index, such as $(0, 2)^\kappa$ is all κ -length index which exclusively include 0 or 2, $(0)^\kappa$ is $\underbrace{(0, 0, \dots, 0)}_{\kappa}$. Then we aggregate all other

$\kappa - 2$ dimension of tensor $\frac{1}{q^{\kappa-2}(\kappa-2)!} \mathbf{C}^{(\kappa)}$ and $\frac{1}{q^{\kappa^*-2}(\kappa^*-2)!} \mathbf{C}^{(\kappa^*)}$, derive the matrices $\widehat{\mathbf{C}}^{(\kappa)}$ and $\widehat{\mathbf{C}}^{(\kappa^*)}$:

$$\widehat{\mathbf{C}}^{(\kappa)} = \frac{1}{4^{\kappa-2}(\kappa-2)!} \begin{bmatrix} 2^{\kappa-2}-1, & 0, & 2^{\kappa-2}, & 0 \\ 0, & 2^{\kappa-2}-1, & 0, & 2^{\kappa-2} \\ 2^{\kappa-2}, & 0, & 2^{\kappa-2}-1, & 0 \\ 0, & 2^{\kappa-2}, & 0, & 2^{\kappa-2}-1 \end{bmatrix} a \quad . \quad (138)$$

$$\widehat{\mathbf{C}}^{(\kappa^*)} = \frac{1}{4^{\kappa^*-2}(\kappa^*-2)!} \begin{bmatrix} 2^{\kappa^*-2}-1, & 2^{\kappa^*-2}, & 0, & 0 \\ 2^{\kappa^*-2}, & 2^{\kappa^*-2}-1, & 0, & 0 \\ 0, & 0, & 2^{\kappa^*-2}-1, & 2^{\kappa^*-2} \\ 0, & 0, & 2^{\kappa^*-2}, & 2^{\kappa^*-2}-1 \end{bmatrix} a^* \quad .$$

Before aggregation with different coarse-grained community structure, we first derive $d^{(\kappa)}$ and $d^{(\kappa^*)}$ since they remain constant after the aggregation:

$$\begin{aligned} d^{(\kappa)} &= \frac{1}{\kappa-1} \frac{a}{4^{\kappa-2}(\kappa-2)!} \frac{2*2^{\kappa-2}-1}{4} \\ &= \frac{a}{4^{\kappa-1}(\kappa-1)!} (2^{\kappa-1}-1) \quad . \end{aligned} \quad (139)$$

$$d^{(\kappa^*)} = \frac{a^*}{4^{\kappa^*-1}(\kappa^*-1)!} (2^{\kappa^*-1}-1)$$

For κ^* -dominated community structure, $\{\{0, 1\}, \{2, 3\}\}$, the aggregated matrices $\widehat{\mathbf{C}}^{(\kappa^*)}$ are:

$$\widehat{\mathbf{C}}_{(\kappa^*)}^{(\kappa)} = \frac{a}{4^{\kappa-2}(\kappa-2)!} \begin{bmatrix} (2^{\kappa-2}-1)/2, & (2^{\kappa-2})/2 \\ (2^{\kappa-2})/2, & (2^{\kappa-2}-1)/2 \end{bmatrix} \quad , \quad (140)$$

$$\widehat{\mathbf{C}}_{(\kappa^*)}^{(\kappa^*)} = \frac{a^*}{4^{\kappa^*-2}(\kappa^*-2)!} \begin{bmatrix} 2^{\kappa^*-2}-\frac{1}{2}, & 0 \\ 0, & 2^{\kappa^*-2}-\frac{1}{2} \end{bmatrix}$$

leading to

$$\text{SNR}_{\text{BH } 01;23} = \frac{\left[-\frac{a}{4^{\kappa-2}(\kappa-2)!} \frac{1}{2} + \frac{a^*}{4^{\kappa^*-2}(\kappa^*-2)!} (2^{\kappa^*-2}-\frac{1}{2}) \right]^2}{2^2[(\kappa-1)d^{(\kappa)} + (\kappa^*-1)d^{(\kappa^*)}]} \quad . \quad (141)$$

For κ -dominated community structure, $\{\{0, 2\}, \{1, 3\}\}$, the aggregated matrices $\widehat{\mathbf{C}}^{(\kappa)}$ are:

$$\widehat{\mathbf{C}}_{(\kappa)}^{(\kappa)} = \frac{a}{4^{\kappa-2}(\kappa-2)!} \begin{bmatrix} 2^{\kappa-2}-\frac{1}{2}, & 0 \\ 0, & 2^{\kappa-2}-\frac{1}{2} \end{bmatrix} \quad , \quad (142)$$

$$\widehat{\mathbf{C}}_{(\kappa)}^{(\kappa^*)} = \frac{a^*}{4^{\kappa^*-2}(\kappa^*-2)!} \begin{bmatrix} (2^{\kappa^*-2}-1)/2, & (2^{\kappa^*-2})/2 \\ (2^{\kappa^*-2})/2, & (2^{\kappa^*-2}-1)/2 \end{bmatrix}$$

leading to

$$\text{SNR}_{\text{BH } 02;13} = \frac{\left[\frac{a}{4^{\kappa-2}(\kappa-2)!} (2^{\kappa-2} - \frac{1}{2}) - \frac{a^*}{4^{\kappa^*-2}(\kappa^*-2)!} \frac{1}{2} \right]^2}{2^2[(\kappa-1)d^{(\kappa)} + (\kappa^*-1)d^{(\kappa^*)}]} . \quad (143)$$

Next, we solve for the switching point $\text{SNR}_{\text{BH } 01;23} = \text{SNR}_{\text{BH } 02;13}$. For convenience, we define

$$\begin{aligned} b &= \frac{a}{4^{\kappa-2}(\kappa-2)!} \\ b^* &= \frac{a^*}{4^{\kappa^*-2}(\kappa^*-2)!} , \end{aligned} \quad (144)$$

then

$$\begin{aligned} \text{SNR}_{\text{BH } 01;23} &= \text{SNR}_{\text{BH } 02;13} \\ (b^* 2^{\kappa^*-2} - \frac{b}{2} - \frac{b^*}{2})^2 &= (b 2^{\kappa-2} - \frac{b}{2} - \frac{b^*}{2})^2 \\ (b^* 2^{\kappa^*-2})^2 - 2^{\kappa^*-2} b b^* - 2^{\kappa^*-2} (b^*)^2 &= (b 2^{\kappa-2})^2 - 2^{\kappa-2} b b^* - 2^{\kappa-2} (b)^2 \\ 2^{\kappa^*-2} (2^{\kappa^*-2} - 1) (b^*)^2 - (2^{\kappa^*-2} - 2^{\kappa-2}) b b^* - 2^{\kappa-2} (2^{\kappa-2} - 1) b^2 &= 0 \\ (2^{\kappa^*-2} b^* - 2^{\kappa-2} b) \underbrace{[(2^{\kappa^*-2} - 1) b^* + (2^{\kappa-2} - 1) b]}_{+} &= 0 \\ \frac{b}{b^*} &= \frac{2^{\kappa^*-2}}{2^{\kappa-2}} \\ \frac{a}{a^*} \frac{4^{\kappa^*-2}(\kappa^*-2)!}{4^{\kappa-2}(\kappa-2)!} &= \frac{2^{\kappa^*-2}}{2^{\kappa-2}} \\ \frac{a}{a^*} &= \frac{2^{\kappa-2}(\kappa-2)!}{2^{\kappa^*-2}(\kappa^*-2)!} \end{aligned} \quad (145)$$

Based on the formula for $|\mathcal{E}^{(\kappa)}|$ in (131), the hyperedge ratio at the switching point is

$$\begin{aligned} \rho_{\text{theo}}^* &= \frac{|\mathcal{E}^{(\kappa)}|}{|\mathcal{E}^{(\kappa^*)}|} = \frac{\frac{2an}{q^\kappa \kappa!} (2^\kappa - 2)}{\frac{2a^* n}{q^{\kappa^*} \kappa^*!} (2^{\kappa^*} - 2)} \\ &= \frac{(2^\kappa - 2)/(4^\kappa \kappa!)}{(2^{\kappa^*} - 2)/(4^{\kappa^*} \kappa^*!)} \frac{a}{a^*} \\ &= \frac{2^{\kappa-2}(\kappa-2)! (2^\kappa - 2)/(4^\kappa \kappa!)}{2^{\kappa^*-2}(\kappa^*-2)! (2^{\kappa^*} - 2)/(4^{\kappa^*} \kappa^*!)} \\ &= \frac{(2^\kappa - 2)/(2^{\kappa+2} \kappa (\kappa-1))}{(2^{\kappa^*} - 2)/(2^{\kappa^*+2} \kappa^* (\kappa^*-1))} \\ &= 2^{\kappa^* - \kappa} \frac{2^{\kappa-1} - 1}{2^{\kappa^*-1} - 1} \frac{\binom{\kappa^*}{2}}{\binom{\kappa}{2}} \end{aligned} \quad (146)$$

However, we still find this switching point has a little bias to the actual transition point, which can be better aligned by:

$$\frac{\text{SNR}_{\text{BH } 01;23}}{\kappa^* + 1} = \frac{\text{SNR}_{\text{BH } 02;13}}{\kappa + 1} , \quad (147)$$

as shown in Figure 16.

H.3 Community structure dominated by hyperedge shape

Beyond the order of hyperedges, their "shape"—the way nodes are distributed across communities—also significantly influences the detection of coarse-grained community structures. To investigate this, we designed an experiment using a hypergraph with a finest community structure of four communities $\{0, 1, 2, 3\}$, where all hyperedges are of order 4. We define two distinct hyperedge shapes based on their node distribution:

- Balanced hyperedges: These 4-order hyperedges span two communities by connecting two nodes from one community and two from another. In our model, these only exist between the community pairs $\{0, 1\}$ or $\{2, 3\}$.
- Imbalanced hyperedges: These 4-order hyperedges span two communities by connecting one node from one community and three from another. In our model, these only exist between the community pairs $\{0, 2\}$ or $\{1, 3\}$.

This setup, illustrated in Figure 17 (a), creates two competing coarse-grained community structures: one based on balanced hyperedges $\{\{0, 1\}, \{2, 3\}\}$ and another based on imbalanced hyperedges $\{\{0, 2\}, \{1, 3\}\}$.

To generate this hypergraph using the HSBM, we define the affinity tensor $\mathbf{C}^{(4)}$ as follows. Let a^* be the affinity parameter for balanced hyperedges and a for imbalanced ones:

$$\mathbf{C}_{\mathbf{z}}^{(4)} = \begin{cases} a, & \mathbf{z} \in \{(0, 0, 0, 2), (0, 0, 2, 0), (0, 2, 0, 0), (2, 0, 0, 0) \\ & (0, 2, 2, 2), (2, 0, 2, 2), (2, 2, 0, 2), (2, 2, 2, 0) \\ & (1, 1, 1, 3), (1, 1, 3, 1), (1, 3, 1, 1), (3, 1, 1, 1) \\ & (3, 3, 3, 1), (3, 3, 1, 3), (3, 1, 3, 3), (1, 3, 3, 3)\} \\ a^*, & \mathbf{z} \in \{(0, 0, 1, 1), (0, 1, 1, 0), (0, 1, 0, 1), \\ & (1, 0, 0, 1), (1, 1, 0, 0), (1, 0, 1, 0), \\ & (2, 2, 3, 3), (2, 3, 2, 3), (2, 3, 3, 2), \\ & (3, 2, 2, 3), (3, 2, 3, 2), (3, 3, 2, 2)\} \\ 0, & \text{otherwise} \end{cases} . \quad (148)$$

For consistency, we denote the expected number of balanced hyperedges as $|\mathcal{E}^{(\kappa^*)}|$ and

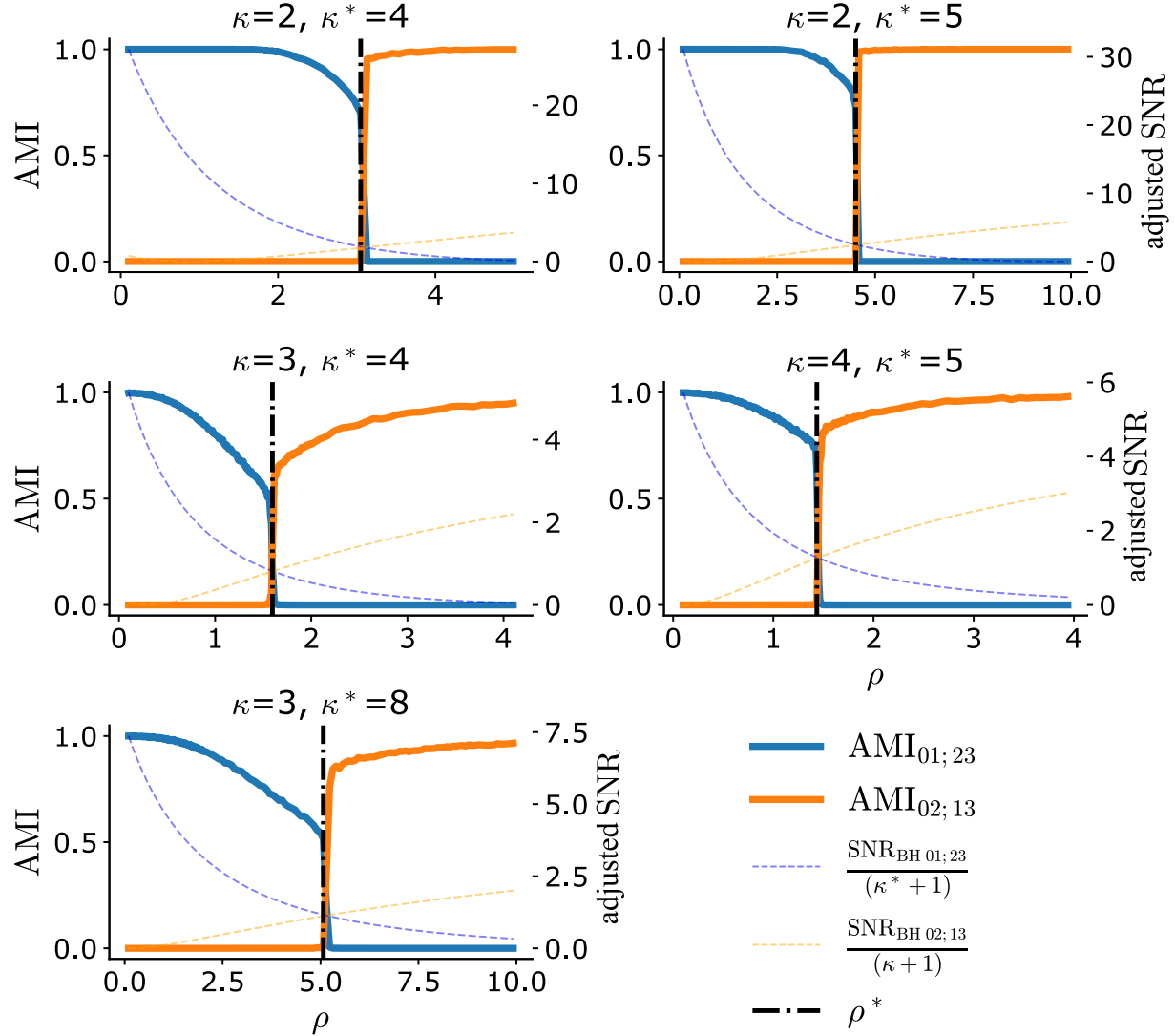
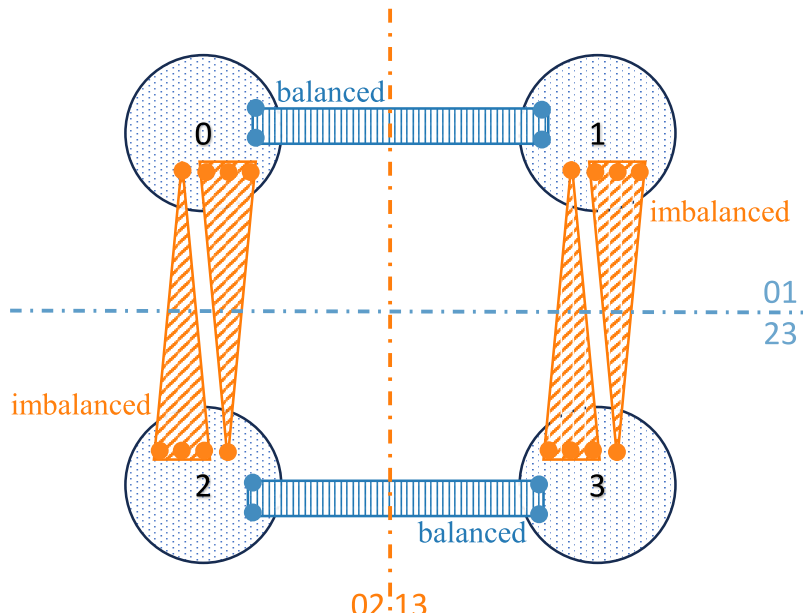


Figure 16: *Experimental results with general κ and κ^* .* All experiments are proceed on $n = 8000$ hypergraphs. For first row, the average degree $d = 50$ for better observing the sharp transition. For others $d = 10$ is enough. We show the $\text{AMI}_{01;23}$ and $\text{AMI}_{02;13}$ as the AMI of detected communities by Bethe Hessian based-spectral clustering to the κ^* and κ dominated community structure.

(a)



(b)

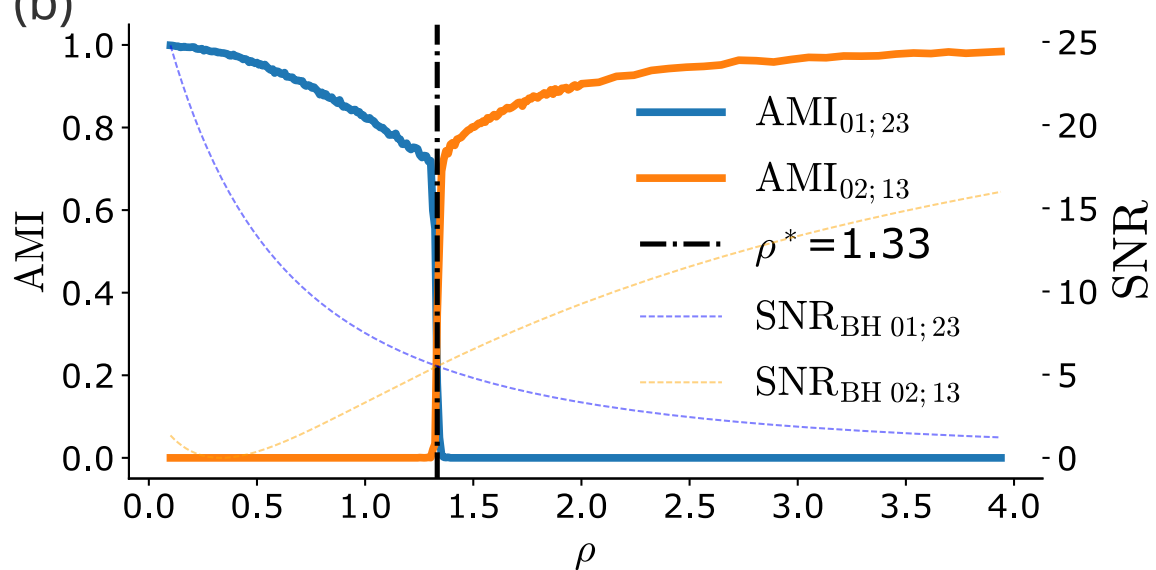


Figure 17: (a) Illustration of community structure of hypergraph used in experiment for exploring the effect of shape to detectability. All the hyperedges are 4-order, only the different shape. The hyperedges shaped by rectangle between communities $\{0, 1\}$ or $\{2, 3\}$ are balanced, the hyperedges shaped by triangle between communities $\{0, 2\}$ or $\{1, 3\}$ are imbalanced. (b) Experimental results with $n = 8000$, $d = 10$, $\kappa = 4$ and $\kappa^* = 4$. We show the AMI_{κ^*} and AMI_{κ} as the AMI of detected communities by Bethe Hessian based-spectral clustering to community structure dominated by balanced and imbalanced 4-order hyperedges.

imbalanced hyperedges as $|\mathcal{E}^{(\kappa)}|$. These can be calculated as:

$$\begin{aligned} |\mathcal{E}^{(\kappa^*)}| &= 2 \binom{n/q}{2} \binom{n/q}{2} \frac{a^*}{n^3} = 2 \frac{(n/q)^4}{4} \frac{a^*}{n^3} = 2 \frac{na^*}{4 * 4^4} \\ |\mathcal{E}^{(\kappa)}| &= 4 \binom{n/q}{3} \binom{n/q}{1} \frac{a}{n^3} = 4 \frac{(n/q)^4}{6} \frac{a}{n^3} = 4 \frac{na}{6 * 4^4} \end{aligned} \quad (149)$$

Using the definitions (133) of average degree d and the hyperedge ratio $\rho = |\mathcal{E}^{(\kappa)}|/|\mathcal{E}^{(\kappa^*)}|$ from previous section, we can express the parameters a and a^* as:

$$\begin{aligned} a &= \frac{6 * 4^4 d \rho}{4(4\rho + 4)} = \frac{6 * 4^2 d \rho}{\rho + 1} \\ a^* &= \frac{4 * 4^4 d}{2(4\rho + 4)} = \frac{2 * 4^3 d}{\rho + 1} \end{aligned} \quad (150)$$

As shown in the experimental results in Figure 17 (b), the Bethe Hessian-based spectral clustering algorithm's preference switches from the balanced to the imbalanced community structure at a point $\rho_{\text{theo}}^* \neq 1$. This empirically confirms that the hyperedge shape directly affects community detectability. To theoretically predict this switching point, we analyze under similar routine to previous sections.

First, we derive the matrix $\widehat{\mathbf{C}}^{(4)}$:

$$\widehat{\mathbf{C}}^{(4)} = \frac{1}{4^{4-2}(4-2)!} \begin{bmatrix} a^* + 2a, & 2a^*, & 2a, & 0 \\ 2a^*, & a^* + 2a, & 0, & 2a \\ 2a, & 0, & a^* + 2a, & 2a^* \\ 0, & 2a, & 2a^*, & a^* + 2a \end{bmatrix} \quad (151)$$

Aggregating this matrix according to the community structure dominated by balanced 4-order hyperedge $\{\{0, 1\}, \{2, 3\}\}$ yields:

$$\widehat{\mathbf{C}}_{(\kappa^*)}^{(4)} = \frac{1}{32} \begin{bmatrix} \frac{3}{2}a^* + a, & a \\ a, & \frac{3}{2}a^* + a \end{bmatrix} \Rightarrow \text{SNR}_{\text{BH } 01;23} = \frac{1}{2^2(4-1)d^{(4)}} \left(\frac{1}{32} \frac{3}{2}a^* \right)^2 \quad (152)$$

Similarly, aggregating for the community structure dominated by imbalanced 4-order hyperedge $\{\{0, 2\}, \{1, 3\}\}$ gives:

$$\widehat{\mathbf{C}}_{(\kappa)}^{(4)} = \frac{1}{32} \begin{bmatrix} \frac{1}{2}a^* + 2a, & a^* \\ a^*, & \frac{1}{2}a^* + 2a \end{bmatrix} \Rightarrow \text{SNR}_{\text{BH } 02;13} = \frac{1}{2^2(4-1)d^{(4)}} \left(\frac{1}{32} (2a - \frac{1}{2}a^*) \right)^2 \quad (153)$$

To find the switching point, we solve the $\text{SNR}_{\text{BH } 01;23} = \text{SNR}_{\text{BH } 02;13}$:

$$\begin{aligned}
\text{SNR}_{\text{BH } 01;23} &= \text{SNR}_{\text{BH } 02;13} \\
\left(\frac{3}{2}a^*\right)^2 &= \left(2a - \frac{1}{2}a^*\right)^2 \\
2(a^*)^2 - 4a^2 + 2aa^* &= 0 \\
(a^* - a)(a^* + 2a) &= 0 \\
a &= a^*
\end{aligned} \tag{154}$$

Last, to find the corresponding ratio of hyperedge counts ρ_{theo}^* , we substitute $a = a^*$ into the ratio formula:

$$\begin{aligned}
\rho_{\text{theo}}^* &= \frac{|\mathcal{E}^{(\kappa)}|}{|\mathcal{E}^{(\kappa^*)}|} = \frac{4 \binom{n/q}{3} \binom{n/q}{1} \frac{a}{n^3}}{2 \binom{n/q}{2} \binom{n/q}{2} \frac{a}{n^3}} \\
&\approx \frac{\frac{(n/q)^4}{3}}{\frac{(n/q)^4}{4}} \\
&= \frac{4}{3}
\end{aligned} \tag{155}$$

This theoretical value of $\rho_{\text{theo}}^* = \frac{4}{3} \approx 1.33$ perfectly aligns with the switching point observed in our experiments (Figure 17 (b)). This means that balanced 4-order hyperedges provide a stronger community signal than imbalanced ones.

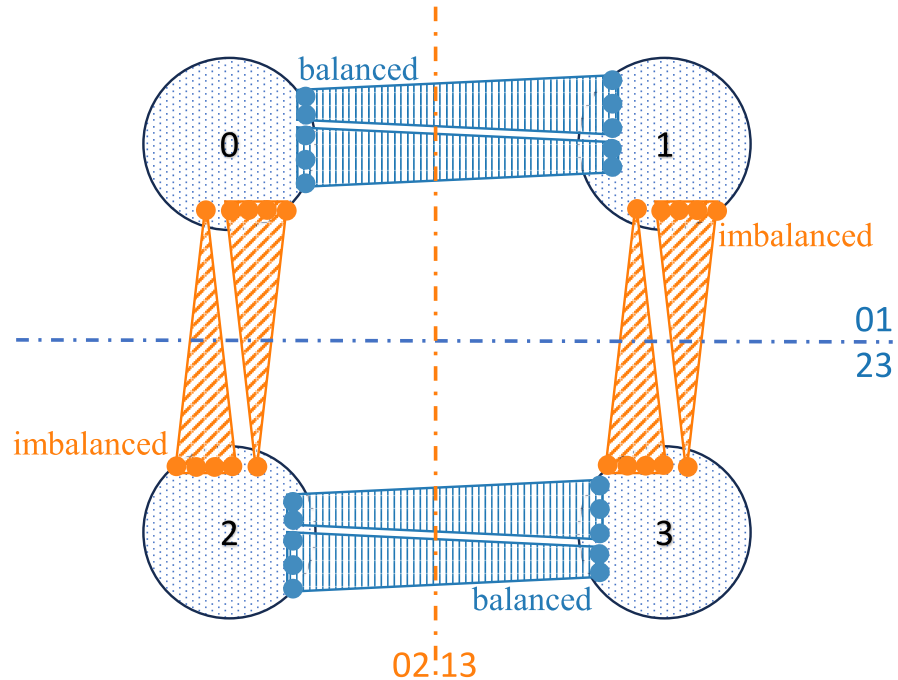
We also proceed similar experiment with 5-order hyperedges, as illustrated in Figure 18 (a). We define the two distinct 5-order hyperedge shapes based on their node distribution:

- More Balanced hyperedges: These 5-order hyperedges span two communities by connecting two nodes from one community and three from another. In our model, these only exist between the community pairs $\{0, 1\}$ or $\{2, 3\}$.
- More Imbalanced hyperedges: These 5-order hyperedges span two communities by connecting one node from one community and four from another. In our model, these only exist between the community pairs $\{0, 2\}$ or $\{1, 3\}$.

Based on the above setup, we define the affinity tensor $\mathbf{C}^{(5)}$ as follows. Let a^* be the affinity parameter for more balanced hyperedges and a for more imbalanced ones:

$$\mathbf{C}_z^{(5)} = \begin{cases} a, & z \in \{z \mid \#\{0 \text{ in } z\} = 3, \#\{2 \text{ in } z\} = 2\} \\ a, & z \in \{z \mid \#\{0 \text{ in } z\} = 2, \#\{2 \text{ in } z\} = 3\} \\ a, & z \in \{z \mid \#\{1 \text{ in } z\} = 3, \#\{3 \text{ in } z\} = 2\} \\ a, & z \in \{z \mid \#\{1 \text{ in } z\} = 2, \#\{3 \text{ in } z\} = 3\} \\ a^*, & z \in \{z \mid \#\{0 \text{ in } z\} = 3, \#\{1 \text{ in } z\} = 2\} \\ a^*, & z \in \{z \mid \#\{0 \text{ in } z\} = 2, \#\{1 \text{ in } z\} = 3\} \\ a^*, & z \in \{z \mid \#\{2 \text{ in } z\} = 3, \#\{3 \text{ in } z\} = 2\} \\ a^*, & z \in \{z \mid \#\{2 \text{ in } z\} = 2, \#\{3 \text{ in } z\} = 3\} \\ 0, & \text{otherwise} \end{cases} \tag{156}$$

(a)



(b)

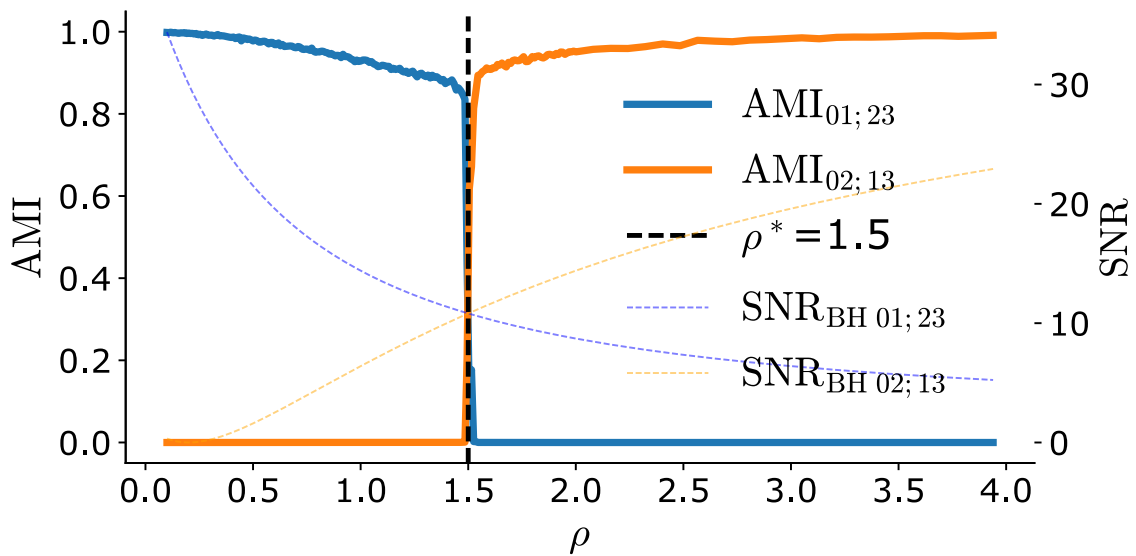


Figure 18: (a) Illustration of community structure of hypergraph used in experiment for exploring the effect of shape to detectability. All the hyperedges are 5-order, only the different shape. The hyperedges shaped by trapezoid between communities $\{0,1\}$ or $\{2,3\}$ are more balanced, composed by 2 nodes in one community, 3 nodes in another. The hyperedges shaped by triangle between communities $\{0,2\}$ or $\{1,3\}$ are more imbalanced, composed by 1 node in one community, 4 nodes in another. (b) Experimental results with $n = 8000$, $d = 10$, $\kappa = 5$ and $\kappa^* = 5$. We show the AMI_{κ^*} and AMI_{κ} as the AMI of detected communities by Bethe Hessian based-spectral clustering to community structure dominated by more balanced and more imbalanced 5-order hyperedges.

For consistency, we denote the expected number of more balanced hyperedges as $|\mathcal{E}^{(\kappa^*)}|$ and more imbalanced hyperedges as $|\mathcal{E}^{(\kappa)}|$. These can be calculated as:

$$\begin{aligned} |\mathcal{E}^{(\kappa^*)}| &= 4 \binom{n/q}{2} \binom{n/q}{3} \frac{a^*}{n^4} = 4 \frac{(n/q)^5}{2!3!} \frac{a^*}{n^4} = 4 \frac{na^*}{2!3!q^5} \\ |\mathcal{E}^{(\kappa)}| &= 4 \binom{n/q}{4} \binom{n/q}{1} \frac{a}{n^4} = 4 \frac{(n/q)^5}{4!} \frac{a}{n^4} = 4 \frac{na}{4!q^5} . \end{aligned} \quad (157)$$

Using the definitions (133) of average degree d and the hyperedge ratio $\rho = |\mathcal{E}^{(\kappa)}|/|\mathcal{E}^{(\kappa^*)}|$, we can express the parameters a and a^* as:

$$\begin{aligned} a &= \frac{4^4 4! d \rho}{5(\rho + 1)} \\ a^* &= \frac{4^4 2! 3! d}{5(\rho + 1)} . \end{aligned} \quad (158)$$

As shown in the experimental results in Figure 18 (b), the Bethe Hessian-based spectral clustering algorithm's preference switches from the more balanced to the more imbalanced community structure at a point $\rho_{theo}^* \neq 1$. This further empirically confirms that the hyperedge shape directly affects community detectability. To theoretically predict this switching point, we analyze under similar routine to previous sections.

First, we derive the matrix $\widehat{\mathbf{C}}^{(4)}$:

$$\widehat{\mathbf{C}}^{(5)} = \frac{1}{4^{5-2}(5-2)!} \begin{bmatrix} 4a^* + 3a, & 6a^*, & 2a, & 0 \\ 6a^*, & 4a^* + 3a, & 0, & 2a \\ 2a, & 0, & 4a^* + 3a, & 6a^* \\ 0, & 2a, & 6a^*, & 4a^* + 3a \end{bmatrix} . \quad (159)$$

Aggregating this matrix according to the community structure dominated by more balanced 5-order hyperedges $\{\{0, 1\}, \{2, 3\}\}$ yields:

$$\begin{aligned} \widehat{\mathbf{C}}_{(\kappa^*)}^{(5)} &= \frac{1}{64 * 6} \begin{bmatrix} 5a^* + \frac{3}{2}a, & a \\ a, & 5a^* + \frac{3}{2}a \end{bmatrix} \\ \Rightarrow \text{SNR}_{\text{BH } 01;23} &= \frac{1}{2^2(5-1)d^{(5)}} \left(\frac{1}{64 * 6} (5a^* + \frac{3}{2}a - a) \right)^2 . \end{aligned} \quad (160)$$

Similarly, aggregating for the community structure dominated by more imbalanced 5-order hyperedges $\{\{0, 2\}, \{1, 3\}\}$ gives:

$$\begin{aligned} \widehat{\mathbf{C}}_{(\kappa)}^{(5)} &= \frac{1}{64 * 6} \begin{bmatrix} 2a^* + \frac{5}{2}a, & 3a^* \\ 3a^*, & 2a^* + \frac{5}{2}a \end{bmatrix} \\ \Rightarrow \text{SNR}_{\text{BH } 02;13} &= \frac{1}{2^2(5-1)d^{(5)}} \left(\frac{1}{64 * 6} (2a^* + \frac{5}{2}a - 3a^*) \right)^2 . \end{aligned} \quad (161)$$

To find the switching point, we solve the $\text{SNR}_{\text{BH } 01;23} = \text{SNR}_{\text{BH } 02;13}$:

$$\begin{aligned}
 \text{SNR}_{\text{BH } 01;23} &= \text{SNR}_{\text{BH } 02;13} \\
 (5a^* + \frac{1}{2}a)^2 &= (\frac{5}{2}a - a^*)^2 \\
 (4a^* + 3a)(6a^* - 2a) &= 0 \\
 \frac{a}{a^*} &= 3
 \end{aligned} \tag{162}$$

Last, to find the corresponding ratio of hyperedge counts ρ_{theo}^* , we substitute $a = a^*$ into the ratio formula:

$$\rho_{\text{theo}}^* = \frac{|\mathcal{E}^{(\kappa)}|}{|\mathcal{E}^{(\kappa^*)}|} = \frac{\frac{a}{4!}}{\frac{a^*}{2!3!}} = \frac{3}{2} \tag{163}$$

This theoretical value of $\rho_{\text{theo}}^* = \frac{3}{2}$ perfectly aligns with the switching point observed in our experiments (Figure 18 (b)). This means that more balanced 5-order hyperedges provide a stronger community signal than more imbalanced ones.

I Notation

node set	\mathcal{V}
node	i, j, k, l
number of nodes	n
edge(hyper) set	\mathcal{E}
edge(hyper)	e, f, g
number of edges(hyper)	m
order of edge(hyper) e	$ e $
order set	\mathcal{K}
order κ hyperedge set	$\mathcal{E}^{(\kappa)}$
number of order κ hyperedges	$m^{(\kappa)}$
average degree	d
diagonal degree matrix	\mathbf{D}
order κ degree of node i	$d_i^{(\kappa)}$
order κ average degree	$d^{(\kappa)}$
order κ degree matrix	$\mathbf{D}^{(\kappa)}$
number of communities	q
community labels	$\vec{\psi}$
adjacent matrix	\mathbf{A}
edge probability matrix(tensor)	Ω
rescaled edge probability matrix(tensor)	\mathbf{C}
incidence matrix	\mathbf{H}
order κ -incidence matrix	$\mathbf{H}^{(\kappa)}$
one-mode projection of $\mathbf{H}^{(\kappa)}$	$\mathbf{A}^{(\kappa)}$
non-backtracking matrix	\mathbf{NB}
non-backtracking matrix of κ -order uniform hyper graph	$\mathbf{NB}^{(\kappa)}$
non-backtracking matrix of nonuniform hyper graph with order set \mathcal{K}	$\mathbf{NB}^{(\mathcal{K})}$
bethe hessian matrix	\mathbf{B}
bethe hessian matrix of κ -order uniform hyper graph	$\mathbf{B}^{(\kappa)}$
bethe hessian matrix of nonuniform hyper graph with order set \mathcal{K}	$\mathbf{B}^{(\mathcal{K})}$

Table 2: Notations